...VELOPMENT OF REFRACTORY CERAMICS THAT CA...
...E PROCESSED AT TEMPERATURES CONSIDERABLY ...
...OWER THAN THEIR MAXIMUM USE TEMPERATURE

Progress Report No. III
Contract No. NOw 62-0710-d
... October 1962 - 1 January 196...
School of Mines
...

DEVELOPMENT OF REFRACTORY CERAMICS THAT CAN BE PROCESSED AT TEMPERATURES CONSIDERABLY LOWER THAN THEIR MAXIMUM USE TEMPERATURE

1 October 1962 - 1 January 1963

Prepared under Navy, Bureau of Weapons
Contract NOw 62-0710-d

Quarterly Progress Report No. III

School of Ceramics
Rutgers, The State University
New Brunswick, New Jersey

Since this is a progress report, the information contained herein is tentative and subject to changes, corrections and modifications.

PREFACE

The undersigned constitute the planning committee for this project. Professor E. J. Smoke is project leader. The experimental work has been carried out by Mr. Peter Fleischner and Mr. Chester Ringel.

SCHOOL OF CERAMICS
RUTGERS, THE STATE UNIVERSITY

Edward J. Smoke
School of Ceramics

John H. Koenig
Professor of Ceramics

Approved:

John H. Koenig, Director
School of Ceramics

January 1, 1963

ABSTRACTS

Part I. Presintering Studies

The presintering study was initiated to determine the densification mechanisms of a high alumina body utilizing the presintering process, an analysis of density determinations and X-ray diffraction results are presented. The formation of a liquid phase is shown.

Part II. Sintering Studies

A study of the densification of pure alumina (C), pure alumina with 0.25% MgO (R) and pure alumina containing 2.0% MgO (CR) was carried out in a vacuum. This investigation has shown that by firing in vacuum, high densities were obtained at comparatively low temperatures for all the compositions investigated. Maximum densities of 3.87, 3.955 and 3.94 were obtained for the C, R and CR compositions respectively at a temperature of 1550°C (2820°F).

TABLE OF CONTENTS

	Page No.
Abstracts	i
I. Presintering Study	1
A. Introduction	1
B. Body Composition	1
C. Summary of Density Determinations	52
D. X-ray Analysis - Discussion	53
E. Liquid Phase	57
F. Sodium Content	58
G. Future Work	58
II. Sintering Studies	59
A. Introduction	59
B. Theoretical Consideration and Methods of Approach	59
C. Experimental Procedure	62
D. Results	75
E. Discussion of Results	111
F. Conclusions	120
G. Future Work	121

I. PRESINTERING STUDY

A. Introduction

This study was initiated in order to better understand the mechanisms occuring in a presintering operation. Utilization of the presintered process enables a high alumina body to densify at a much lower temperature and to a much greater extent than a conventionally fabricated body of the same composition. Once these mechanisms are determined and controlled, it should be possible to obtain the optimum body under a given set of conditions. This will play a vital role in the overall objective of this effort, the lowering of the firing temperature of ceramics for radome application, yet retaining all the desireable engineering properties.

B. Body Compositions

The compositions under investigation are shown in Figure 1 on page . As seen from the figure, the alumina content increases from 71.8% to 95% by weight, while the remainder of the body composition is added wholly silica, magnesia, or fixed ratios of silica and magnesia.-

C. Analysis of Density Determinations

The density determinations with regard to presintering temperature, final firing temperature, and composition were shown in the previous report. Curves of density vs. presintering temperature and density vs. final firing temperature for

Figure 1

COMPOSITIONS CHOSEN IN Al_2O_3-MgO-SiO_2

PHASE DIAGRAM

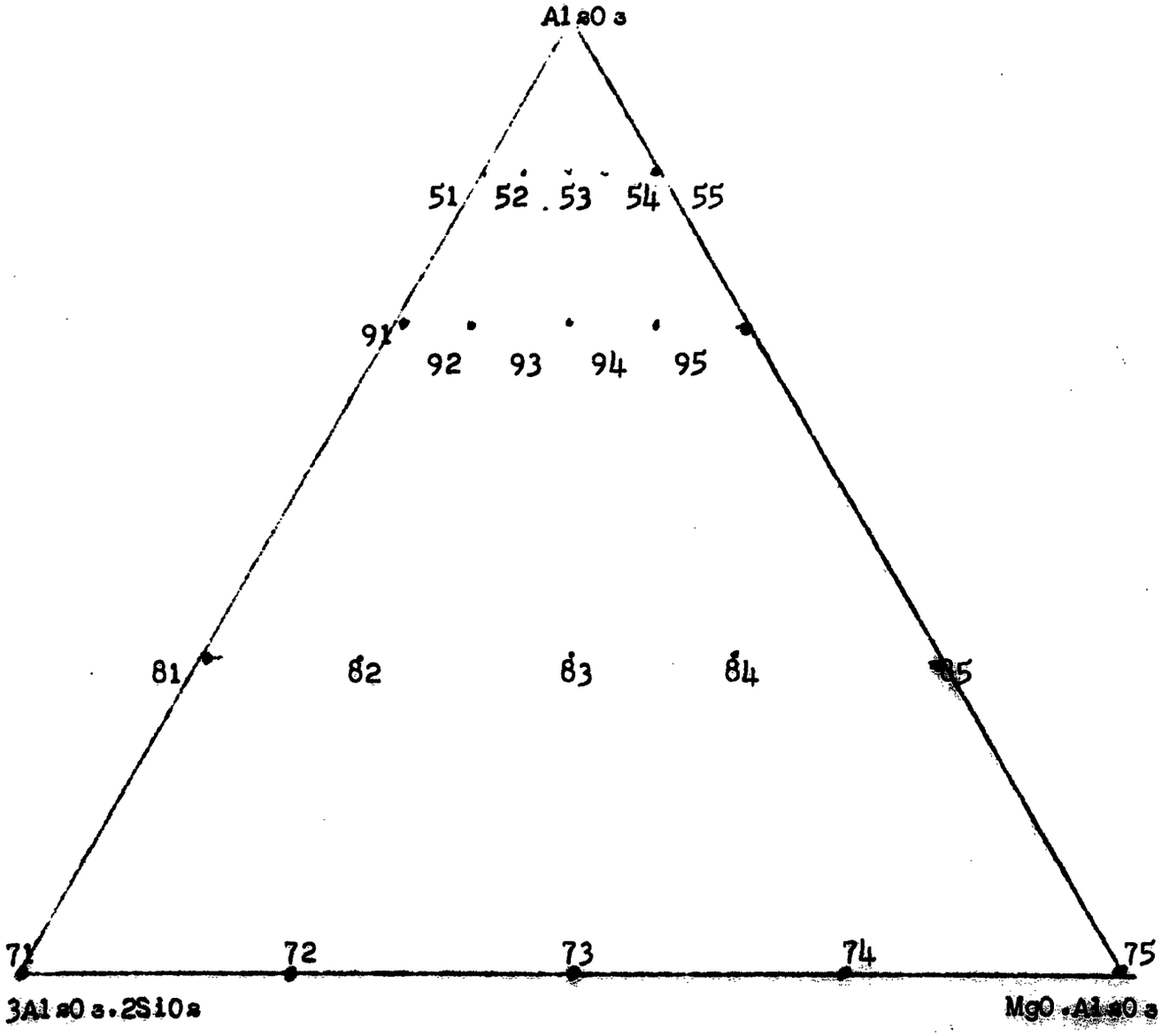

each composition are shown in this report. An analysis of density with respect to composition, presintering temperature, and final firing temperature will be presented.

Al$_2$O$_3$-SiO$_2$ Binary - Series 71, 81, 91, and 51

The density vs. presintering temperature and density vs. final firing temperature curves of the binary Al$_2$O$_3$-SiO$_2$ series 71, 81, 91, and 51, are shown on pages - . As seen from the curves, the density of bodies in this range composition increases as the final firing temperature increases. It would appear that densification is taking place by diffusional means as indicated by the increasing density with increasing temperature. An incongruity exists in the density vs. presintering temperature curve of series 71, 81, and 91. It would be expected that the density should increase with increasing presintering temperature, however, the curve of these series increases to 2600°F, decreases at 2700°F, and increases again at 2800°F. The series 51 shows an increase in density with an increasing presintering temperature.

The results obtained in the Al$_2$O$_3$-SiO$_2$ binary are very encouraging, in that relatively low porosities were obtained for this type composition. The series 51 composition attains a moisture absorption of less than one per cent while possessing a relatively high density.

Figure 2

Density versus Final Firing Temperature

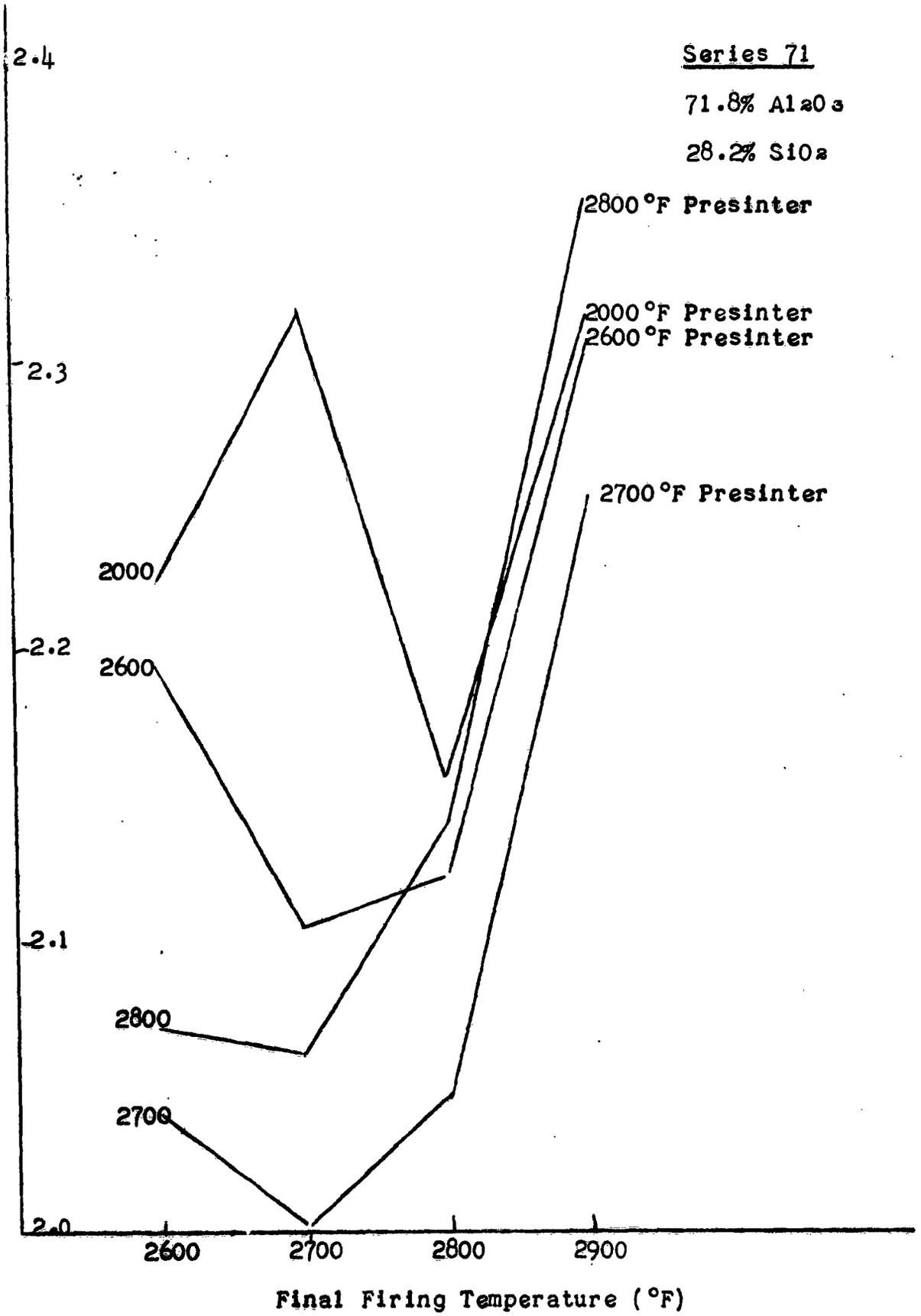

Figure 3

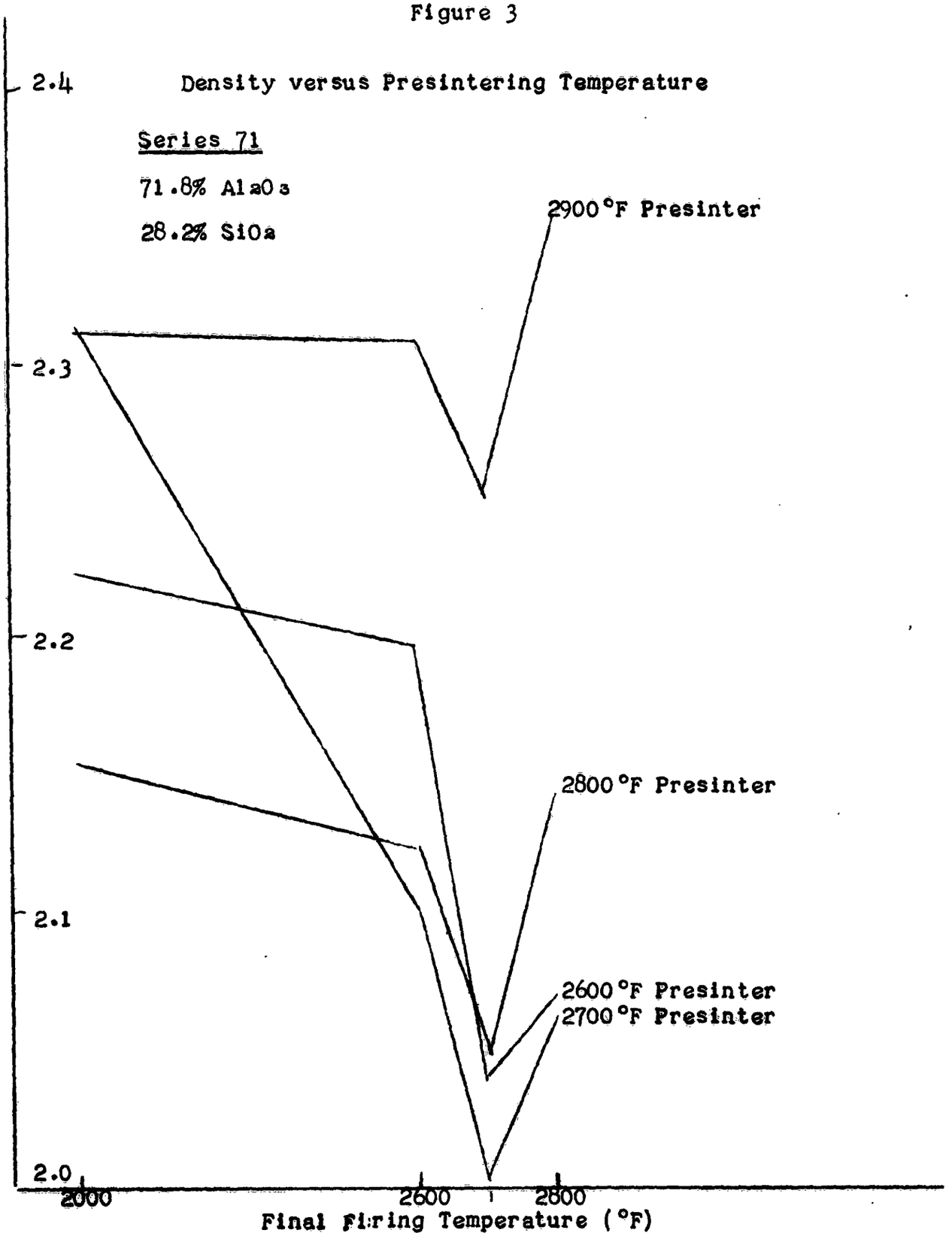
Density versus Presintering Temperature
Series 71
71.8% Al2O3
28.2% SiO2
2900 °F Presinter
2800 °F Presinter
2600 °F Presinter
2700 °F Presinter
2.4
2.3
2.2
2.1
2.0
2000
2600
2800
Final Firing Temperature (°F)

Figure 4

Density versus Final Firing Temperature

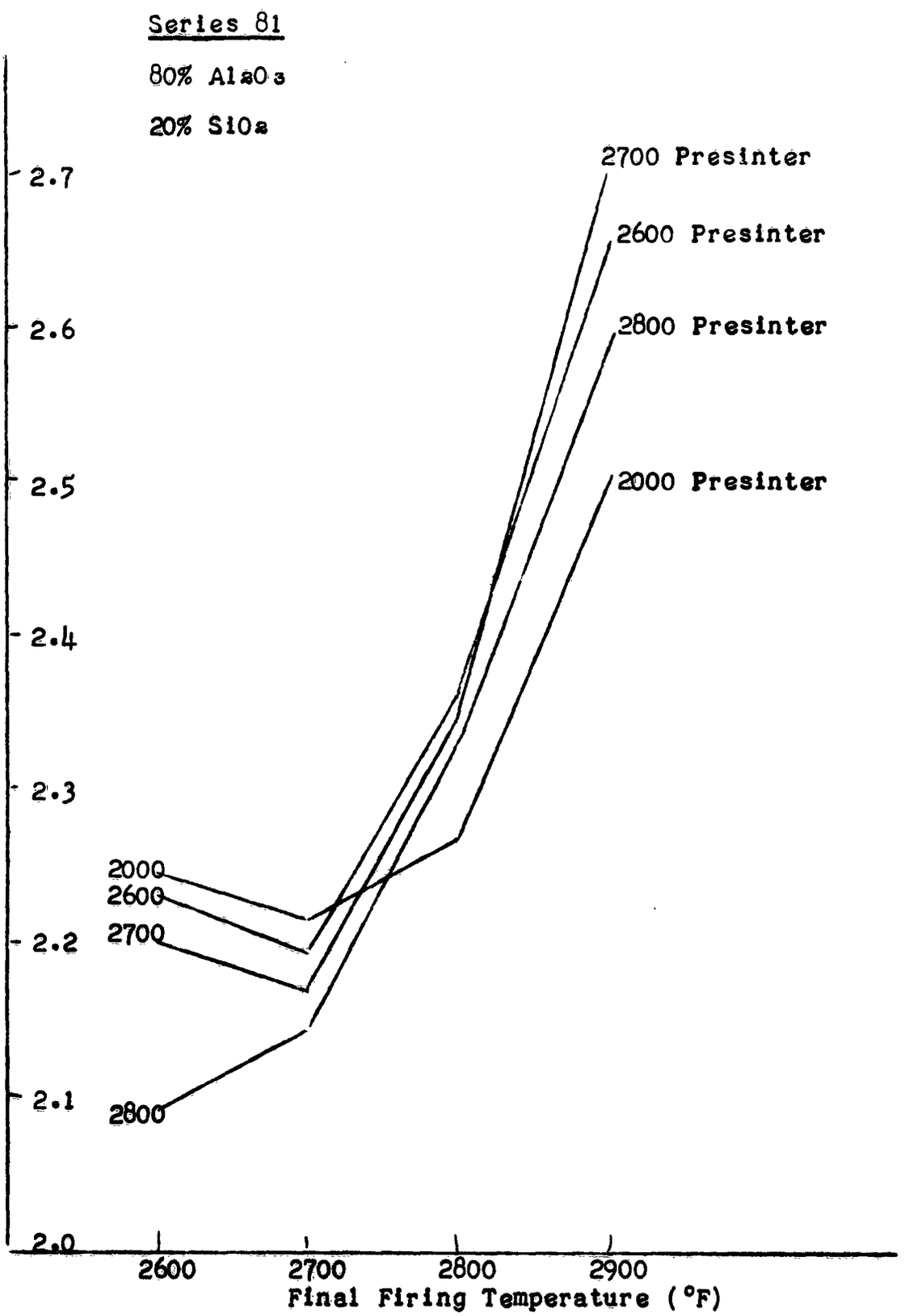

Figure 5

Density versus Presintering Temperature

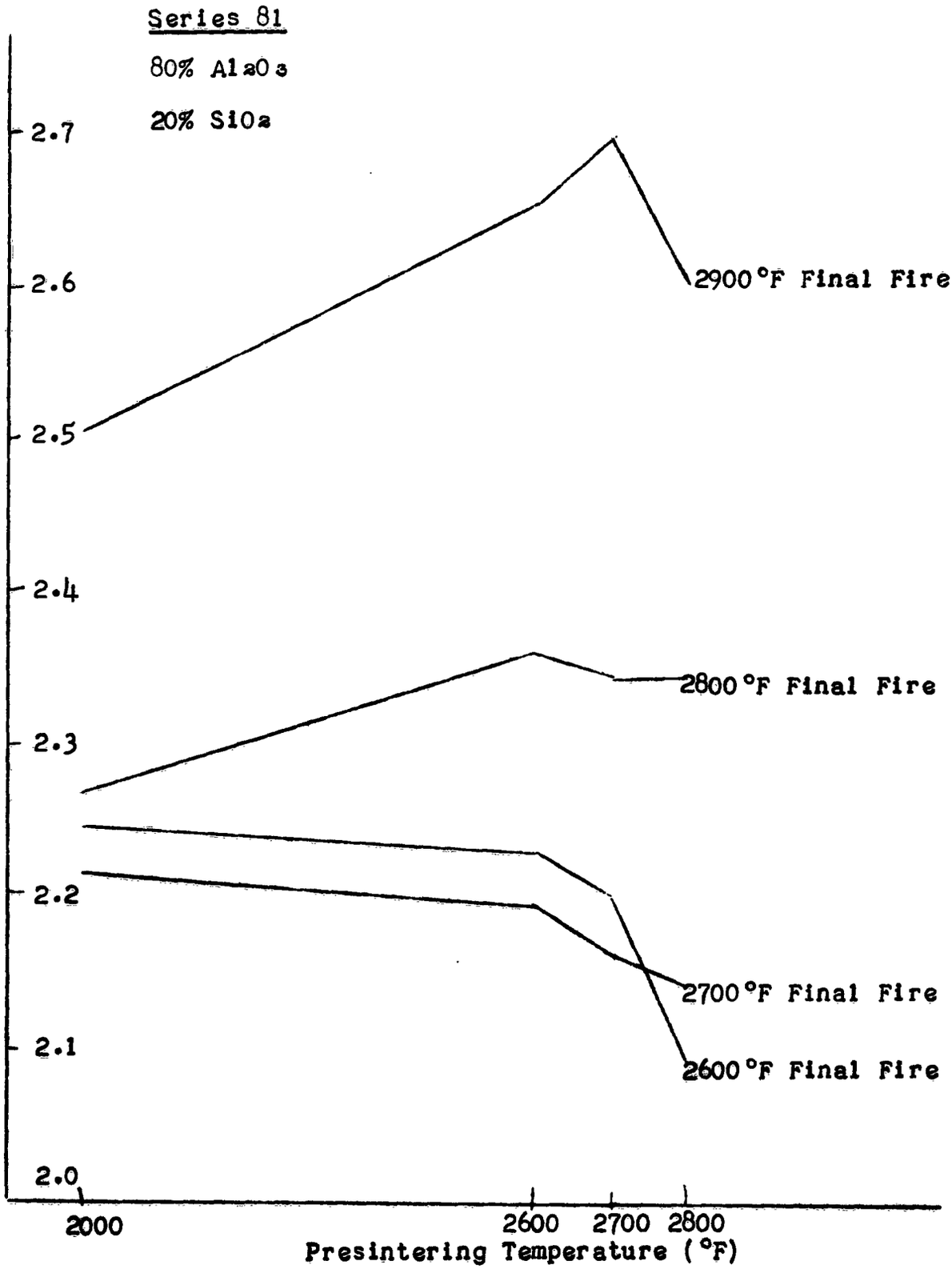

Figure 6

Density versus Final Firing Temperature

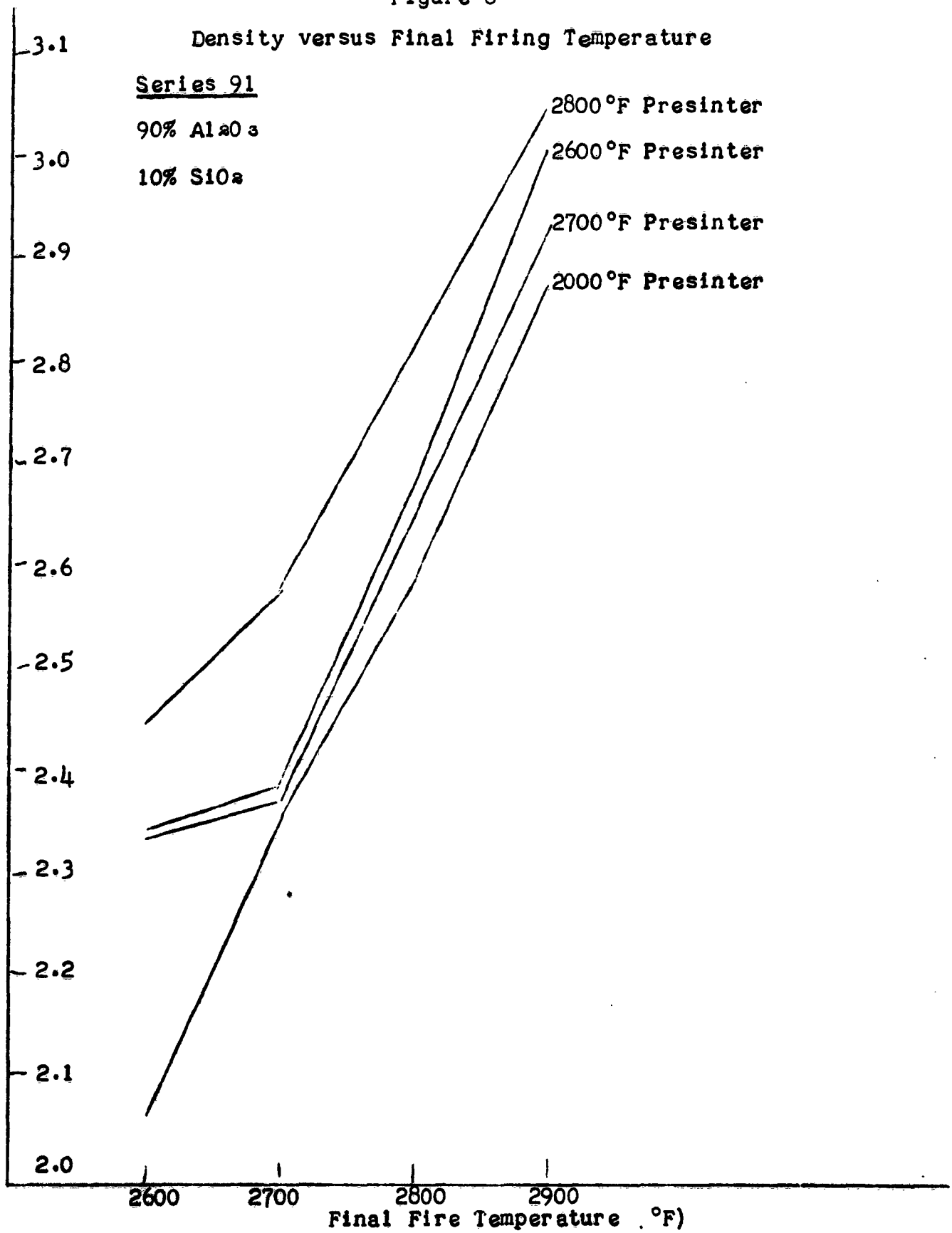

Figure 7

Density versus Presintering Temperature

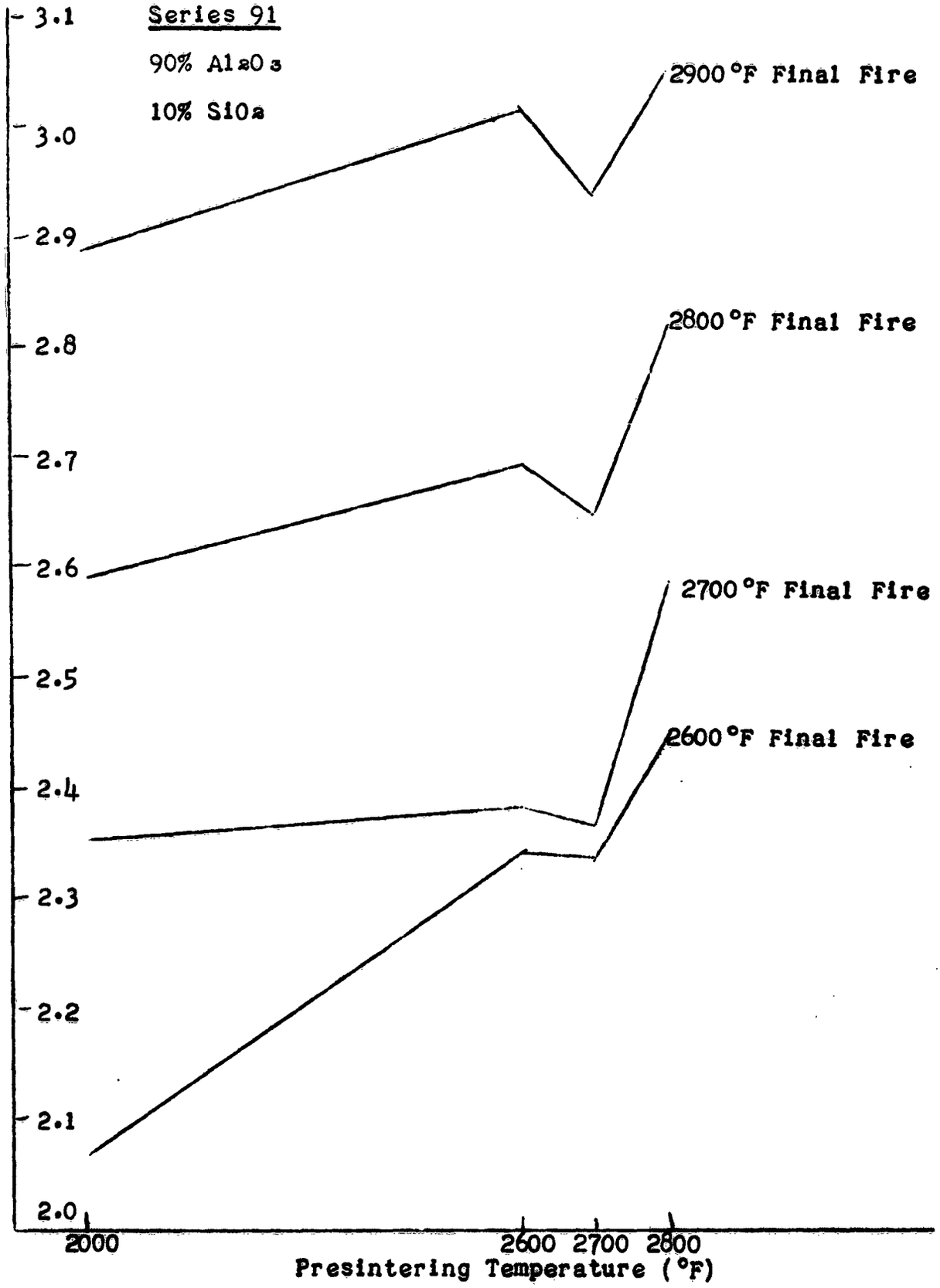

Figure 8

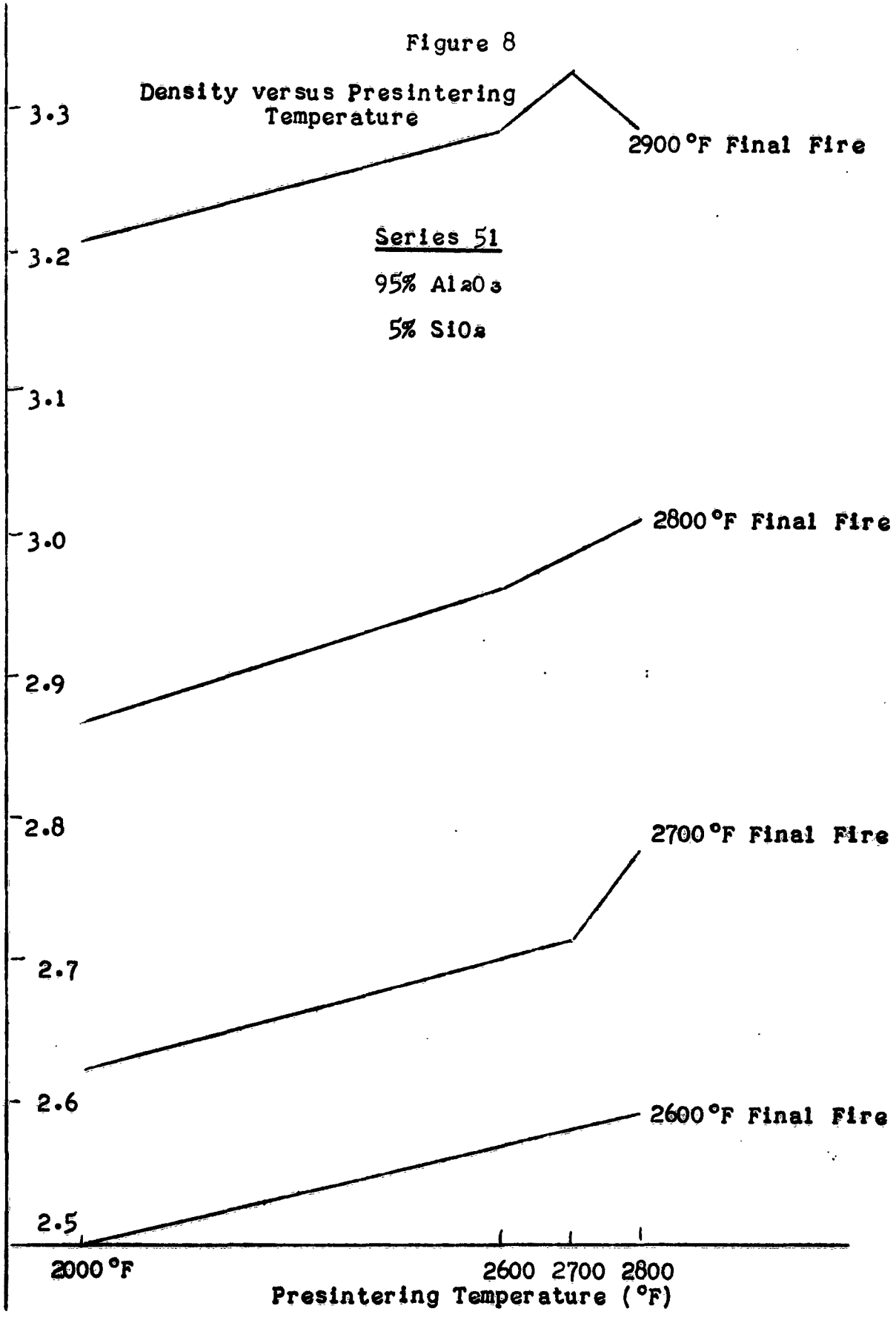
Density versus Presintering Temperature
3.3
3.2
3.1
3.0
2.9
2.8
2.7
2.6
2.5
2900 °F Final Fire
Series 51
95% Al2O3
5% SiO2
2800 °F Final Fire
2700 °F Final Fire
2600 °F Final Fire
2000 °F
2600 2700 2800
Presintering Temperature (°F)

Figure 9

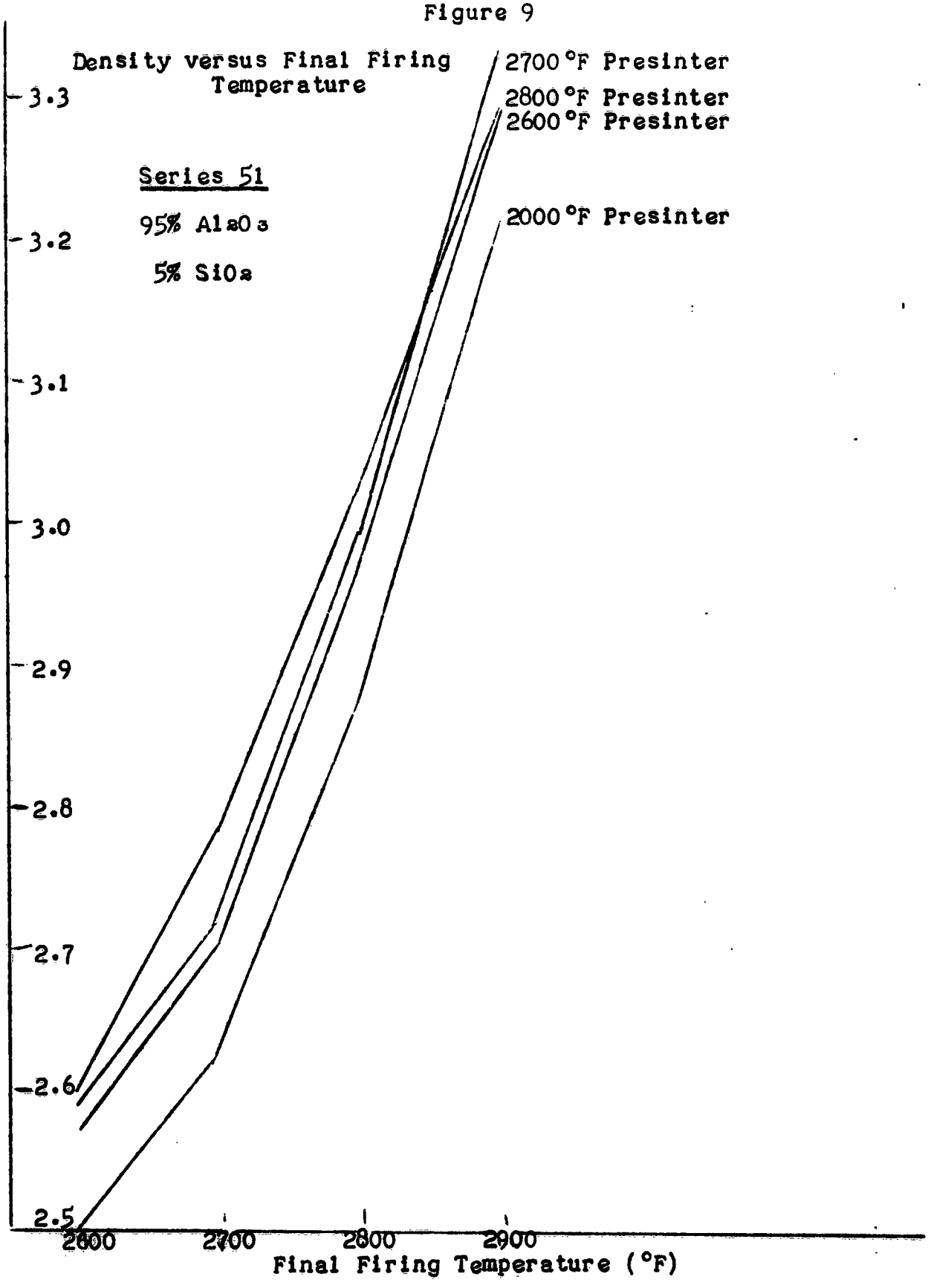
Density versus Final Firing Temperature
Series 51
95% Al2O3
5% SiO2
2700 °F Presinter
2800 °F Presinter
2600 °F Presinter
2000 °F Presinter
3.3
3.2
3.1
3.0
2.9
2.8
2.7
2.6
2.5
2600
2700
2800
2900
Final Firing Temperature (°F)

THE TEMPERATURE UTILIZED TO PRODUCE

OPTIMUM BODIES OF EACH SERIES

Series 71	Density	Moisture Absorption	Presintering Temperatures	Final Firing Temperature
71.8% Al_2O_3	2.353	10.0%	2800°F	2900°F
28.2% SiO_2				
Series 81				
80.0% Al_2O_3	2.699	5.5%	2700°F	2900°F
20.0% SiO_2				
Series 91				
90.0% Al_2O_3	3.051	3.4%	2800°F	2900°F
10.0% SiO_2				
Series 51				
95.0% Al_2O_3	3.331	0.9%	2700°F	2900°F
5.0% SiO_2				

Al$_2$O$_3$ - MgO Binary - Series 75, 85, 95, and 55.

An analysis of the density vs. presintering temperature and density vs. final firing temperature curves of the Binary Al$_2$O$_3$-MgO are shown on pages . As seen from the curves, the density increases with an increase in final firing temperature. This increasing density with increasing temperature is indicative of diffusional mechanisms of sintering. The density increases with increasing presintering temperature to 2600°F, levels off to 2700°F, and decreases slightly at 2800°F. The large increase in density between compositions presintered at 2000°F and compositions presintered at 2600°F indicates that for compositions in this binary to achieve maturity, a presintering fire of at least 2600°F is necessary.

The temperatures utilized to produce optimum bodies of each series are shown below:

	Density	Moisture Absorption	Presintering Temperature	Final Firing Temperature
Series 75 71.8% Al$_2$O$_3$ 28.1% MgO	3.338	0.00%	2800°F	2900°F
Series 85 80% Al$_2$O$_3$ 20% MgO	3.448	0.00%	2700°F	2800°F

Figure 10

Density versus Presintering Temperature

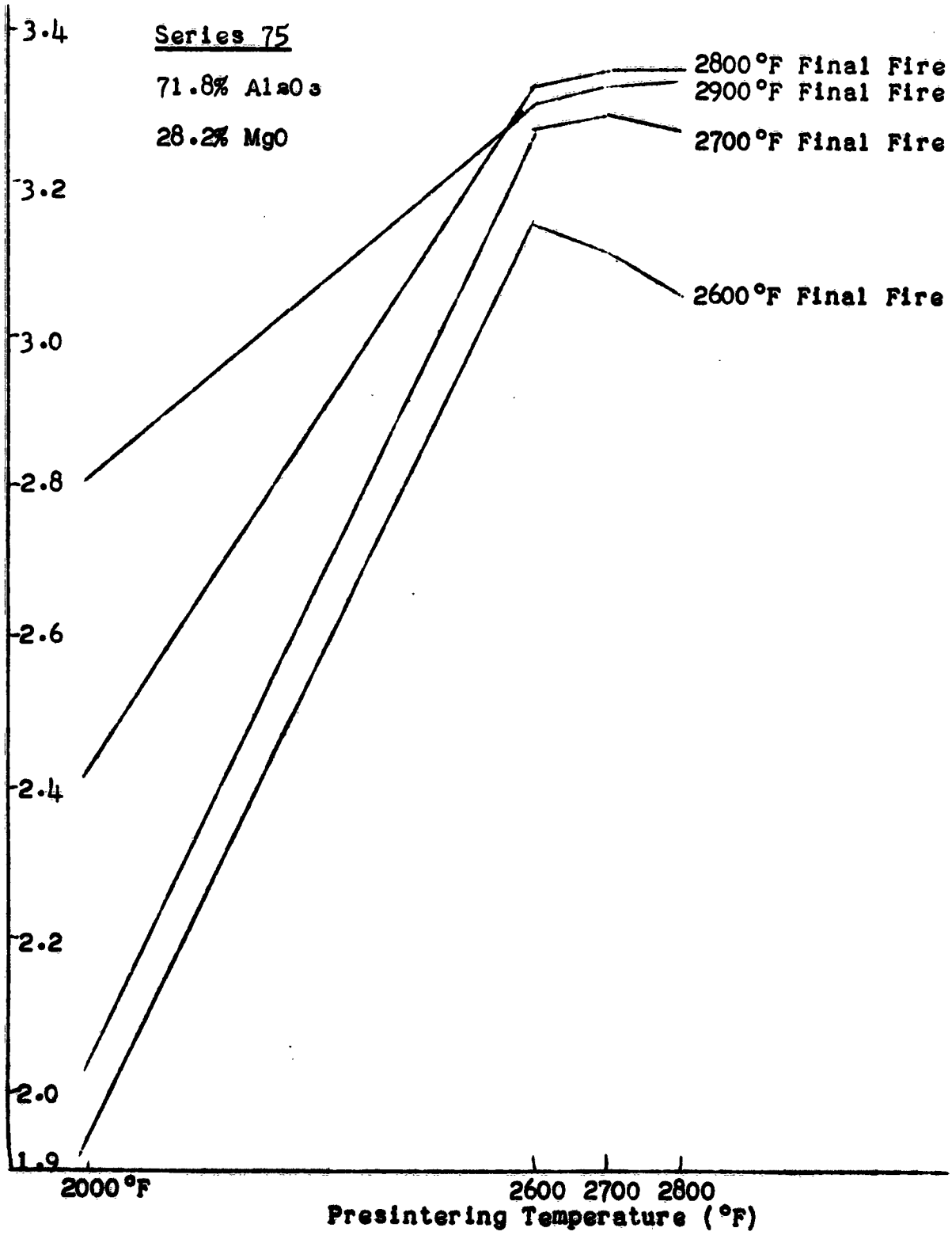

Figure 11

Density versus Final Firing Temperature

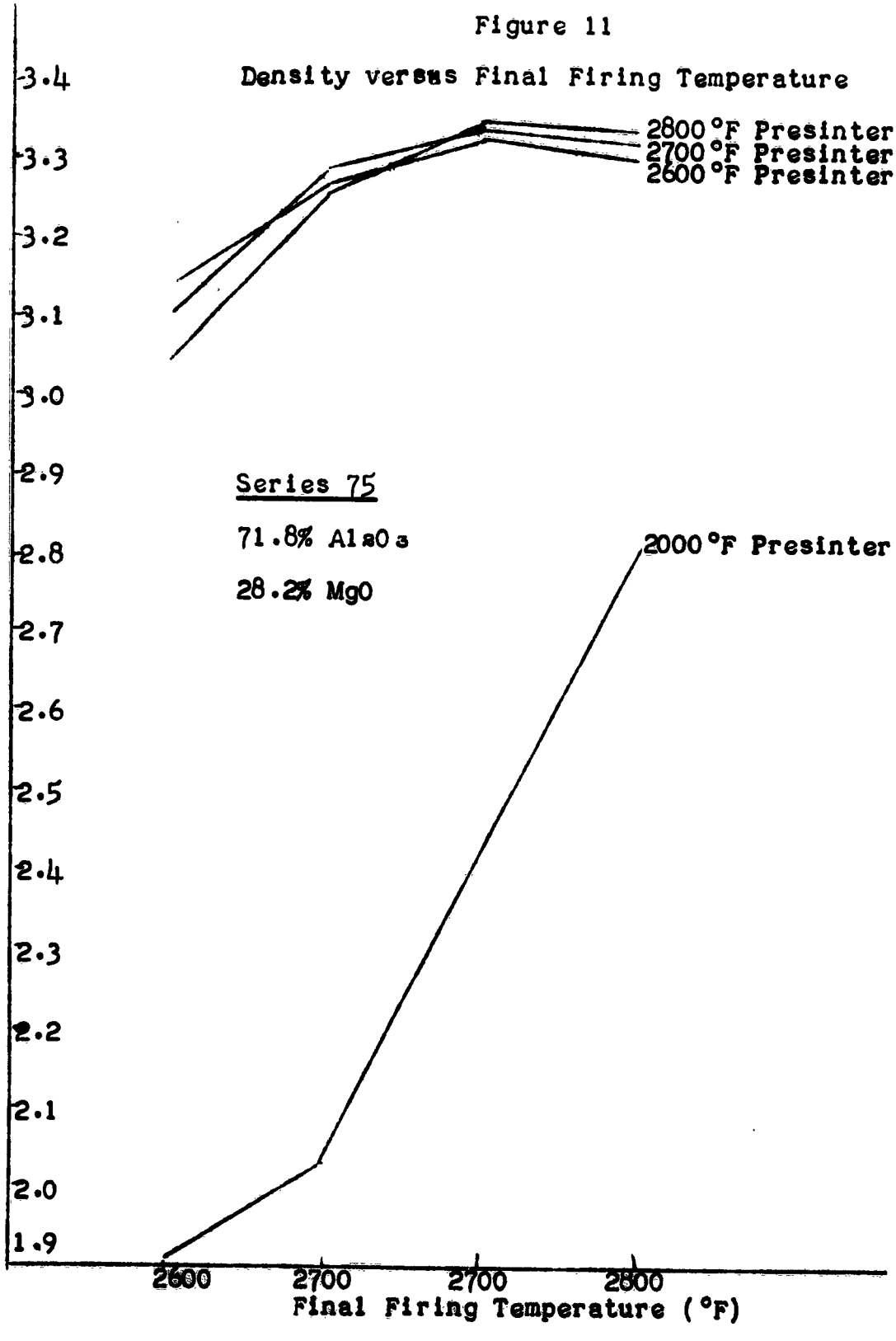

Figure 12

Density versus Presintering Temperature

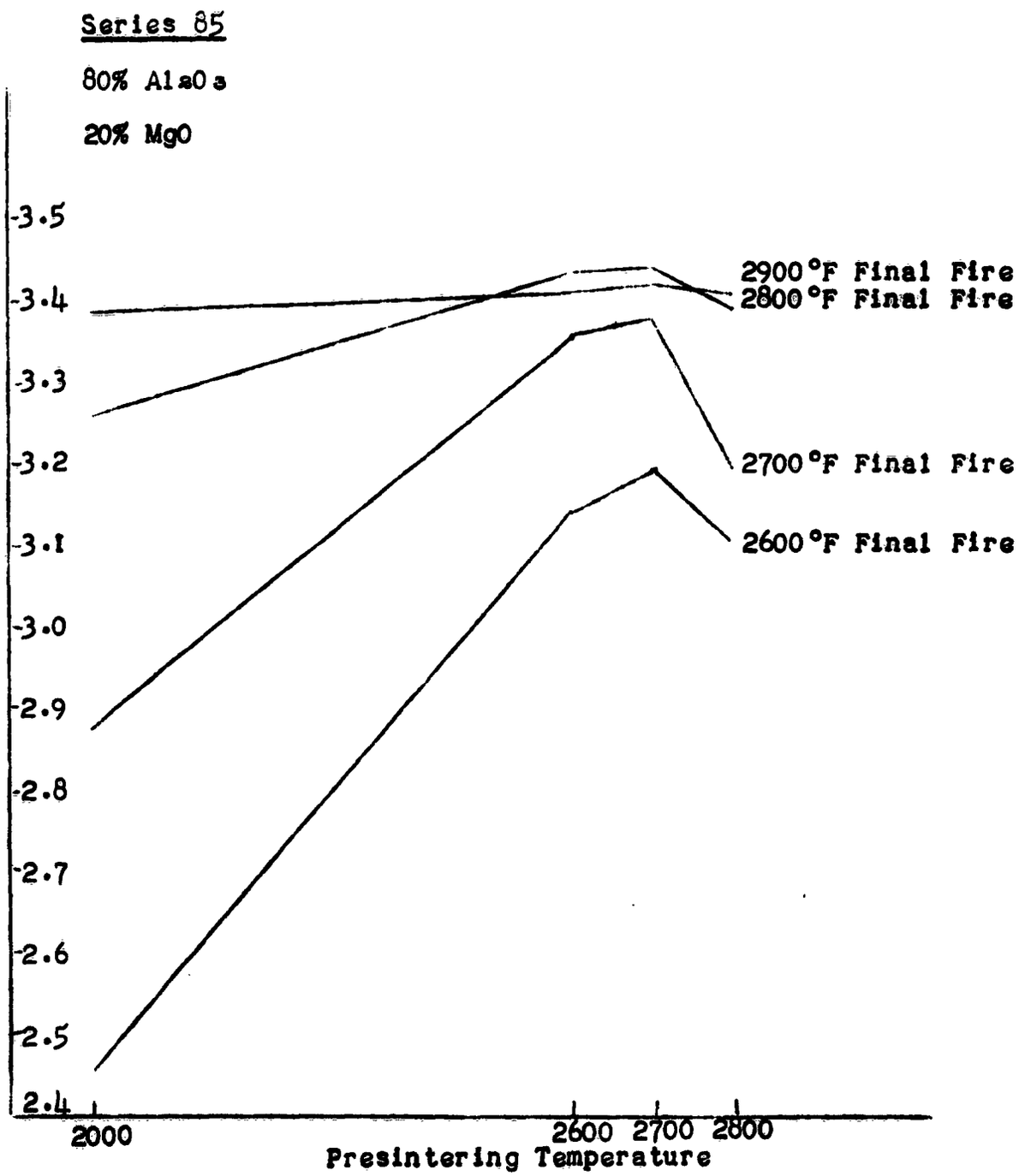

Figure 13

Density versus Final Firing Temperature

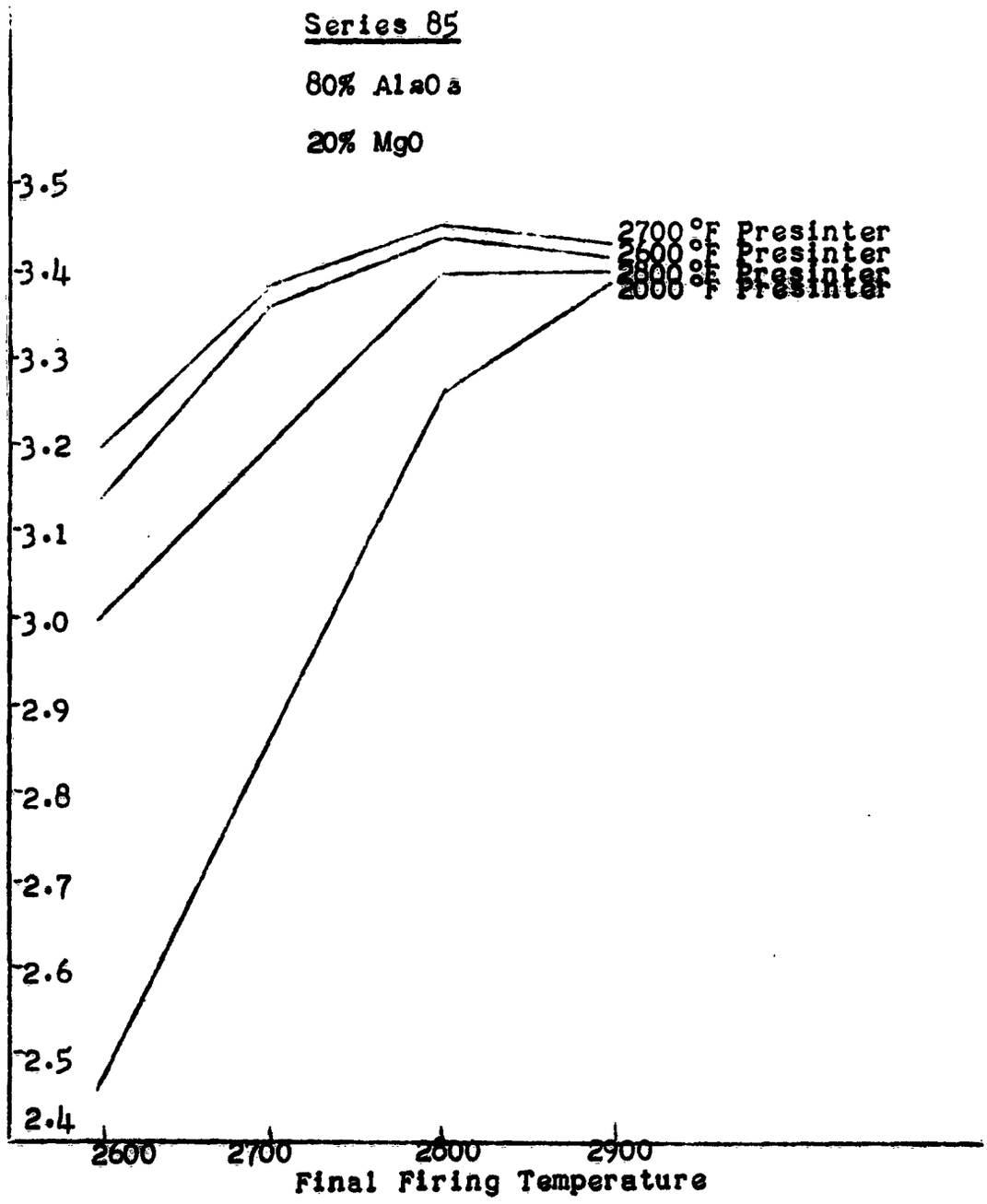

Figure 14

Density versus Presintering Temperature

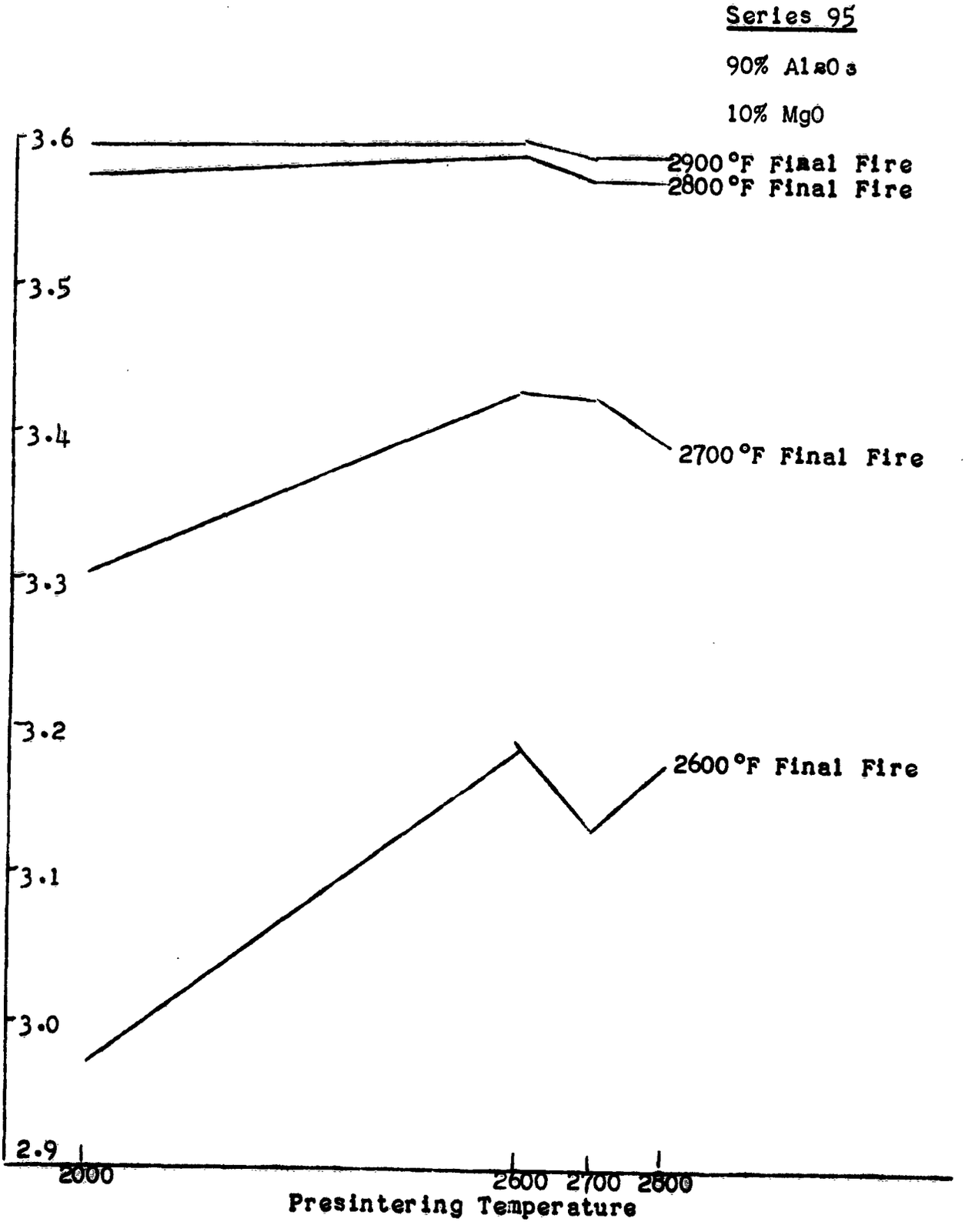

Figure 15

Density versus Final Firing Temperature

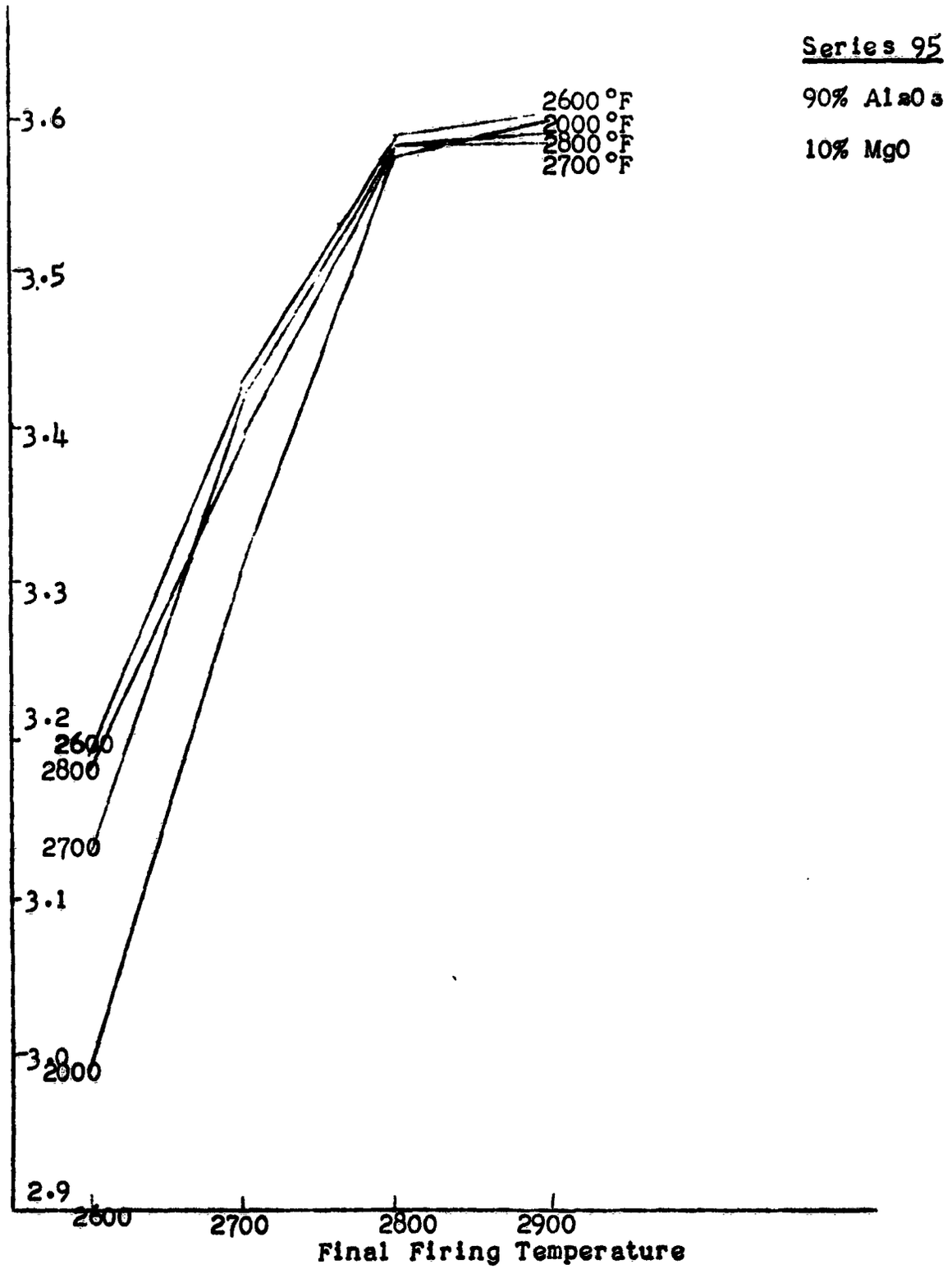

Figure 16

Density versus Presintering Temperature

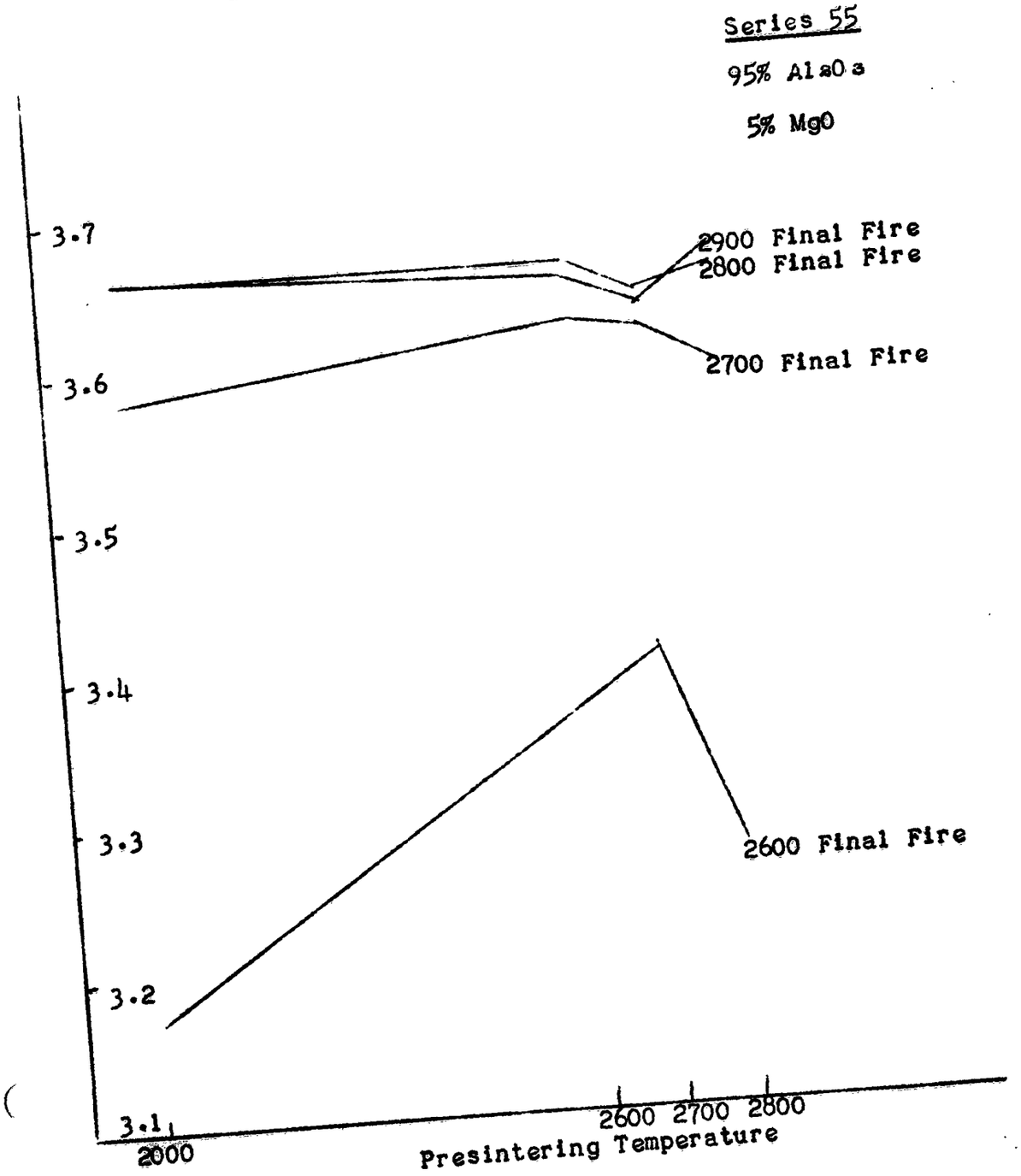

Figure 17

Density versus Final Firing Temperature

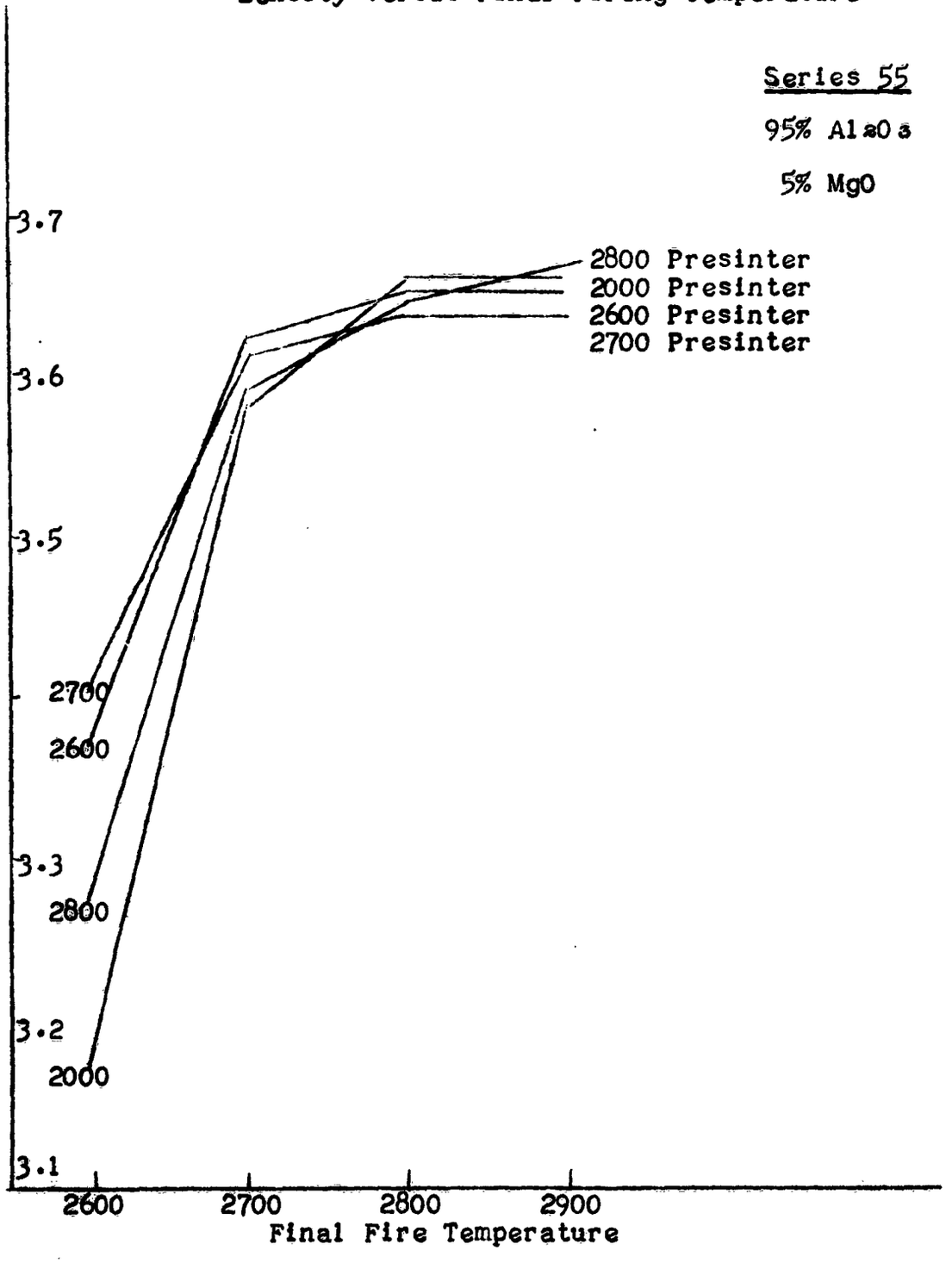

Series 95 90% Al_2O_3 10% MgO	3.600	0.00%	2600°F	2900°F
Series 55 95% Al_2O_3 5% MgO	3.664	0.00%	2800°F	2900°F

As the results indicate all series attained maturity with relatively high densities. These results are significant in that all compositions are non porous at 2700°F and reach maximum density at 2800°F. These bodies contain no silica additions, to form a liquid. This means that these compositions can be fired to 3496°F before a eutectic liquid is attained, and yet they mature at 2800°F, almost 700°F below liquid formation.

Al_2O_3-SiO_2-MgO Ternary - Series 72, 82, 92, and 52

The density vs. presintering temperature and density vs. final firing temperature curves of the series 72, 82, 92, and 52 are shown on pages . As seen from the curves, the final fire density of bodies in this range of compositions increases initially with an increase in temperature, levels off in the intermediate range, and finally decreases at the high temperatures. The density vs. presintering temperature curves show similar type of results. These curves are indicative of densification occuring with aid of a liquid phase.

Figure 18

Density versus Presintering Temperature

Series 72

71.8% Al_2O_3
21.15% SiO_2
7.05% MgO

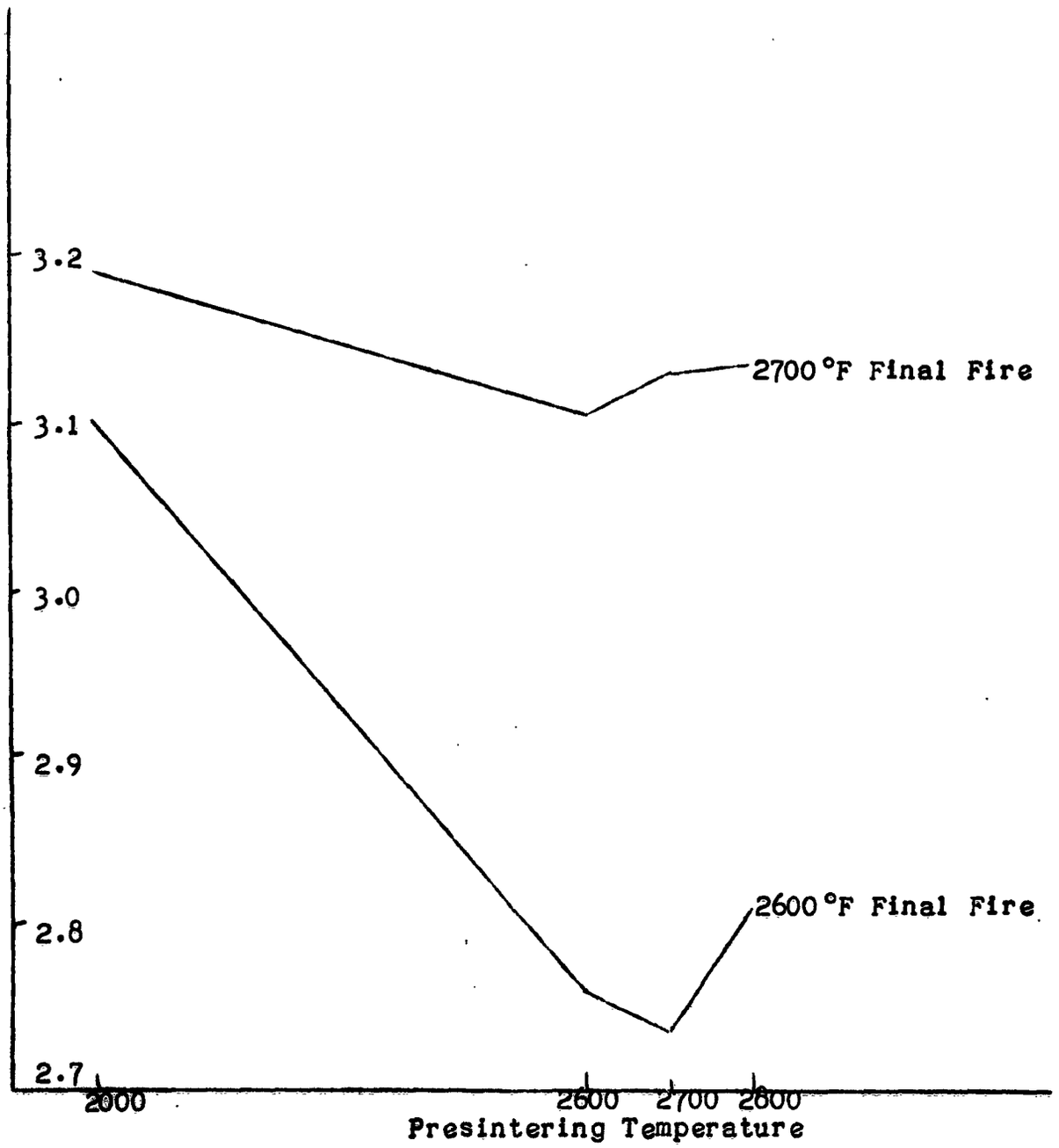

Figure 19

Density versus Final Firing

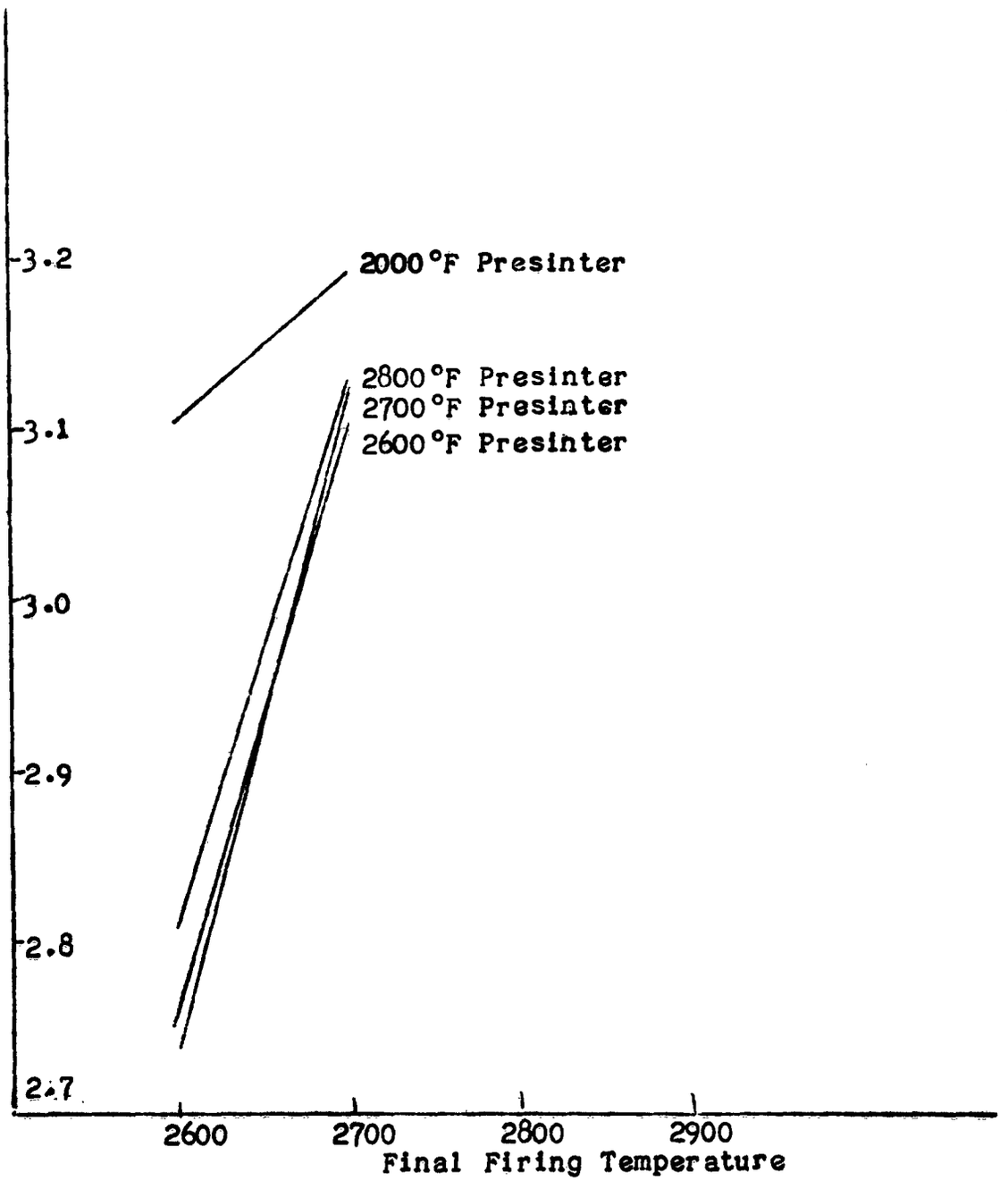

Figure 20

Density versus Presintering Temperature

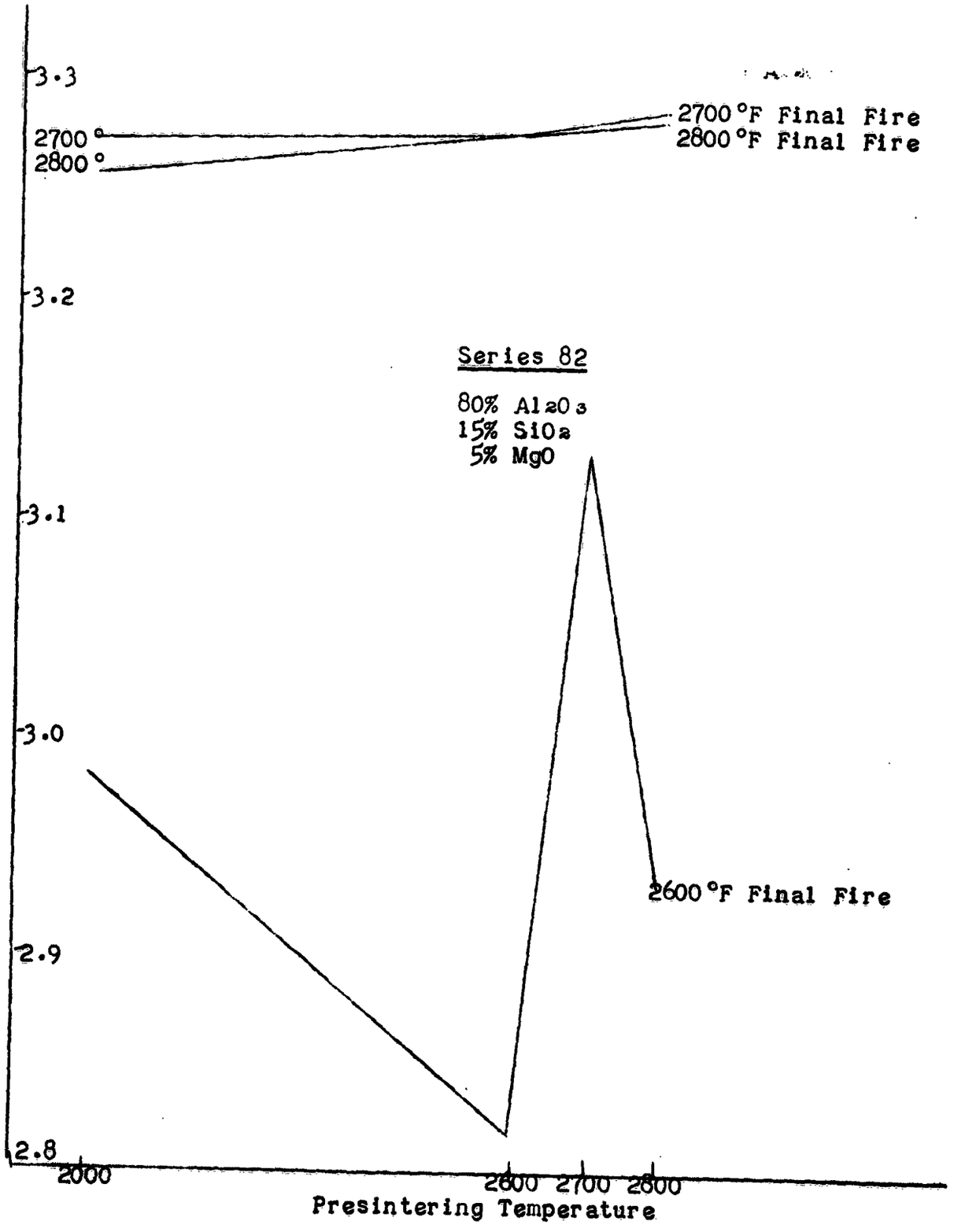

Figure 21

Density versus Final Firing Temperature

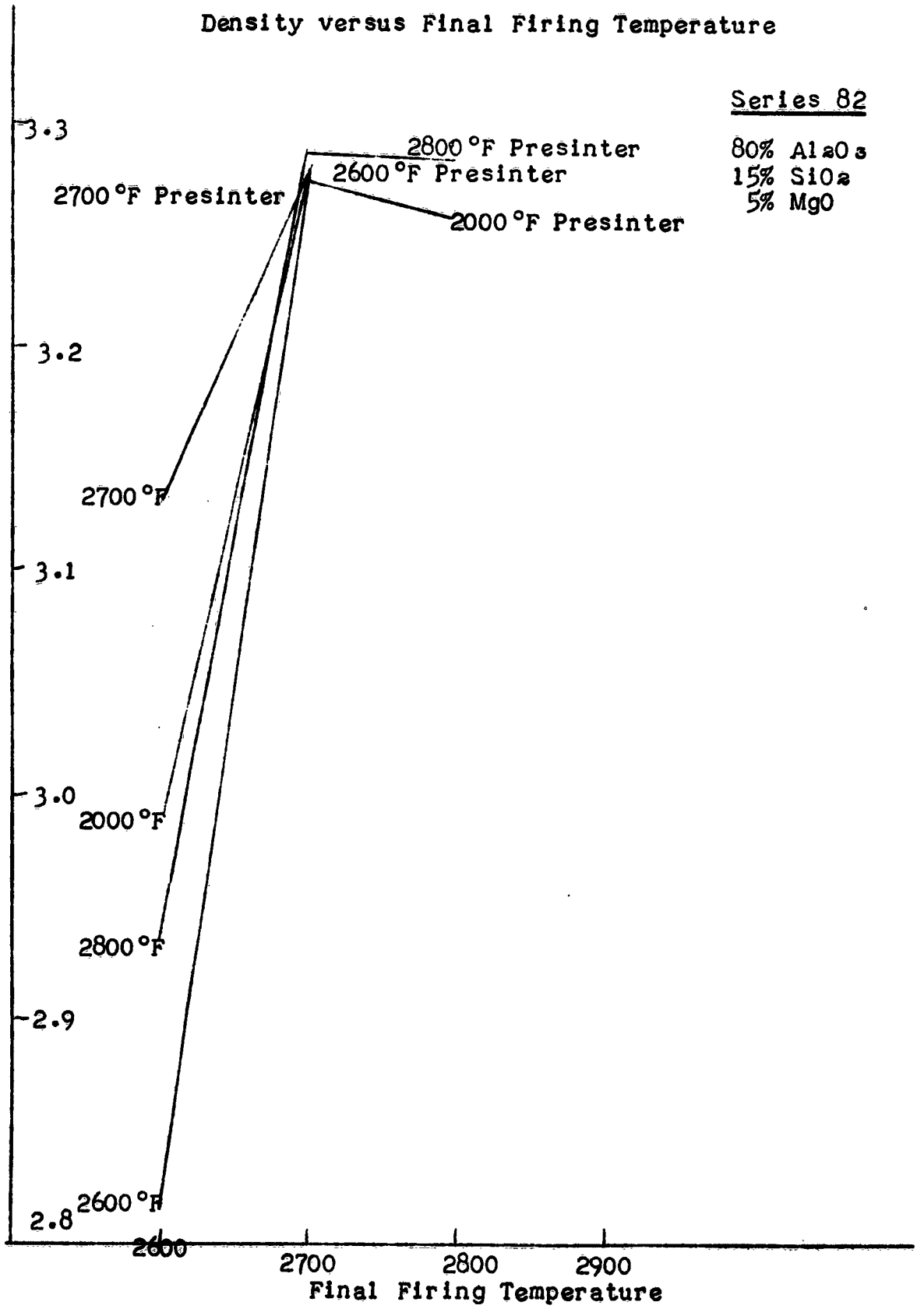

Figure 22

Density versus Presintering Temperature

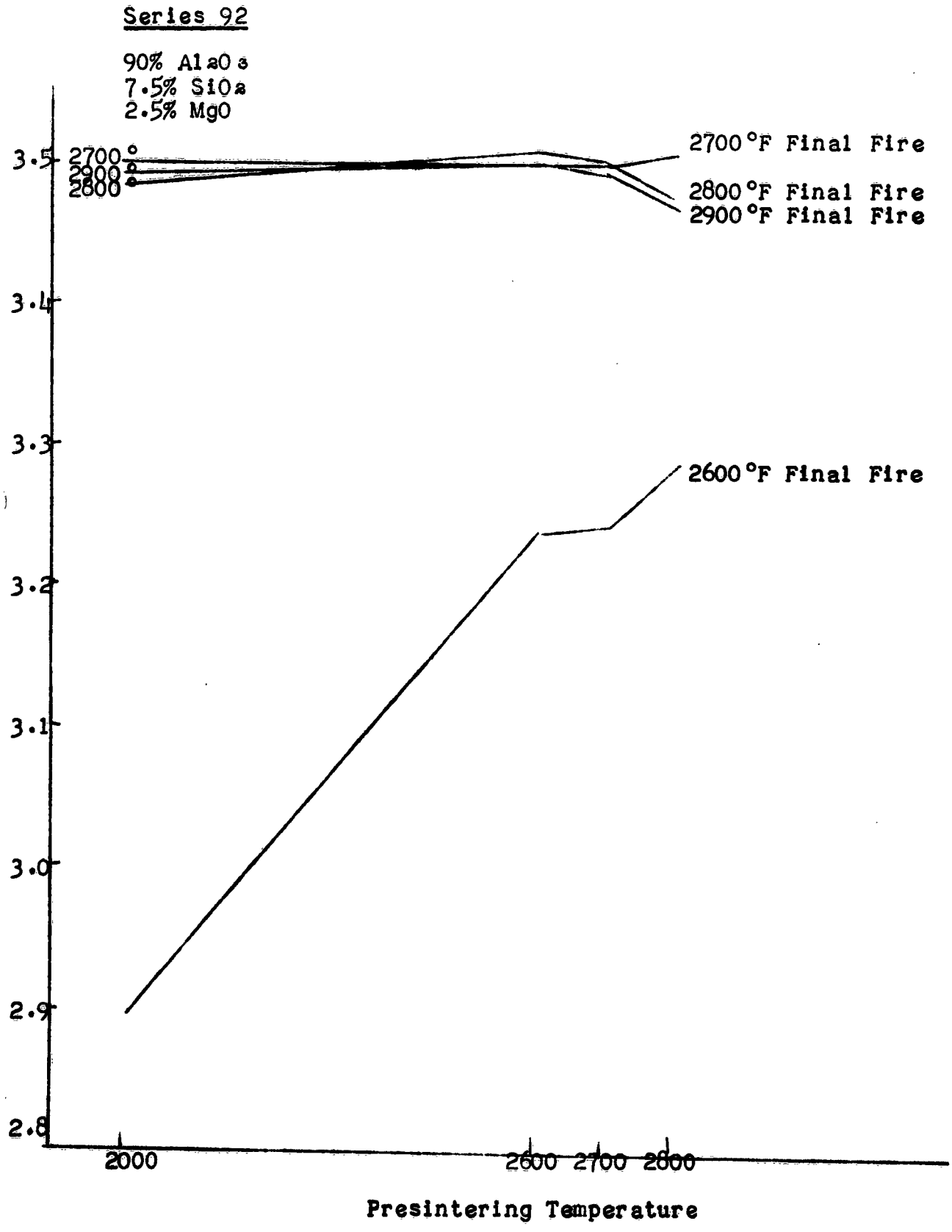

Figure 23

Density versus Final Firing Temperature

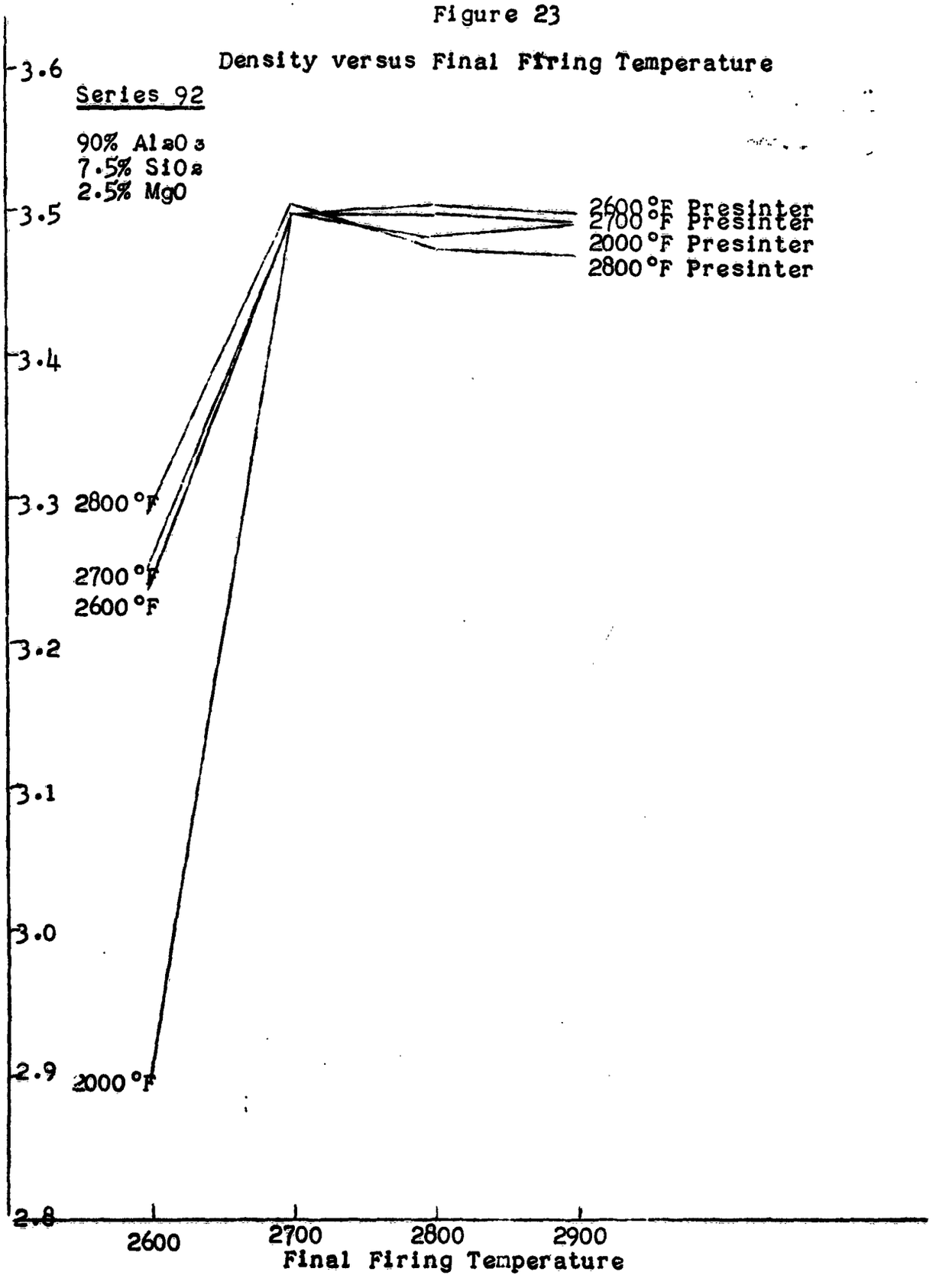

Figure 24

Density versus Final Firing Temperature

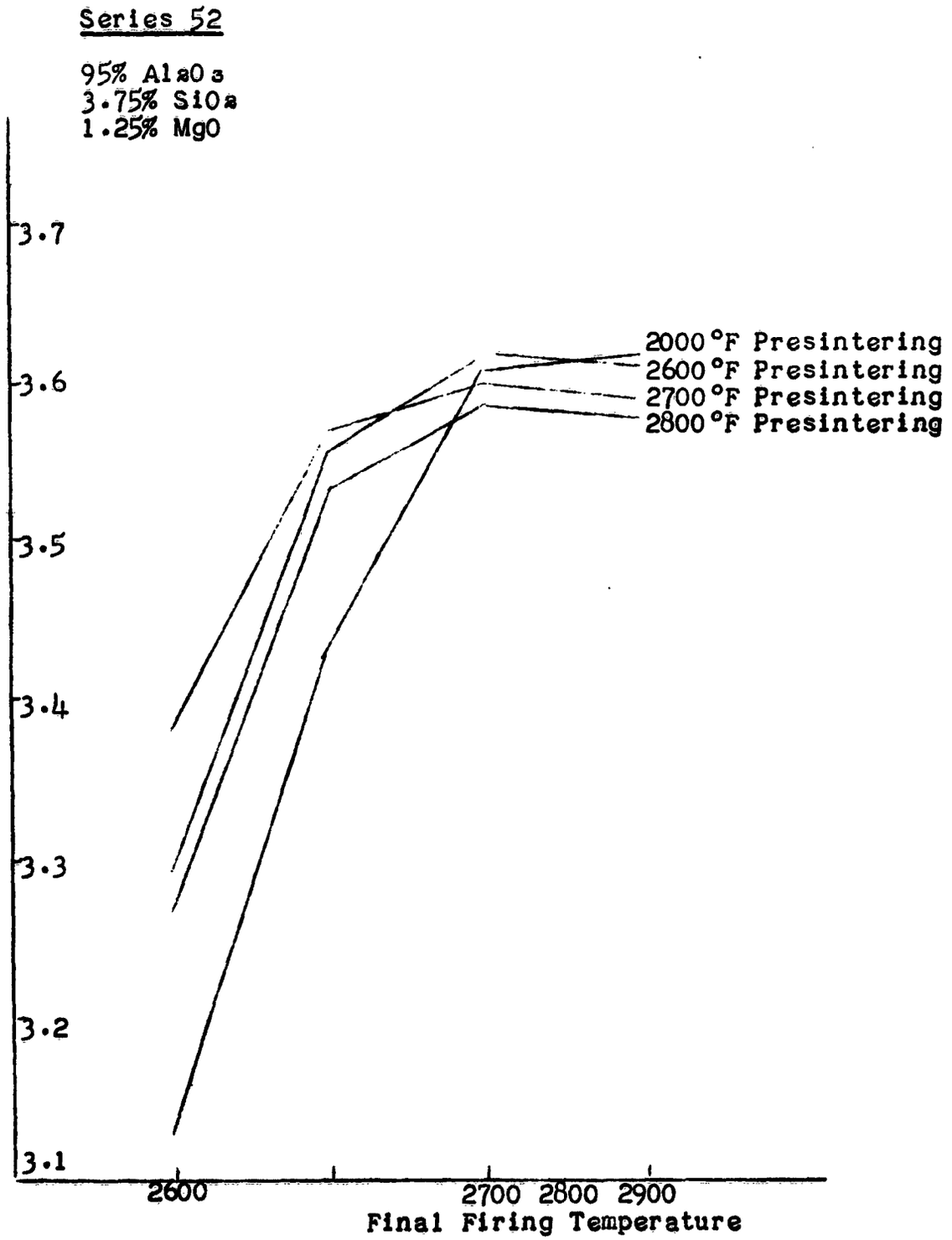

Figure 25

Density versus Presintering Temperature

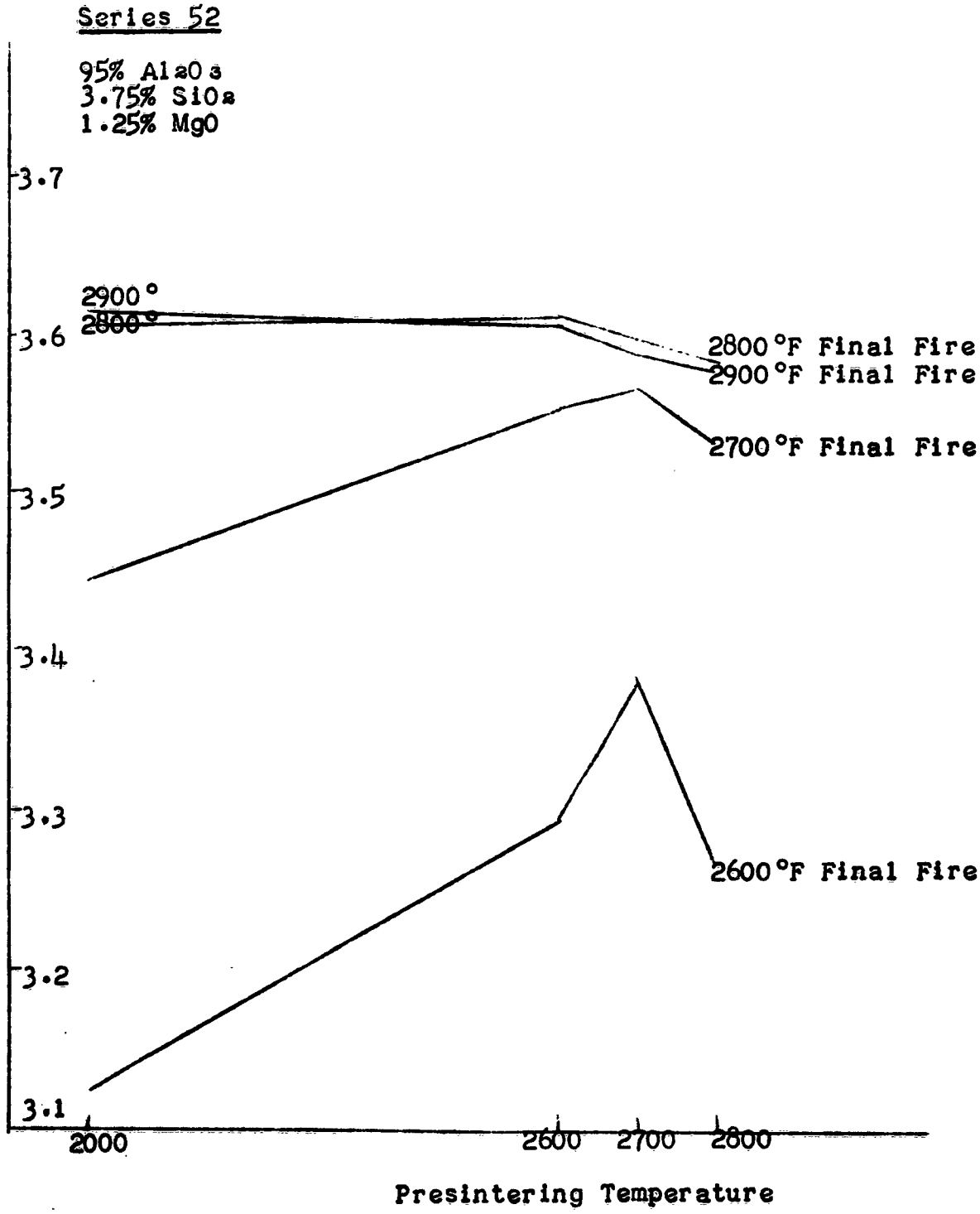

Compositions in the low alumina range, Series 72, and 82, when fired to 2800°F contained a liquid of such high fluidity, which reacted with the sagger, that density determinations were impossible to perform.

The optimum bodies of each series showed the following results:

	Density	Moisture Absorption	Presintering Temperature	Final Fire Temperature
Series 72	3.193	0.00%	2000°F	2700°F
71.8% Al_2O_3				
21.15% SiO_2				
7.05% MgO				
Series 82	3.287	0.00%	2800°F	2700°F
80.0% Al_2O_3				
15.0% SiO_2				
5.0% MgO				
Series 92	3.508	0.00%	2800°F	2700°F
90.0% Al_2O_3				
7.5% SiO_2				
2.5% MgO				
Series 52	3.615	0.00%	2600°F	2800°F
95.0% Al_2O_3				
3.75% SiO_2				
1.25% MgO				

These series of compositions attain a relatively high density and mature about 2700°F. A liquid phase is formed which acts to promote densification at a low temperature. This liquid attains such a high degree of fluidity that any surface in contact with the specimen at 2800°F, in the case of Series 72 and 82, will draw the liquid phase away from the specimen. This will be discussed in more detail in this report under the heading of Liquid Phase.

Al$_2$O$_3$-SiO$_2$-MgO Ternary - Series 73, 83, 93, and 53

The density vs. presintering temperature and density vs. final firing temperature curves of the series 73, 83, 93, and 53 are shown on pages . As seen from the curves, the final fired density increases initially with an increase in temperature, levles off in the intermediate range, and finally decreases at the high temperatures. These curves are of the same general nature as the curves of the series 72, 82, 92, and 52. This series of compositions relies on a liquid phase for densification at low temperatures. The decrease in density when overfiring occurs is not as great as the series 72, 82, 92, and 52, indicating that a lesser quantity of liquid is being formed. The density vs. presintering temperature curves generally show higher densities occuring with a presintering fire of 2600°F and slightly lower densities occuring at the higher presintering temperatures.

Figure 26

Density versus Presintering Temperature

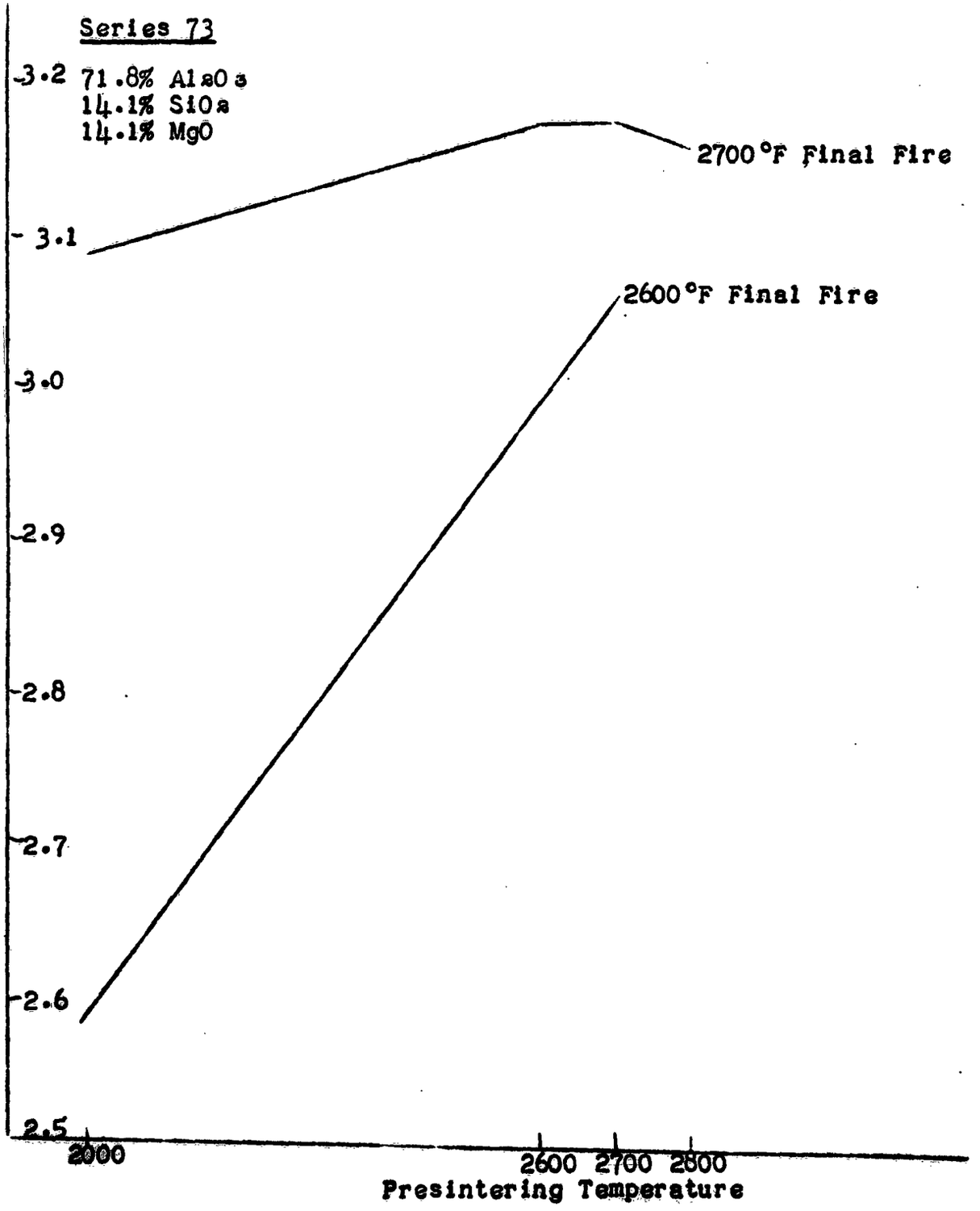

Figure 27

Density versus Final Firing Temperature

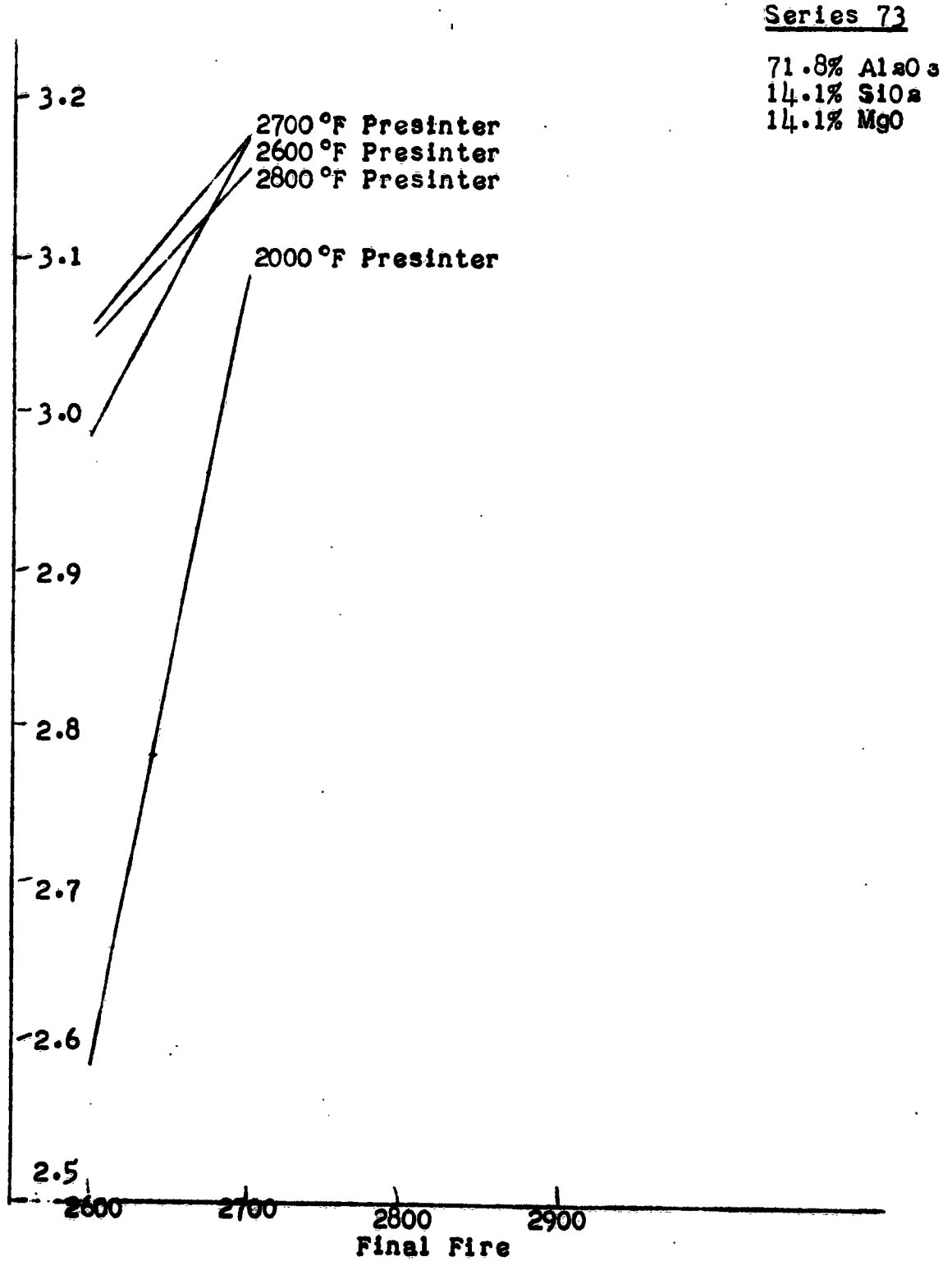

Figure 28

Density versus Presintering Temperature

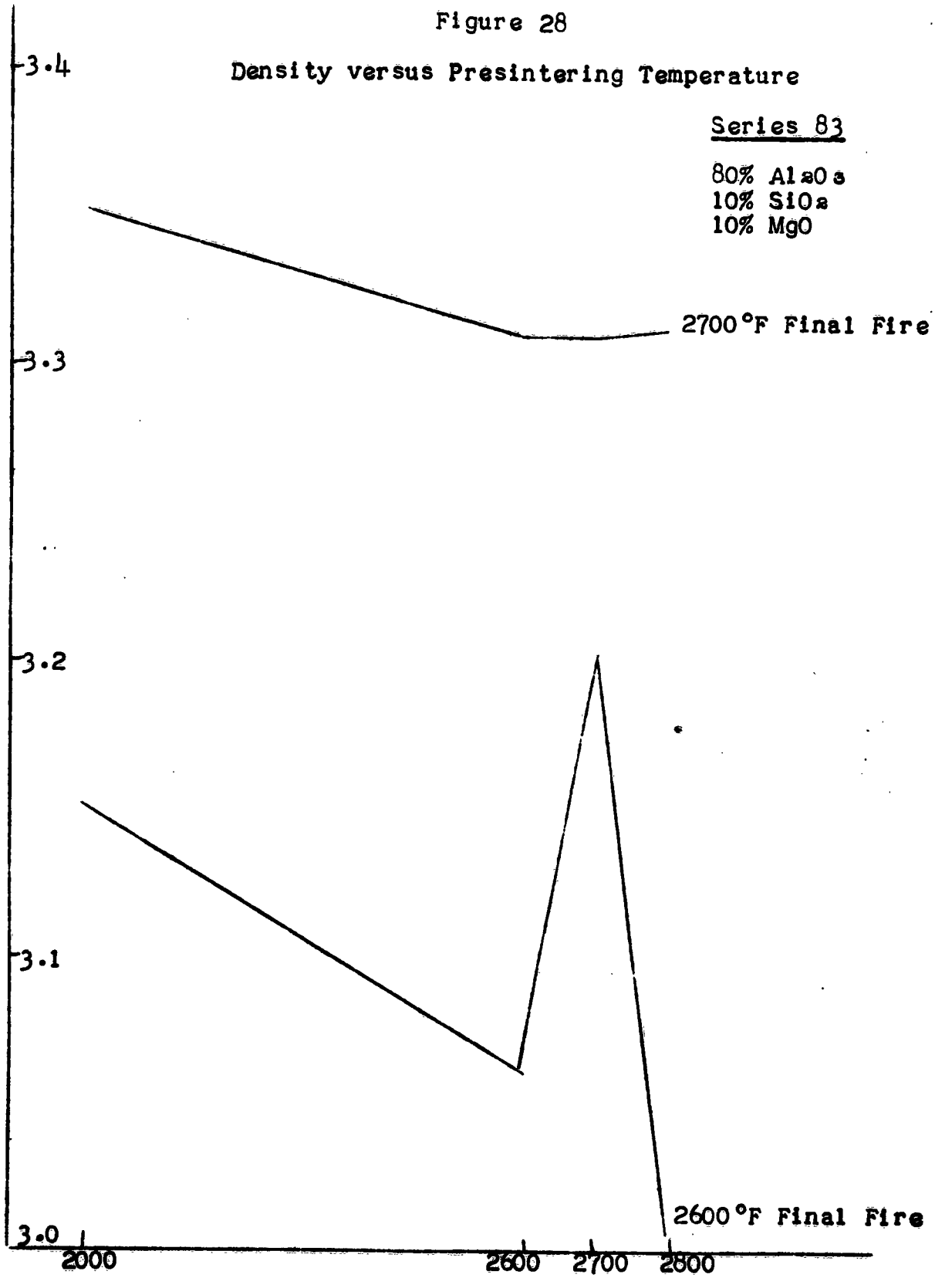

Figure 29

Density versus Final Firing Temperature

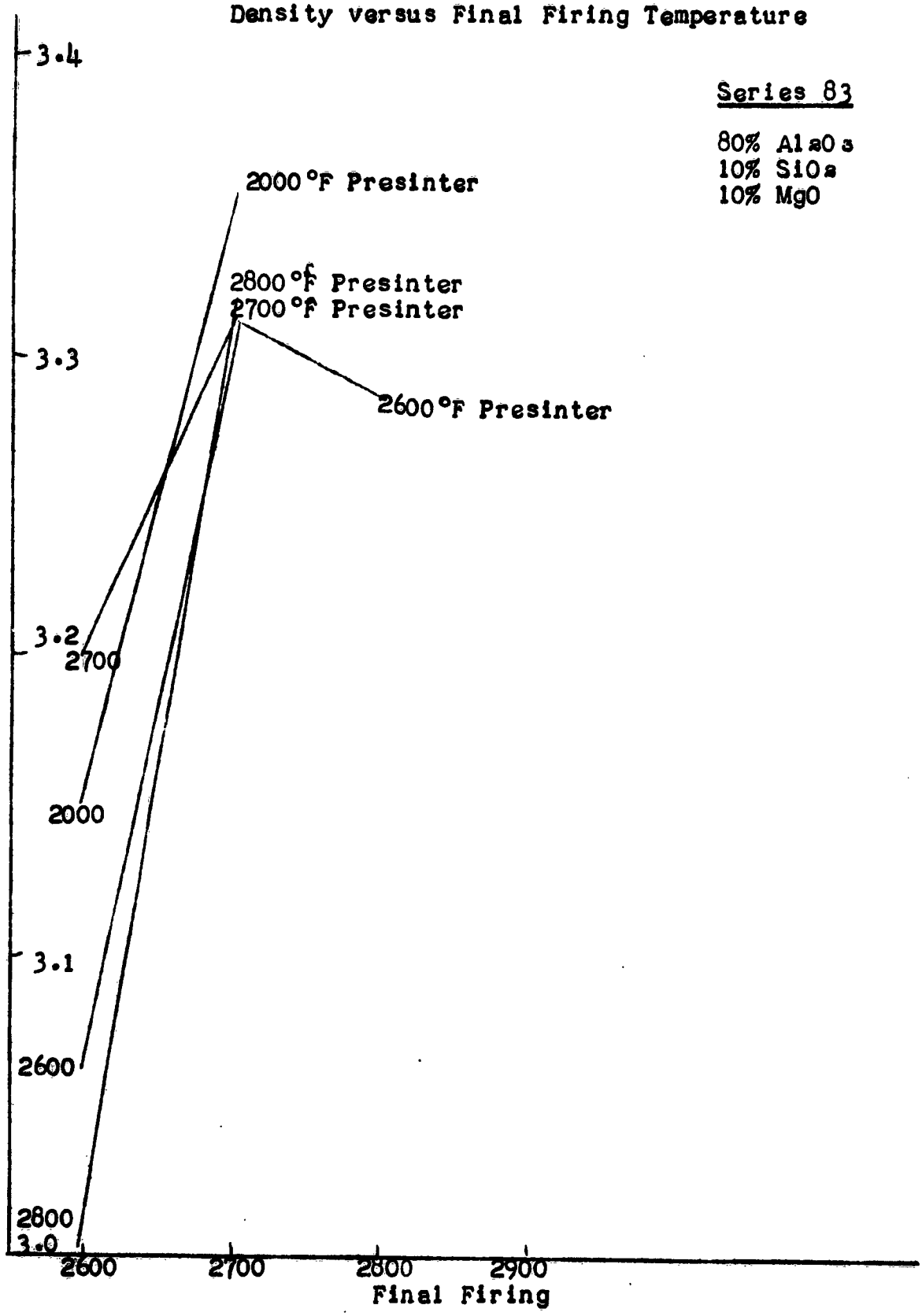

Figure 30

Density versus Presintering Temperature

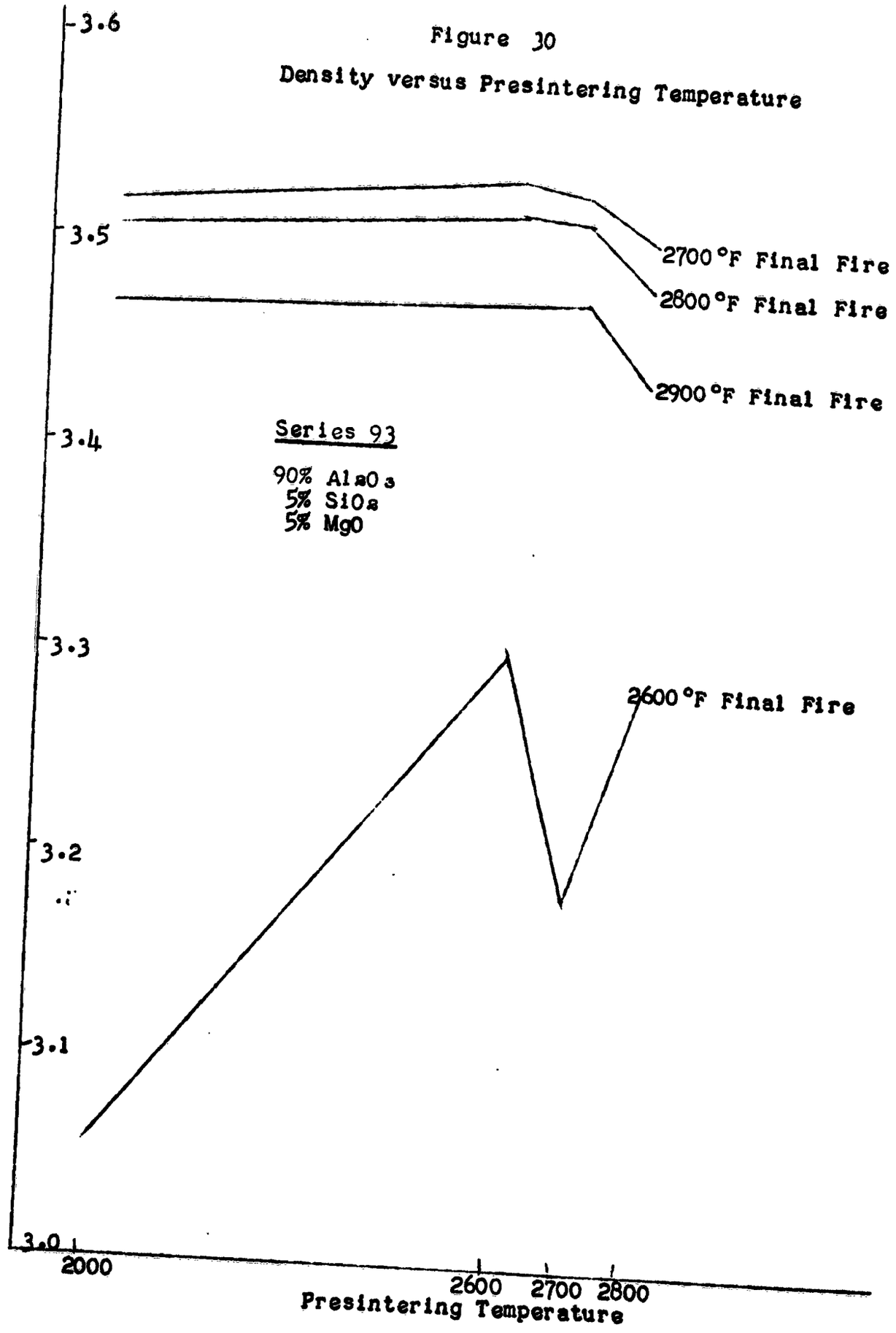

Figure 31

Density versus Final Firing Temperature

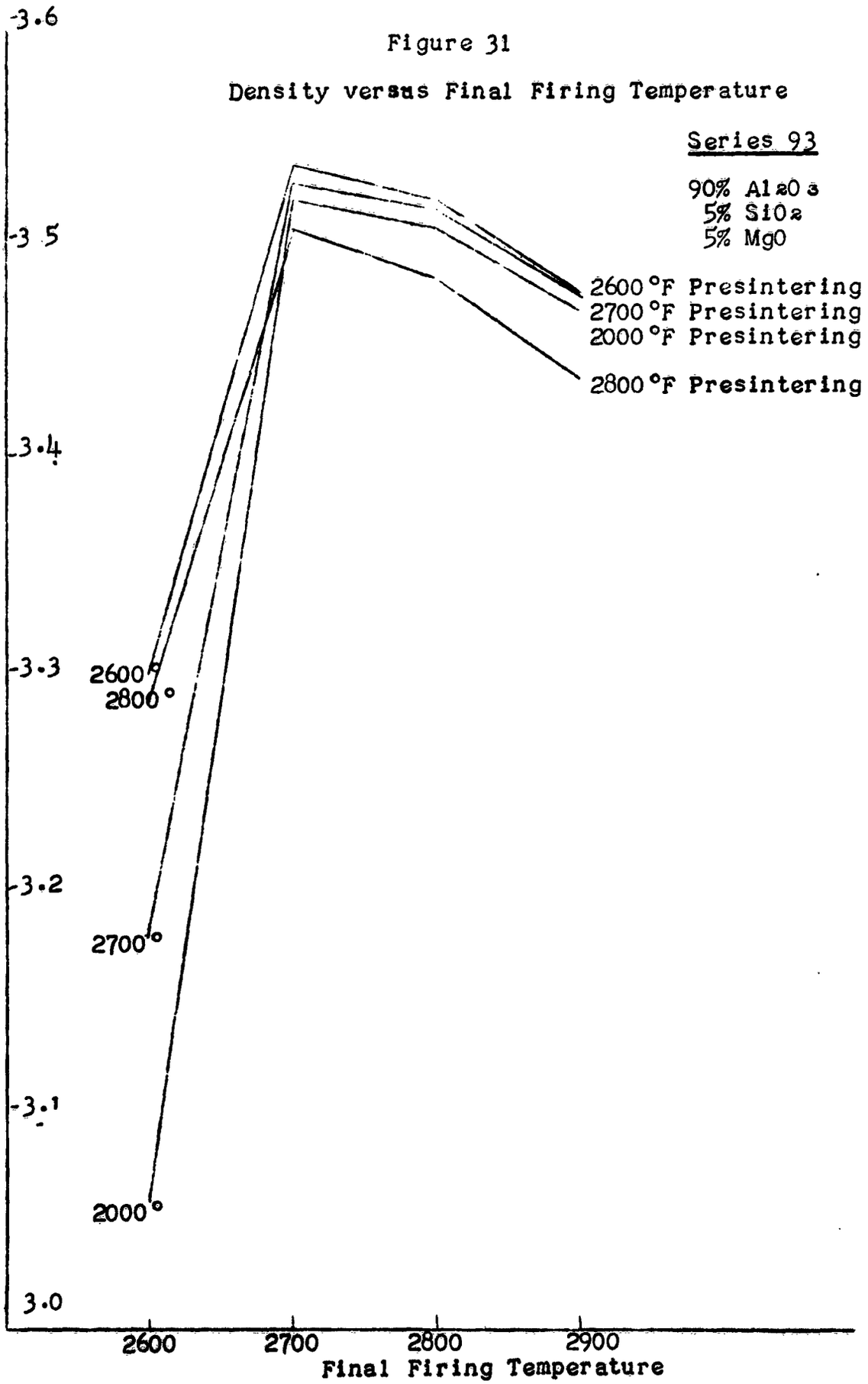

Figure 32

Density versus Presintering Temperature

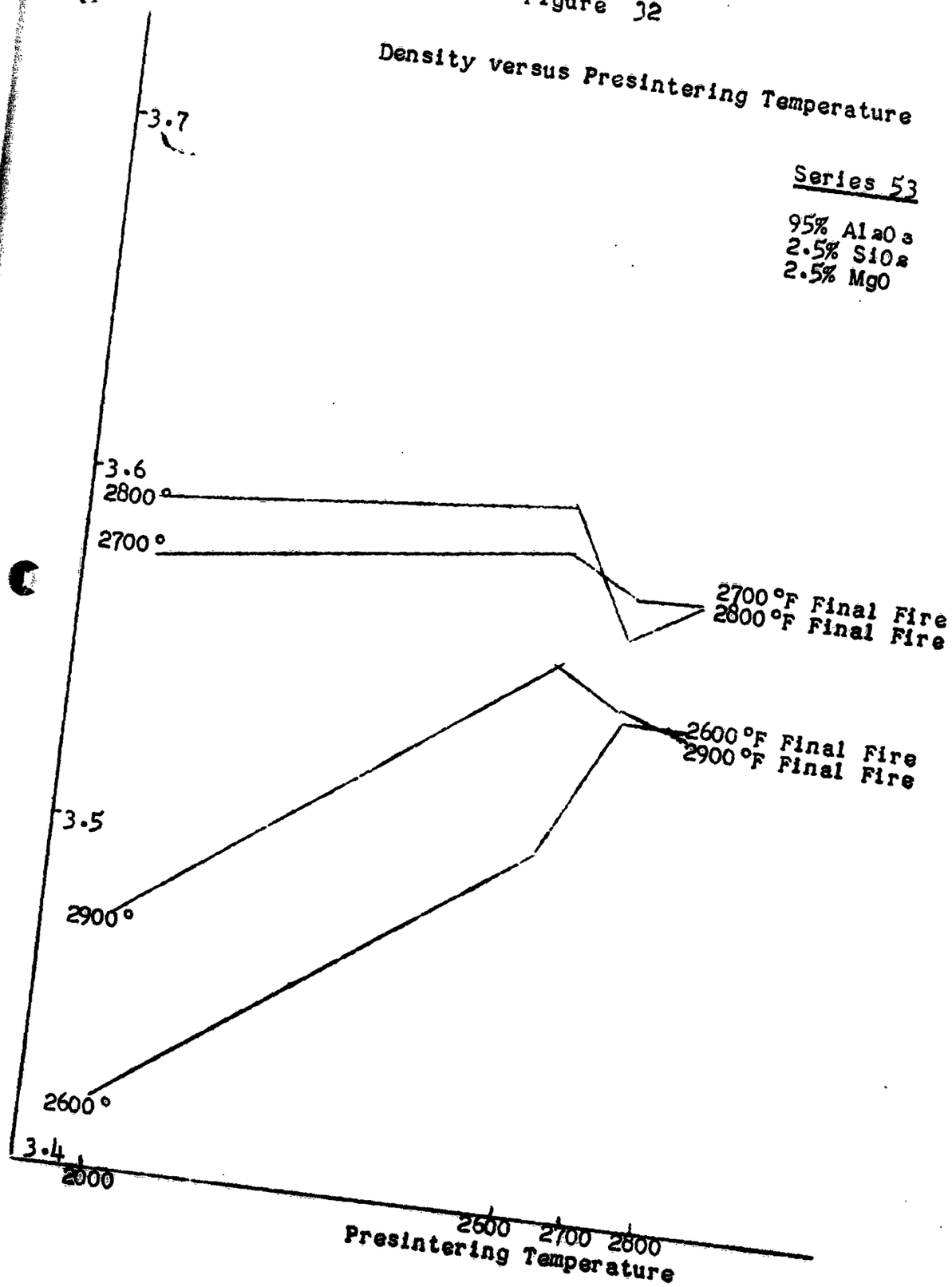

Figure 33

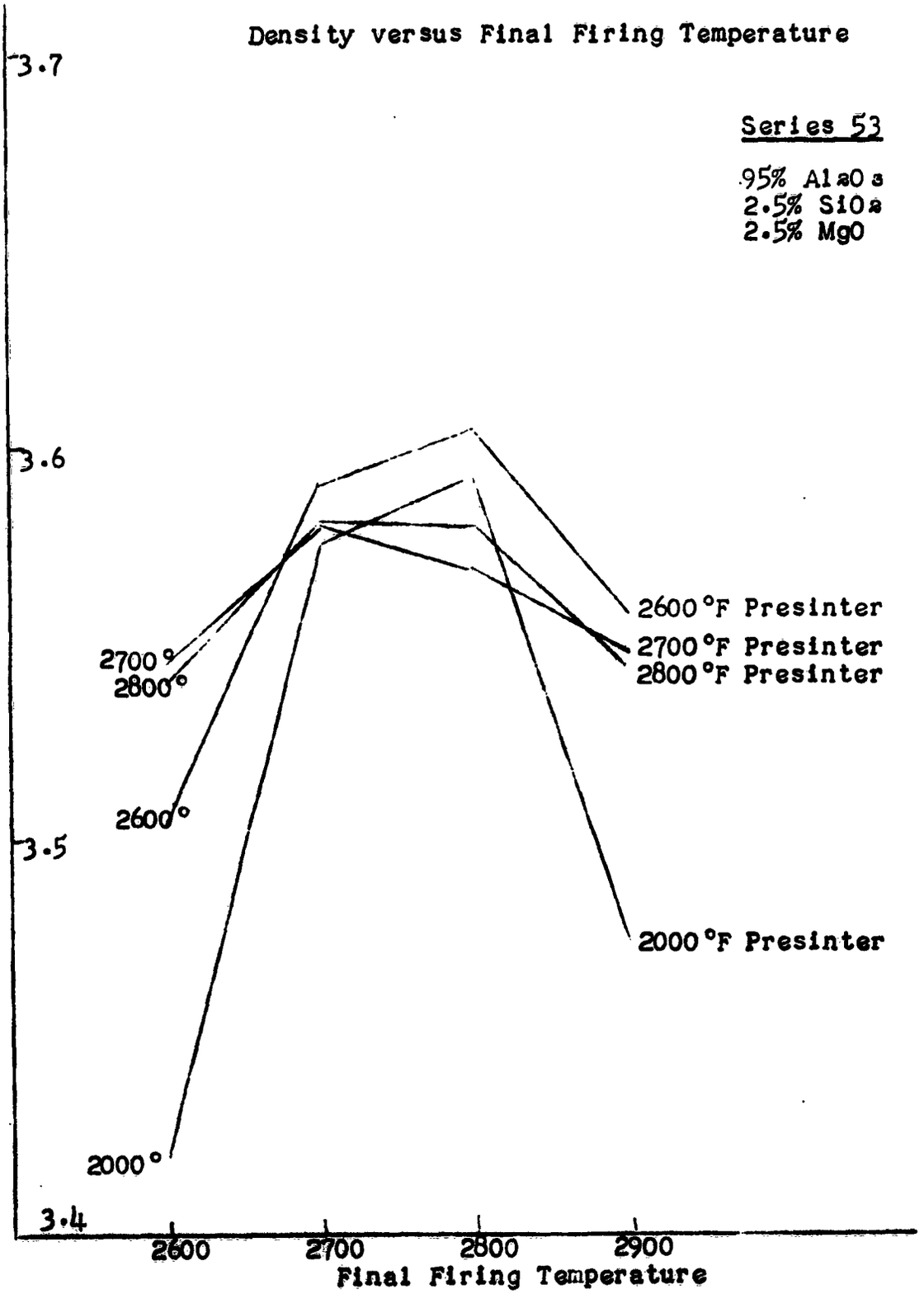
Density versus Final Firing Temperature
3.7
3.6
3.5
3.4
Series 53
95% Al2O3
2.5% SiO2
2.5% MgO
2600 °F Presinter
2700 °F Presinter
2800 °F Presinter
2000 °F Presinter
2700°
2800°
2600°
2000°
2600
2700
2800
2900
Final Firing Temperature

The optimum bodies of each composition show the following properties;

	Density	Moisture Absorption	Presintering Temperature	Final Firing Temperature
Series 73	3.176	0.00%	2700°F	2700°F
71.8% Al_2O_3				
14.1% SiO_2				
14.1% MgO				
Series 83	3.352	0.00%	2000°F	2700°F
80.0% Al_2O_3				
10.0% SiO_2				
10.0% MgO				
Series 93	3.533	0.00%	2600°F	2700°F
90.0% Al_2O_3				
5.0% SiO_2				
5.0% MgO				
Series 53	3.605	0.00%	2600°F	2800°F
95% Al_2O_3				
2.5% SiO_2				
2.5% MgO				

This series acts in much the same manner as Series 72, 82, 92, and 52. The compositions mature about 2700°F with relatively high densities. A liquid phase is being formed in the final firing to promote densifiation. This liquid attains a high degree of fluidity in the high temperature firings.

Al_2O_3-SiO_2-MgO - Series 74, 84, 94, and 54

The density vs. presintering temperature and density vs. final firing temperature curves of the series 74, 84, 94, and 54 are shown on pages . As seen from the curves, the final fired density increases initially with an increase in temperature, levels off in the intermediate range, and finally decreases at the high temperatures. These curves are of the same general nature as the series 72, 82, 92, and 52. This series of compositions relies on a liquid phase for densification at low temperatures. The primary difference between the 72, 82, 92, and 52 series and the 74, 84, 94, and 54 series is the amount of liquid phase formed. This effect can be noted by the degree of overfiring and percentage decrease in density, exhibited by the two series. The 74, 84, 94, and 54 series show only a slight decrease in density upon overfiring, while the series 72, 82, 92, and 52 show marked decreases in density. In general, the density vs. presintering temperature curves show that an increase in presintering temperature will increase the density .

This series densifies in much the same manner as Series 72, 82, 92, and 52, with the formation of a liquid phase in the final firing. The compositions attain a high density and mature in the range of 2700-2800°F. The optimum presintering temperature is 2800°F, however, the compositions may be presintered at 2600 or 2700°F with little decrease in the final fired density.

Figure 34

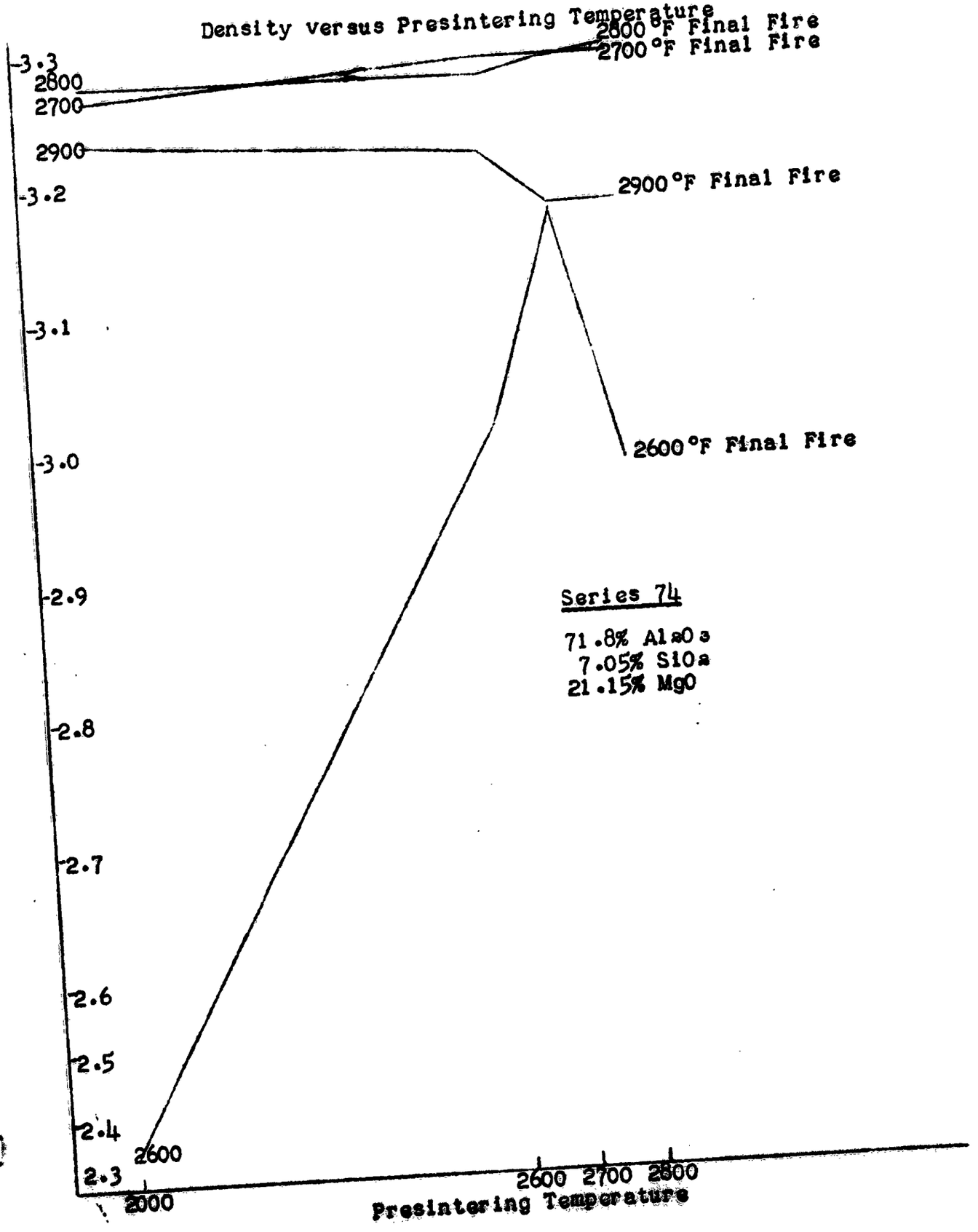
Density versus Presintering Temperature
2800 °F Final Fire
2700 °F Final Fire
2900 °F Final Fire
2600 °F Final Fire
3.3
3.2
3.1
3.0
2.9
2.8
2.7
2.6
2.5
2.4
2.3
2800
2700
2900
2600
Series 74
71.8% Al2O3
7.05% SiO2
21.15% MgO
2000
2600 2700 2800
Presintering Temperature

Figure 35

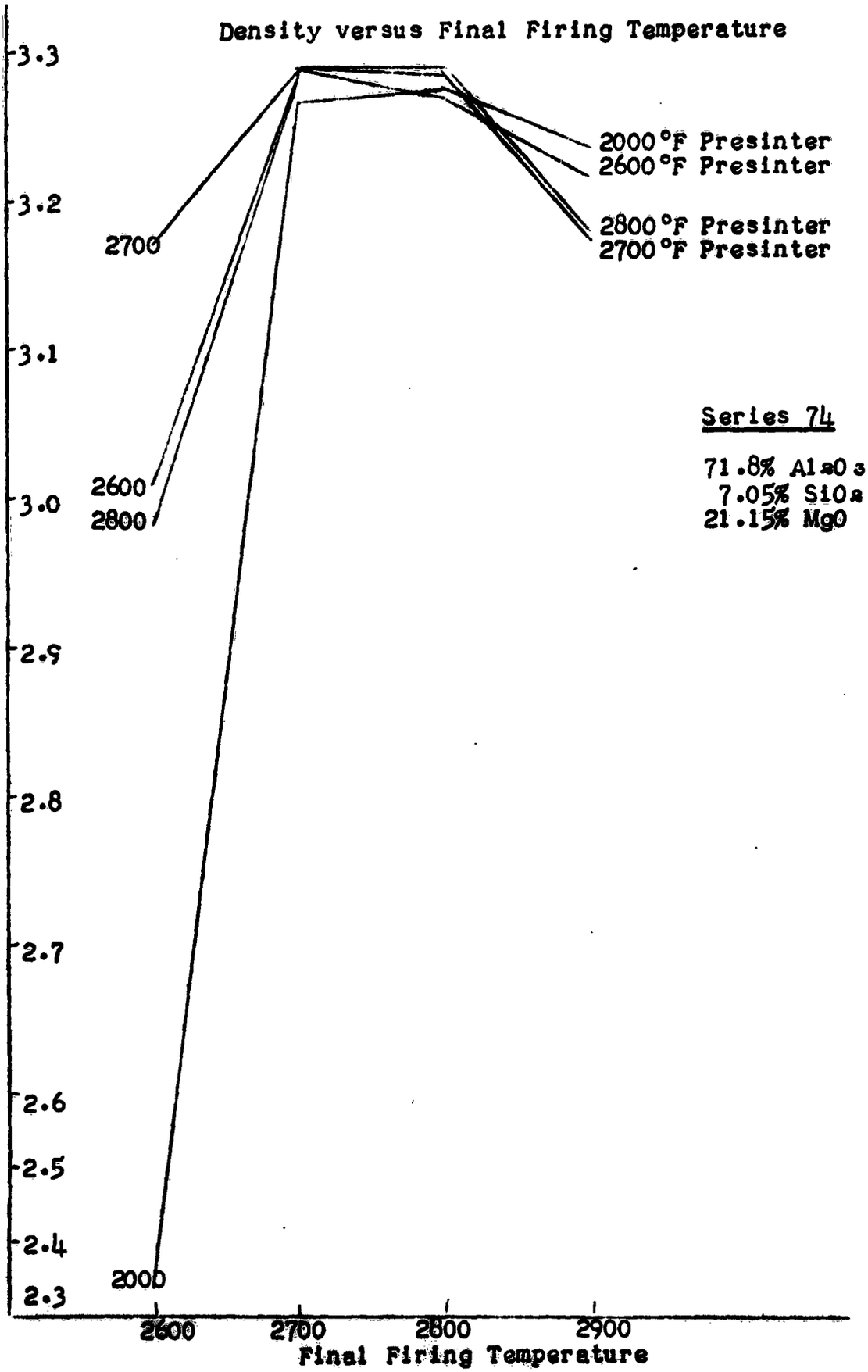
Density versus Final Firing Temperature
3.3
3.2
3.1
3.0
2.9
2.8
2.7
2.6
2.5
2.4
2.3
2700
2600
2800
2000
2000 °F Presinter
2600 °F Presinter
2800 °F Presinter
2700 °F Presinter
Series 74
71.8% Al2O3
7.05% SiO2
21.15% MgO
2600
2700
2800
2900
Final Firing Temperature

Figure 36

Density versus Presintering Temperature

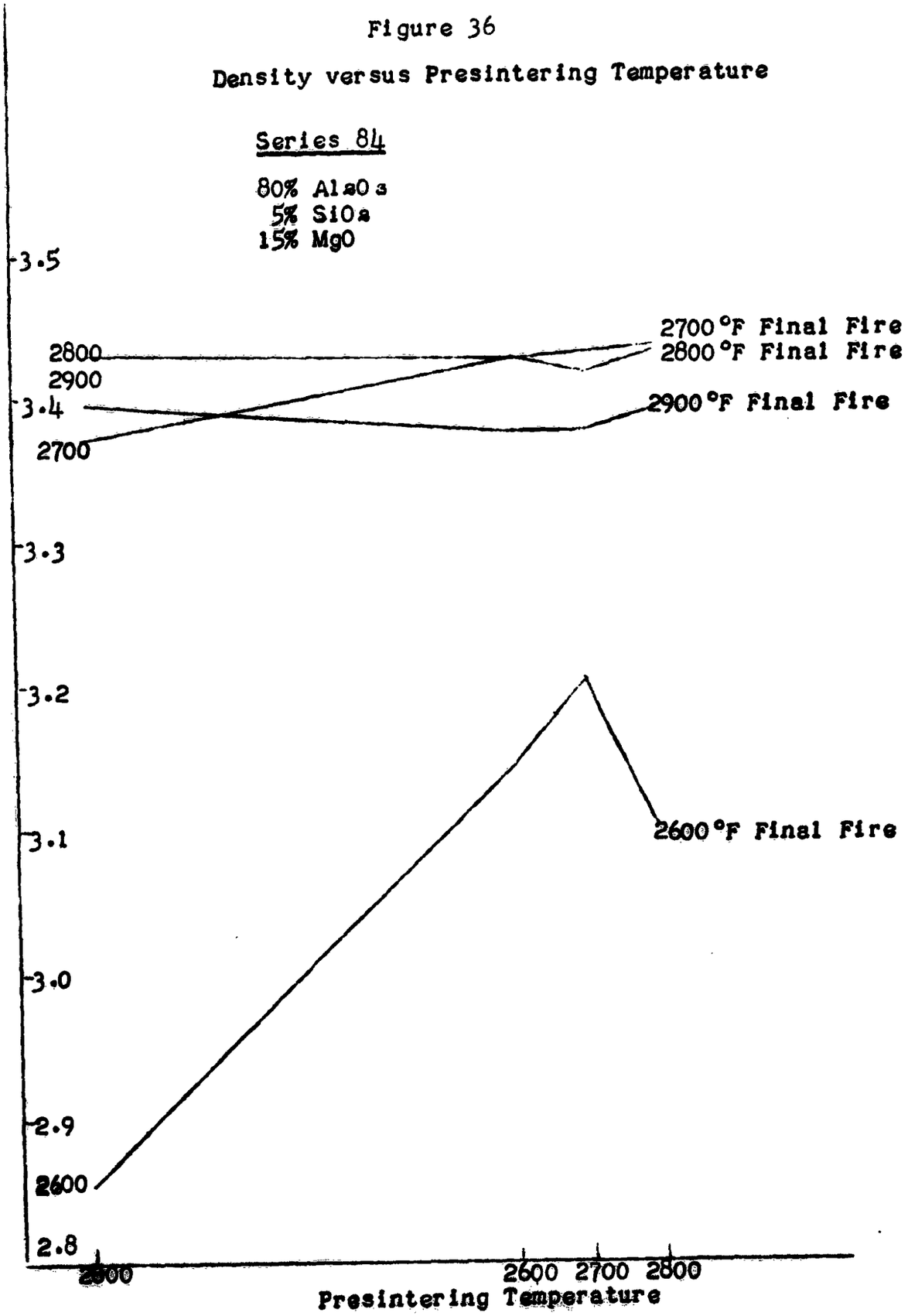

Figure 37

Density versus Final Firing Temperature

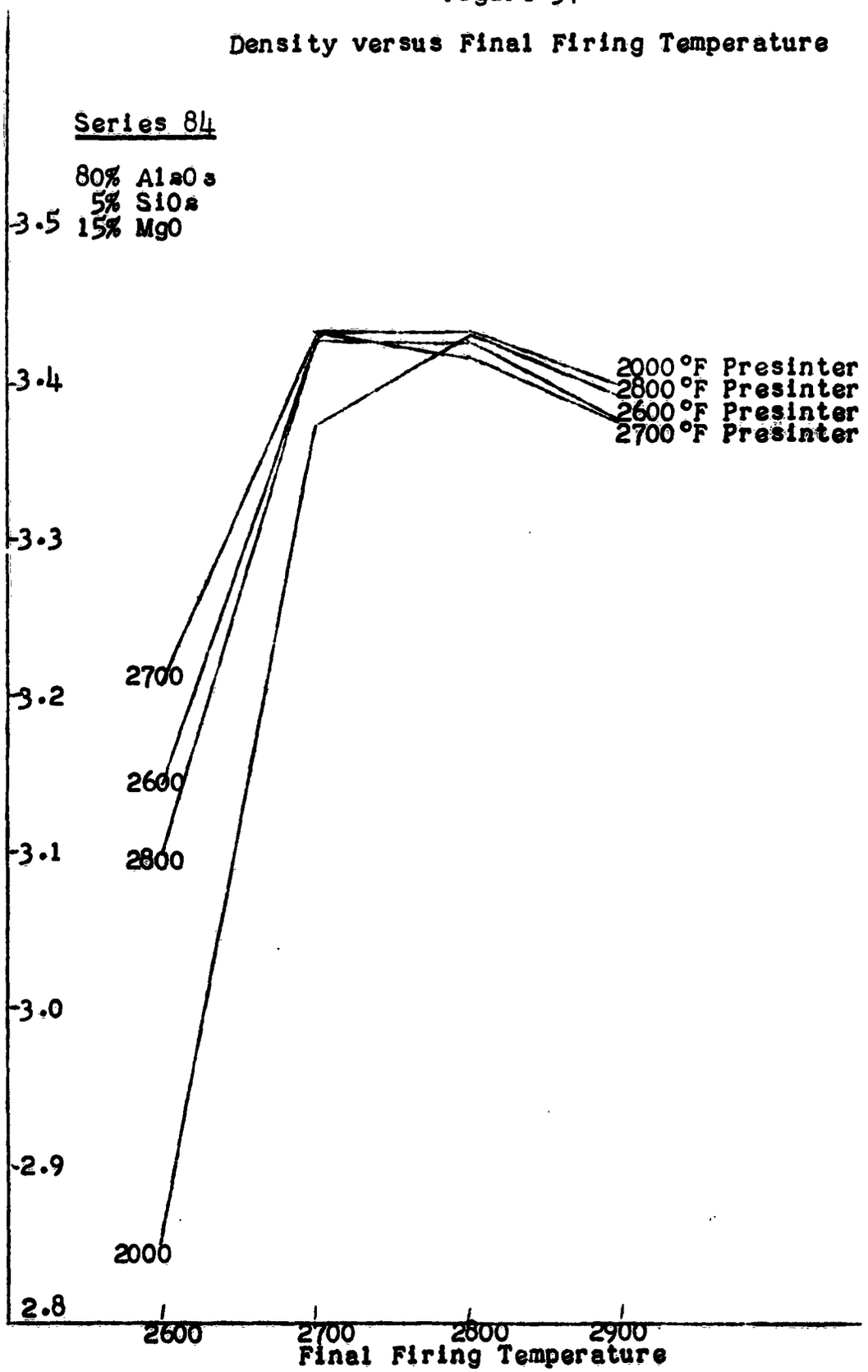

Figure 38

Density versus Presintering Temperature

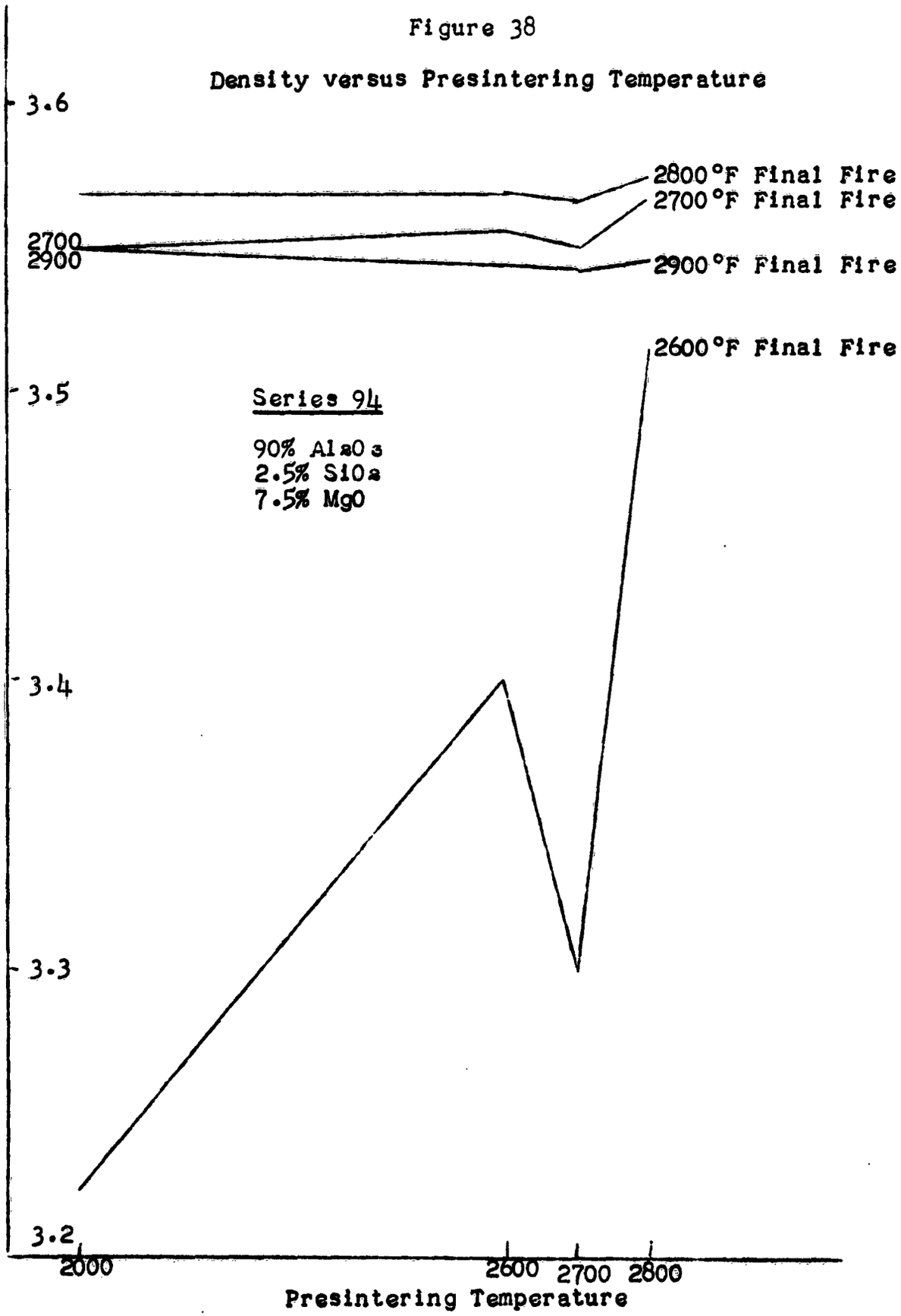

Figure 39

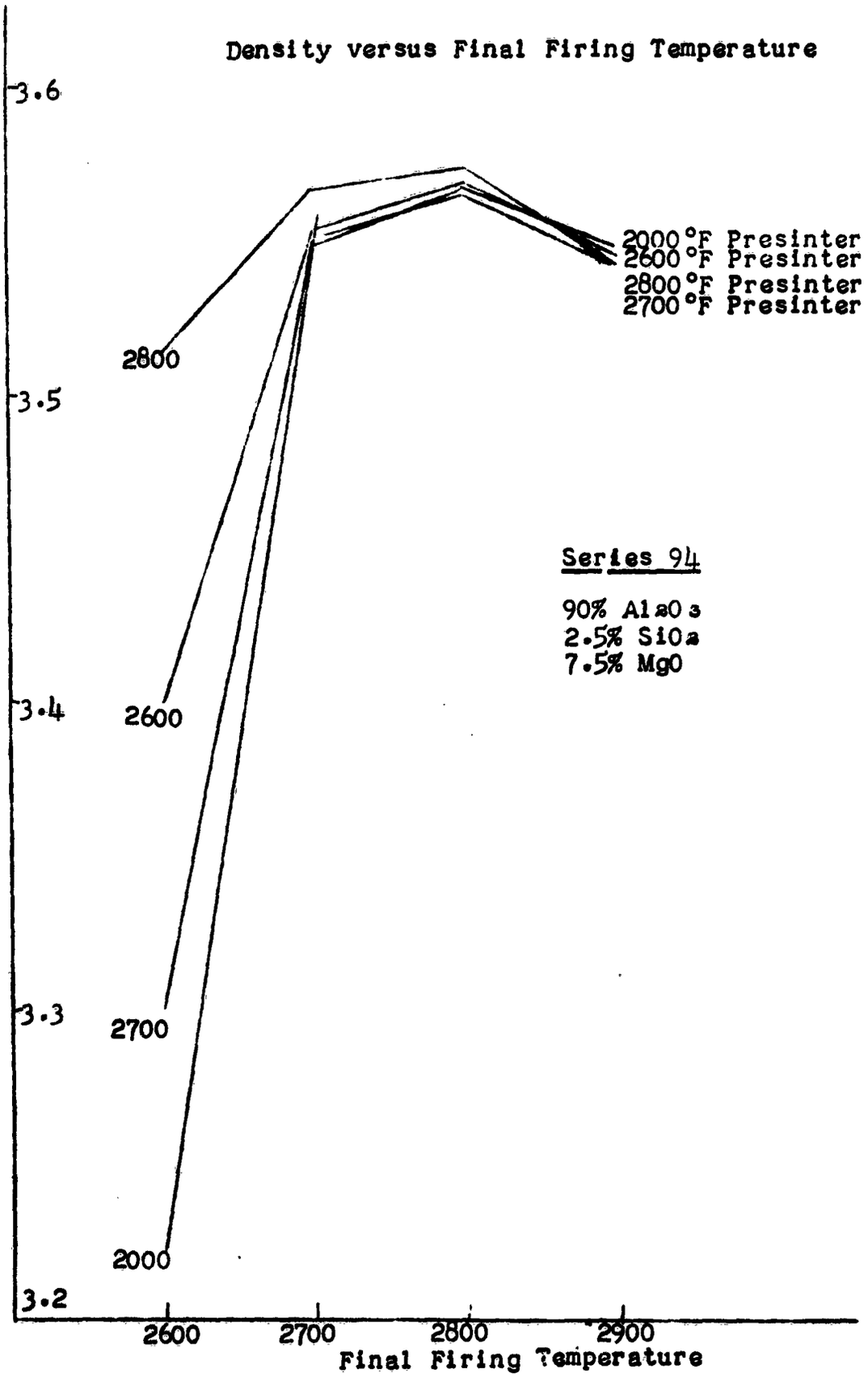
Density versus Final Firing Temperature
3.6
3.5
3.4
3.3
3.2
2800
2600
2700
2000
2000 °F Presinter
2600 °F Presinter
2800 °F Presinter
2700 °F Presinter
Series 94
90% Al2O3
2.5% SiO2
7.5% MgO
2600
2700
2800
2900
Final Firing Temperature

Figure 40

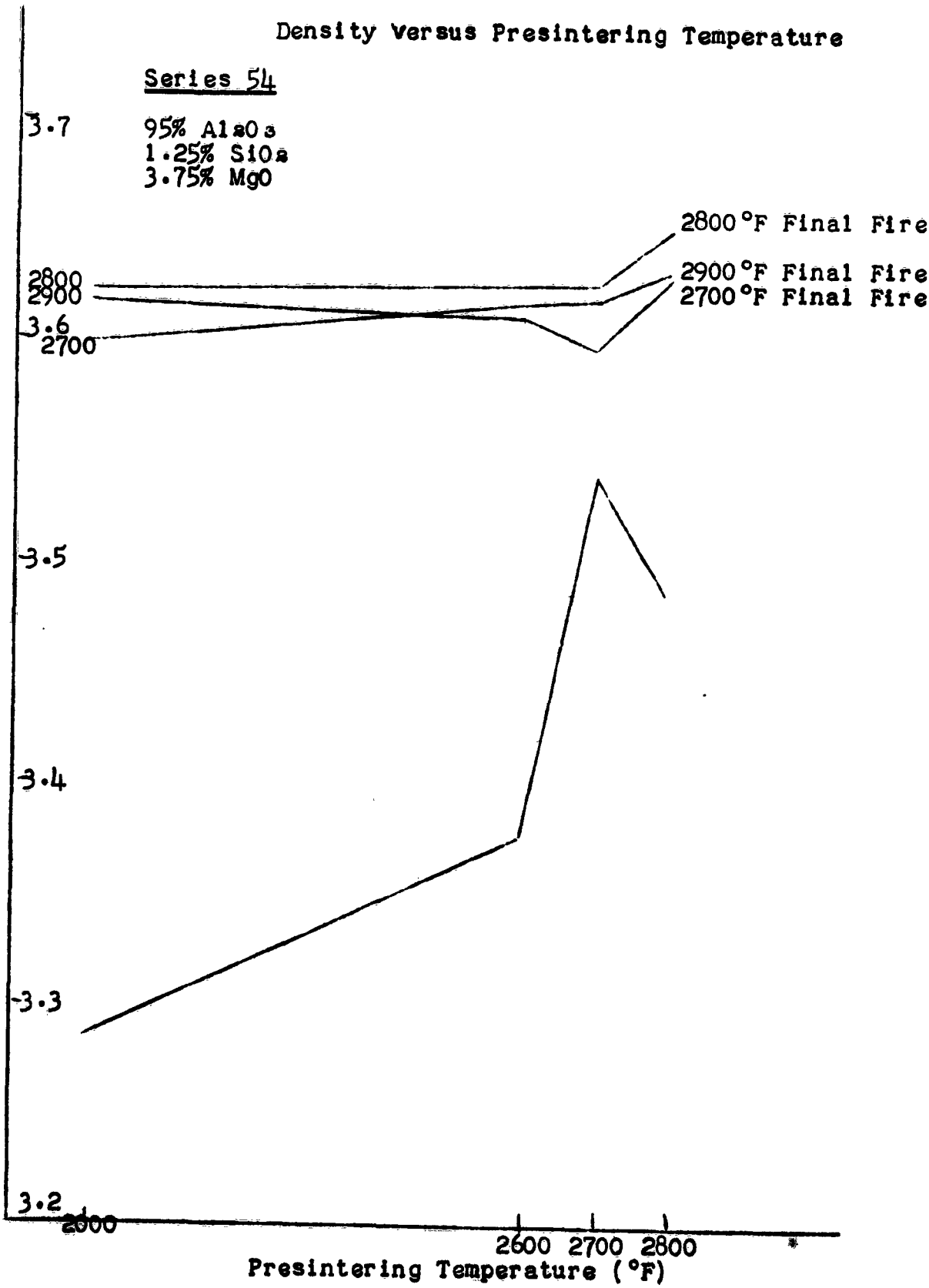
Density versus Presintering Temperature
Series 54
95% Al2O3
1.25% SiO2
3.75% MgO
2800 °F Final Fire
2900 °F Final Fire
2700 °F Final Fire
3.7
3.6
3.5
3.4
3.3
3.2
2800
2900
2700
2600
2600 2700 2800
Presintering Temperature (°F)

Figure 41

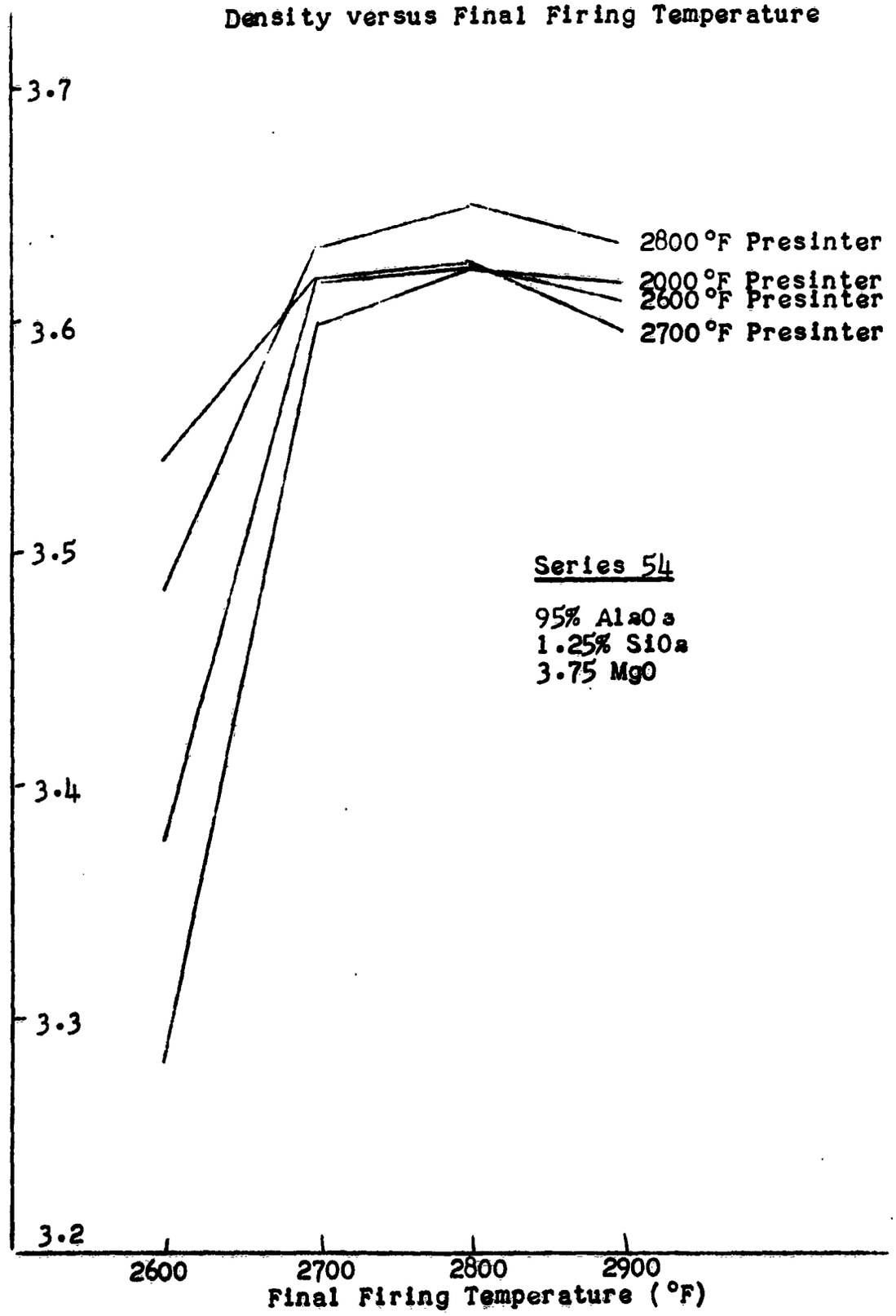
Density versus Final Firing Temperature
3.7
3.6
3.5
3.4
3.3
3.2
2800 °F Presinter
2000 °F Presinter
2600 °F Presinter
2700 °F Presinter
Series 54
95% Al2O3
1.25% SiO2
3.75 MgO
2600
2700
2800
2900
Final Firing Temperature (°F)

The optimum bodies of each composition show the following properties:

	Density	Moisture Absorption	Presintering Temperature	Final Firing Temperature
Series 74	3.290	0.00%	2800°F	2700°F
71.8% Al_2O_3				
21.15% MgO				
7.05% SiO_2				
Series 84	3.435	0.00%	2800°F	2700°F
80% Al_2O_3				
15% MgO				
5% SiO_2				
Series 94	3.574	0.00%	2800°F	2800°F
90.0% Al_2O_3				
7.5% MgO				
2.5% SiO_2				
Series 54	3.650	0.00%	2800°F	2800°F
95.0% Al_2O_3				
3.75% MgO				
1.25% SiO_2				

C. Summary of Density Determinations

With the exception of Series 71, 81, 91, and 51, all compositions attained high densities and matured in the range 2700-2800°F. It was generally found that these compositions could be presintered in the range of 2600-2800°F with little change in final fired density.

In the ternary compositions, densification was attributed to the formation of a liquid phase in the final firing. The relative amount of liquid formation is generally tied up in the amount of SiO_2 added as a raw material. The greater the initial silica additions, the greater the amount of liquid phase, exhibited. The magnesia plays a vital role in the densification. The magnesia reacts to from spinel, acts as a flux for the silica liquid, and there is evidence that the magnesia acts to breakdown the mullite that is formed and thus produce more silica for liquid formation. The density was found to increase as the alumina content increased, and as the magnesia content was increased at the expense of the silica.

In the binary compositions, densification was attributed to diffusional processes. This was evidenced by the increasing density with increasing firing temperature, and the knowledge that a eutectic liquid will not form in the firing temperature utilized. The compositions in the Al_2O_3-SiO_2 binary did not mature, however low porosities were exhibited in the high alumina compositions at high temperatures. Compositions in the Al_2O_3-MgO binary matured at relatively low temperatures, 2800°F, with

relatively high densities, approximately 97% theoretical density. The excellent results in this binary are attributed to an extremely fine particle size raw material and to excellent diffusional characteristics of the spinel grains.

D. X-ray Analysis - Discussion

The phases present as shown through X-ray analysis were presented in the previous reports. This will be a discussion of the results shown by X-ray analysis.

Al_2O_3-MgO Binary - Series 75, 85, 95, and 55

In the Al_2O_3-MgO binary, only two phases, spinel and alumina, were present above 2600°F. Only after the lowest presintering fire of 2000°F was there evidence of MgO. The spinel content was found to increase as the presintering temperature and final firing temperature increased. This increase in the amount of spinel present was indicated by the increasing height of the spinel peaks from the X-ray chart. The phase reaction to form spinel, Al_2O_3+MgO -- Al_2O_3.MgO, approaches completion when either the presintering fire or final fire is performed at 2700°F or above.

Al_2O_3-SiO_2 Binary - Series 71, 81, 91, and 51

In the Al_2O_3-SiO_2 binary, only three phases; alumina, mullite, and α-cristobalite were present above 2600°F. Only after the lowest presintering fire of 2000°F was there evidence

of α-quartz. A presintering fire below 2800°F produces a raw material containing as its major phases alumina and α-cristobalite, and its minor phase mullite. Presintering above 2800°F produces a raw material with alumina and mullite as the major phase, and α-cristobalite is now the minor phase. X-ray analysis after the final firing indicates that mullite and alumina are always the major phases, with small α-cristobalite peaks present. The phase reaction to form mullite, $2SiO_2 + 3Al_2O_3 \rightarrow 3Al_2O_3 \cdot 2SiO_2$, does not reach completion in the temperatures utilized for firing. In general, the mullite peaks increased in size with an increasing firing temperature.

Al$_2$O$_3$-SiO$_2$-MgO Ternary - Series 72, 82, 92, and 52

The X-ray analysis of Series 72, 82, 92, and 52 show a rather complex pattern. After a presintering fire of 2000°F, alumina and α-quartz are the major phases with mullite, MgO, and spinel as minor phases. Presintering at 2600°F results in alumina and cordierite as major phases, with mullite, spinel, and α-cristobalite as minor phases. Presintering at both 2700°F and 2800°F shows that mullite and alumina are the major phases, with spinel and α-cristobalite as minor phases.

In general, the X-ray pattern after final firing at a specific temperature showed relatively the same phase peaks for all presintering temperatures. With a final firing of 2600°F, mullite and alumina are the principal phases, with

spinel, cordierite, and α-cistobalite as minor phases. But, after a final firing of 2700°F, the lowest temperature of zero moisture absorption, alumina and spinel are the principal phases, with mullite and -cristobalite as minor phases. By firing to 2800°F, alumina, spinel, and mullite are major phases, and α-cristobalite is the only minor phase.

The liquid phase begins to form below 2700°F, the incongruent melting of the cordierite, and become quite fluid at 2800°F. The decrease in the mullite peaks at 2700°F, suggests that the mullite is breaking down to form free alumina and silica which forms more liquid. It is assumed that the large percentage of magnesia acts to break down the mullite.

Al₂O₃-MgO-SiO₂ Ternary - Series 73, 83, 93, and 53

The X-ray analysis of Series 73, 83, 93, and 53 show a rather complex pattern. After a presintering fire of 2000°F, alumina is the only major phase, with α-quartz, spinel, and MgO as the minor phases. Presintering at 2600°F produces alumina and spinel as the major phases. With a presintering fire of 2700°F, alumina and spinel are major phases, with mullite and α-cristobalite as minor phases. Presintering at 2800°F produces alumina, mullite, and spinel as major phases, with α-cristobalite as a minor phase.

After a final firing of 2600°F, alumina, spinel, and mullite are major phases, with sapphirine and α-cristobalite the minor phases. With a final firing of 2700°F, alumina and spinel were

found to be the major phases, with mullite and α-cristobalite the minor phases. Presintering at 2800°F resulted in alumina mullite, and spinel as the major phases, with α-cristobalite as the only minor phase.

The x-ray analysis shows the same pattern for phase formation in this series that was shown in the series 72, 82, 92, and 52. The mullite peaks decrease substantially at 2700°F and return again at 2800°F. This would suggest that the mullite is instrumental in the formation of the liquid phase necessary for densification at these low temperatures.

Al$_2$O$_3$-SiO$_2$-MgO Ternary - Series 74, 84, 94, and 54.

Presintering at any of the temperatures produces spinel and alumina as major phases. At 2000°F, the minor phase are α-quartz, MgO, and mullite. At 2600°F, the minor phases are mullite, sapphirine, and α-cristobalite. At 2700°F and 2800°F the minor phases are: mullite and α-cristobalite.

After final firing at all temperatures alumina and spinel are the major phases. Final firing at 2600°F, produces strong sapphirine and mullite minor peaks with weak α-cristobalite peaks. Final firing at 2700°F produces weak mullite and α-cristobalite peaks. With a final firing of 2800°F, the mullite peaks are still classified as minor peaks but are increasing in size over those shown at 2700°F.

E. Liquid Phase

In the course of final firing to 2800°F it was noticed that Series 72, 82, 73, and 83 reacted with the sagger. Closer examination revealed that a liquid was coming out of the sample discs resulting in reaction with the sagger.

It was felt that if this liquid phase could be isolated and identified valuable information could be gained as to its formation.

The first attempt to isolate the liquid phase consisted fo hanging the sample on a platinum wire and firing to 2800°F in a platinum wound resistance furnace. It was hoped that the liquid would drip into a quenching pan. However, the surface tension of the liquid prevented any separation to occur.

The second attempt was to place the sample on a platinum foil, fire to 2800°F, and then quench in water. After quenching, the platinum foil was removed to expose the bottom of the specimen. The specimen was coated with a thin layer of some glass such as to give the appearance of a clear glaze. The question arose if glass surface would remain if the specimen was cooled slowly. The same procedure cooling slowly produced the same result.

This verifies the theory that a liquid phase enhances the densification process. This liquid is quite fluid at 2800°F. It seems that the liquid occupies only the interstices of the alumina matrix, since the piece did not deform under the action of liquid flow.

This thin glass coating was not in sufficient quantity or easily removable to allow for investigation of the chemical make up of the liquid. Further work in this area will be pursued.

F. Sodium Content

The compositions under investigation contain approximately 0.5% sodium. This impurity is introduced with the alumina (A-14 0.04%, and the magnesium carbornate 0.40%). It was questioned whether the sodium was responsible for the fluidity obtained in the liquid phase.

A composition of series 72 was prepared using only very pure materials. The composition was presintered at 2600°F utilizing the presintering process. Firing on platinum foil 2800°F revealed a glassy coating similar to the composition containing 0.5% sodium.

This would indicate that the sodium is not primarily responsible for the high fluidity of the liquid phase.

G. Future Work

1. Analysis of Glassy Phase
2. Thermal Expansion Study
3. Equilibrium Study

II. SINTERING STUDIES

A. Introduction

Recent developments in the densification of aluminum oxide have shown that small additions of magnesium oxide permit theoretical density to be reached. It has also been found that specific atmospheres are required to obtain void free structures. These developments suggest further study of densification in the alumina-magnesia system.

The object of this investigation is to reduce the firing temperature and maintain all the desirable engineering properties of pure alumina and 2.0% MgO. This was done by determining the sintering characteristics of pure alumina with small additions of magnesia when fired in vacuum. Grain growth, density, porosity, shrinkage, pore size and pore location are studied as a function of time and temperature.

B. Theoretical Considerations and Methods of Approach

1. Theoretical Considerations

a. Additives

Additives have considerable effect of the densification of aluminum oxide. The most commonly used additive for producing dense aluminum oxide is magnesia. Coble[1] and Bruch[2] have been able to produce alumina of theoretical density using 0.25% MgO. Coble postulates that magnesia enhances the sintering

[1] R. L. Coble, "Sintering Crystalline Solids, Part I and II," J. of Appl. Phy., 32(5) (1961), 787-99.

[2] C. A. Bruch, "Sintering Kinetics for the High Density Alumina Process," Am. Ceram. Soc. Bulletin, 41(12) (1962), 799-806.

rate of aluminum oxide and therefore, eliminates exaggerated grain growth.

It is felt that the enhancement of the sintering rate is due primarily to the formation of an oxygen deficient solid solution. If this formation occurs, there will be an increase in the number of vacancies above that found at equilibrium. Since vacancy concentration is the driving force for sintering, the increase in vacancy concentration will increase the diffusion coefficient and consequently, the sintering rate will increase.

As seen from the phase diagram [3], a solid solution spinel phase exists in equilibrium with alumina when there is less than 98.5% alumina. In this case, some of the magnesia should go into the alumina matrix as a solid solution and the remainder as a second phase. Therefore, the resultant sintering for a composition containing less than 98.5% alumina should be different from a composition containing more than 99.0% alumina [4]. Because of the probable formation of spinel crystals at the grain boundary, there should be a difference in grain size between the above two compositional ranges.

b. Atmospheres

Atmospheres, as well as additives, have a prominent effect on sintering. Experiments undertaken by Kuczynski [5]

[3] E. M. Levin, H. F. McMurdie and F. P. Hall, Phase Diagrams for Ceramists (The American Ceramic Society, 1956) Figures 78 & 79.

[4] R. Arlett, Personal Communication

[5] G. C. Kuczynski, Kinetics of High Temperature Processes (Edited by W. D. Kingery. Technology Press Cambridge, Mass. and J. Wiley and Sons, Inc., New York, 1959)

have shown that a dry hydrogen atmosphere increases the diffusion coefficient of alumina by many orders of magnitude over atmospheres of wet hydrogen and air. Coble [6] has shown that when firing alumina with 0.25% magnesia, the only atmospheres where exaggerated grain grows does not occur are dry hydrogen, dry oxygen and vacuum.

As in the case of additives, dry hydrogen should aid in the formation of additional anionic vacancies over and beyond those found at equilibrium. Dry oxygen should form additional cationic vacancies, and thereby increase the diffusion coefficient. Vacuum may act to reduce the total gas pressure within each pore, and as a result, potential required to collapse the pore will be reduced.

2. Method of Approach

Since atmospheres and additives have considerable effect on sintering, it was felt that a further investigation of these variables should be undertaken. The compositions investigated were: 100% alumina, 99.75% alumina-0.25% magnesia, and 98.0% alumina-2.0% magnesia (signified as C, R and CR respectively). In order to see the effect vacuum has on densification, firings were done in a vacuum.

Utilizing the compositions investigated, a comparison between the effect of a solid solution and the effect of a second phase on densification was made. The 0.25% magnesia

[6] R. L. Coble, "Firing Alumina in Various Atmospheres," J. Am. Ceram. Soc., 45(3) (1962), 123-27.

composition was used because it is in the solid solution region reported by Arlett [7], and because of previous work done with it [8, 9]. Vacuum was used because exaggerated grain growth does not occur with it and the 0.25% magnesia composition[10]. In addition, detailed description of the effect of vacuum on the total densification process does not exist.

C. Experimental Procedure

1. Raw Material

The materials needed for this study are high purity alumina of uniform small particle size and a high purity form of magnesia that will uniformly distribute itself in the alumina. With this in mind, the following raw materials were selected for this investigation:

Alumina

Linde "A" alumina - Linde Company

Single crystal alumina

Purity - 99.9 Al_2O_3

Spectrographic Analysis for Main Impurities

Si---------From 0.01% to 0.05%

Fe---------0.01%

---

[7] R. Arlett, Personal Communication

[8] R. L. Coble, "Firing Alumina in Various Atmospheres," J. Am. Ceram. Soc., 45(3) (1962), 123-27.

[9] R. L. Coble, "Sintering Crystalline Solids, Part I and II, J. of Appl. Phy., 32(5) (1961), 787-99.

[10] Same as 8

Grain size - 0.3 microns

Grain shape - spherical[11]

Magnesia

"Baker's" magnesium nitrate crystals

Formula - $Mg(NO_3)_2.6H_2O$

Chemical Analysis

Insol. Mat.----0.005% SiO_2----0.003%

SO_4----0.0008% Ba---- < 0.005%

Ca---- < 0.02% Fe----0.0002%

Alkali Salts----0.10%

PO_4----0.0003%

H. M. (as Pb)----0.0005%

Cl----0.0005%

2. Compositions

The three compositions under investigation in this study are as follows: 100% Al_2O_3, 99.75% Al_2O_3 and 0.25% MgO, and 98% Al_2O_3 and 2.0% MgO. The source of alumina is "Linde A" and the source of magnesia is magnesium nitrate. The batch formulae for these compositions based on a hundred gram batch are as follows:

1. C - 100% alumina

---

[11] J. Pappis and W. D. Kingery, "Electrical Properties of Single-Crystal and Polycrystalline Alumina at High Temperatures," J. Am. Ceram. Soc., 44(9) (1961), 459-64.

2. R - 99.75% alumina

   99.75 grams "Linde A"

   3.09 millliliters of magnesium nitrate solution containing 0.081 grams MgO/ millliliter.

3. CR - 98% alumina

   98 grams "Linde A"

   24.7 millliliters of magnesium nitrate solution containing 0.081 grams MgO/ millliliter.

3. Fabrication and Examination

   a. Fabrication

One hundred gram batches were prepared of the three compositions under investigation. "Linde A" was weighed out in an analytical balance and placed in a glass jar. Magnesium nitrate solution, in the proper proportion, was added to the batch. Five hundred millliliters of distilled water was then added to form a slurry. The glass jar was sealed and agitated for half an hour, and the slurry poured into a pan covered with aluminum foil. The residual slurry was removed from the glass jar by repeated washings with distilled water and added to the pan. Next, the slurry was dried dried and placed into a jar. The residual material sticking to the aluminum foil was carefully scraped off and placed into the jar-making sure that no agglomeration had occurred. (The use of aluminum foil

eliminates most contamination except for a possible small amount of aluminum metal which has a smaller effect than most other impurities). The dried material was agitated in the glass jar for 30 minutes and then removed and placed in an alumina mortar andpestle where sufficient distilled water to prepare a powdered compact was added. The batch was remixed and ground. In order to avoid the sticking of the batch to the die, one piece of paper was placed on each punch face. Discs of the raw material were prepared in a hydraulic press with a 5/8" die, pressed to 50,000 psi and then removed and stored in a desiccator.

b. Firings and Density

Before placing the specimen in the furnace, its initial diameter was measured with a micrometer caliper. One specimen of each composition was placed in the furnace and fired to the predetermined time and temperature. The same firing was repeated a number of other times at random to see if the same physical data could be obtained. After firing all three compositions for four different lengths of time (1, 3, 5, 7 hours) and for four different temperatures (1550, 1650, 1700, 1750°C) the samples were removed from the furnace and their final diameters measured. Density and total porosity of the specimens were determined by the water immersion technique.

c. Microscopic Examination

Both polished sections and fragments were prepared for microscopic examination. The maximum, minimum and average

grain sizes, as well as pore sizes and pore locations, were determined for each composition and sintering treatment. From the above data the sintering characteristics of each composition in vacuum could be found.

d. Sintering Equipment

A photograph showing the equipment used for this study is shown in the final report of Navy contract number NOw 61-0211-c. The following equipment was used:

1. Electrical components
   a. Powerstat
   b. 10 KVA transformer
2. High Temperature resistance furnace
3. Vacuum equipment
   a. Vacuum valve
   b. Diffusion pump
   c. Mechanical vacuum pump
4. Vacuum measuring equipment
   a. Thermocouple vacuum gauge
   b. Discharge gauge

1. Electrical Components

The electrical power enters the powerstat (right side of Figure 1) and then goes through the 10 KVA transformer to the furnace.

The electrical power for this study was a 230 volt and 60 ampere. The current from this source is fed into a Superior Electric Co. Powerstat capable of carrying 15.6 KVA. The current th

Powerstat capable of carrying 15.6 KVA. The current then goes through a 0-50 ampere ammeter to a 10 KVA transformer. The 10 KVA transformer is capable of delivering 1000 amperes at 10 volts. In order to heat the molybdenum heating element within the furnace, large amperage is necessary. The primary current of the 10 KVA transformer can be seen on the 0-50 ampere ammeter. The furnace temperature is controlled and varied by the powerstat.

2. Vacuum Components

The vacuum system consists essentially of a mechanical vacuum pump backed up by an oil diffusion pump which is located below the vacuum valve. This system is attached to the bottom of the furnace (Figure 1). There are two pressure measuring devices for the system: a thermocouple gauge and a discharge gauge. The thermocouple gauge, capable of measuring pressures between 1000 and five microns of mercury, is located between the mechanical pump and the diffusion pump. The discharge gauge, located near the atmosphere outlet valve of the furnace, is capable of measuring pressures between 25 and 10^{-3} microns of mercury. The mechanical pump can reduce the pressure in the system to about 25 microns of mercury. The oil diffusion pump is turned on after the mechanical pump has reduced the pressure to less than five hundred microns. The oil diffusion pump has a capacity of 275 liters per second and will take the system down to a pressure of about a tenth of a micron of mercury

The vacuum valve is located below the furnace. The valve must be opened when vacuum firings are carried out. To protect the vacuum equipment in case of any emergency, the valve can be closed manually.

3. The furnace

The high temperature resistance furnace used in this study is basically similar to the furnace described by N. N. Ault and F. H. Mc Ritchie (22, 23). (See Figure 1). This furnace is equipped for operation in vacuum and inert or reducing atmospheres.

The heating element is a cylindrical sheet of molybdenum 0.005" thick which is placed between two copper contact cones that act as electrical contact for the heating element. In addition, contact between the heating element and the contact cone is established by placing a brass split ring in the heating element and having this ring exert a pressure against both the heating element and the contact cone. In order to sight directly on the specimens to be fired, the heating element has a gap of about 1/16". The specimens are placed on molybdenum discs 0.005" thick which are suspended within the heating element by means of a tungsten wire which is welded to the bottom of the top water jacket of the furnace. In order to measure the temperature within the furnace, a Leads and Northrup optical pyrometer, recently recalibrated, was used. Black body conditions were

approached by sighting on the specimen through a 1/16" slit in the heating element. Figure 2, found in Quarterly progess report No. II Navy Contract No. NOw 61-0211-c, is a sketch of the furnace.

The furnace shell is made of copper and is water cooled. To contain the heat, the furnace interior is silver plated and a cylindrical radiation shield has been placed between the furnace wall and heating element. To aid in maintaining uniform temperature, molybdenum radiation shields have been placed above and below the specimen stands, near both the upper and lower water jackets. In order to maintain a vacuum when other atmospheres are not used, vacuum tight needle valves were placed on both the atmosphere inlet and outlet connections. Because the furnace contains no insulating materials, no problem arises in the out gassing of these materials under vacuum. In addition, since no insulating materials are present, this furnace has a very fast current-temperature response.

4. Measurement of Temperature

Temperatures were measured using a recently recalibrated "Leeds and Northrup" optical pyrometer. The heat absorbed by the fused silica window in the furnace when temperatures were observed was taken into account, using the data obtained by Mc Nally, Peters and Ribbe[12]. Their method was to sight

[12] R. N. Mc Nally, F. I. Peters and P. H. Ribbe, "Laboratory Furnace for Studies in Controlled Atmospheres; Melting Points of MgO in a N₂ atmosphere and of Cr₂O₃ in N₂ and in Air Atmospheres," J. Am. Ceram. Soc., 44(10) (1961), 491-93.

on a variable tungsten filament with an optical pyrometer and measure the difference in temperature with an without the window in place. Figure 2A shows the correction that was applied to the observed temperature to obtain the true temperature.

A molybdenum shield, which was rotated to cover or expose the vitreous silica window, was placed in the furnace[13] (See Figure 2). This shield was placed in the furnace to inhibit condensation of molybdenum on the vitreous silica window and was rotated to the opened position only when readings were taken.

4. Determination of Physical Variables

a. Bulk Density, Moisture Absorption and Total Porosity

The bulk densities and moisture absorptions of the compositions under investigation were determined for each time and temperature used, by the water immersion technique utilizing an analytical balance. Each specimen was weighed dry. After boiling for two hours in water the wet and suspended weights of the samples were measured. The moisture absorption, bulk density, and total porosity were calculated according to the following formulas [14];

$$(10) \quad \text{Bulk Density (g/cc)} = D_B = \frac{D}{W-S}$$

---

[13] D. Lupfer, Personal Communications

[14] A. I. Andrews, Ceramic Tests and Calculations, (J. Wiley and Sons, Inc., New York, 1947) 37-8.

Figure 2A

RADIATION ABSORPTION OF VITREOUS SILICA

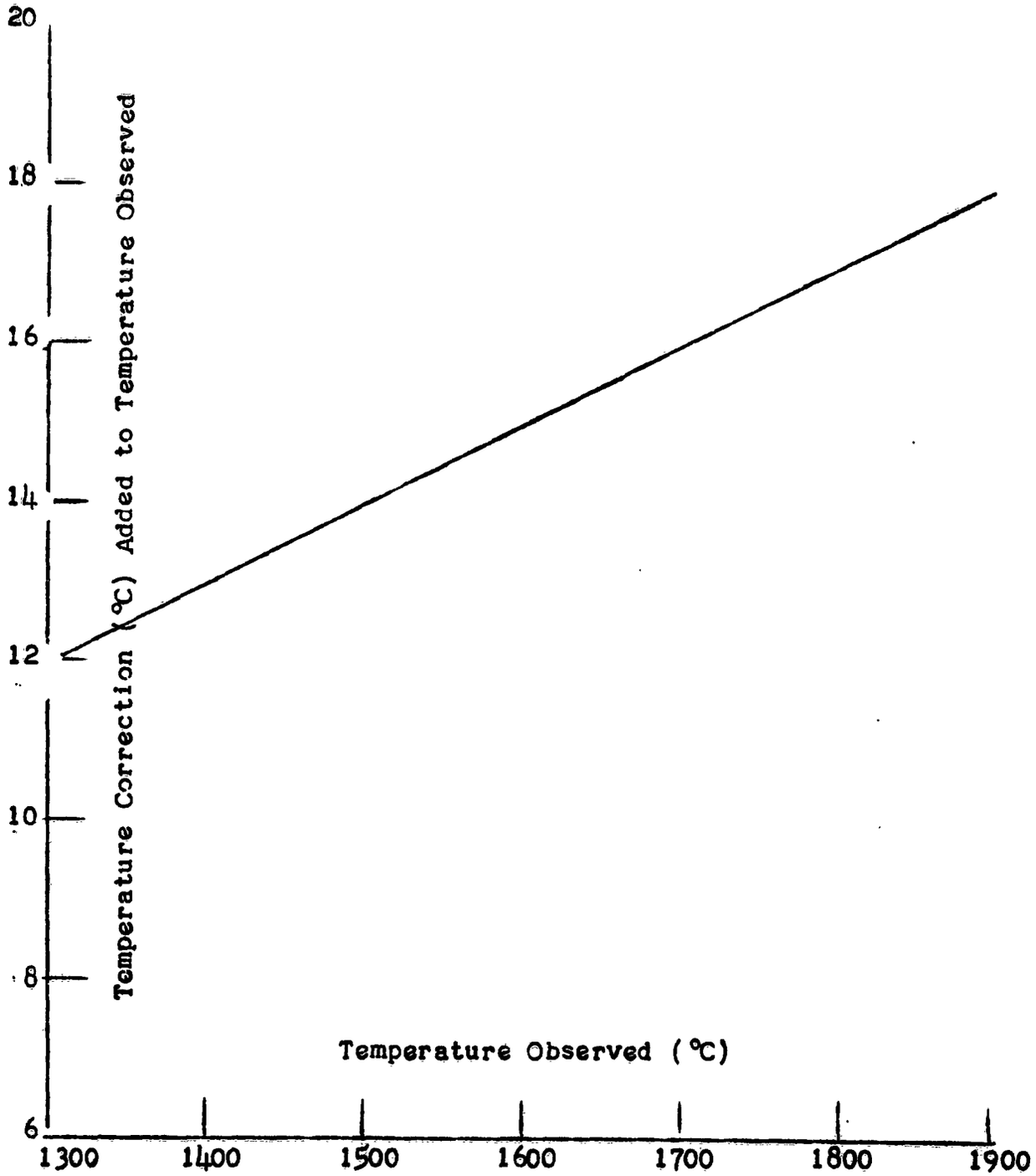

(11) Moisture Absorption (%) = $\frac{W - D}{D} \times 100$

(12) Total Porosity [15]* = P(%) = $(1 - \frac{D_B}{D_T}) \times 100$

Where: D = Dry weight

W = Wet Weight

S = Suspended weight

b. Linear shrinkage

The linear shrinkage of the bodies prepared for this investigation were measured using a micrometer caliper. Four measurements of the diameter of the specimen were taken before the specimen was sintered and four after sintering. The average value of the initial and final diameters were taken and the linear shrinkage was determined as follows:

(13) Linear Shrinkage = $\frac{D_1 - D_F}{D_1}$

Where: D_1 = Initial diameter

D_F = Final Diameter

5. Petrographic Determination

a. Sample Preparation

Two techniques were used to examine the microstructure of the compositions investigated: the fragmentation method

15 Chemical Engineering Handbook, Third Edition, (Edited by J. H. Perry, McGraw-Hill Book Company, Inc. 1950) 110-20.

*It is assumed that the true density of the compositions under investigation are the same as the true density of alumina. The true density of aluminum oxide is 3.987 g/cc. The true densities of magnesia and magnesium aluminate are 3.58 and 3.60 g/cc respectively. The error in assuming the theoretical density of alumina for the 2.0% magnesia composition is 0.2%, which is well within experimental error. This error was calculated using the additive law for the density of a multicomponent system.

and the polished section method [16].

The fragmentation technique was used for most of the samples. Specimens were crushed and ground in an alumina mortar with a pestle until the powdered sample felt smooth when rubbed between the index finger and thumb. Next, a small amount of the specimen was placed on a microscope slide and mixed with an oil whose index of refraction was close to the index of refraction of the material investigated. A glass cover was placed over the ground specimen and oil and, using transmitted light, observed under the microscope.

The polished section technique was used primarily to verify the fragmentation technique. A specimen, with "Lucite" added, was placed in a mold and pressure was applied as the temperature was raised. Upon cooling, the "Lucite" solidified around the specimen. Using the "Automet" polishing machine, the cooled sample was polished first for ten minutes on a course "Three M" diamond wheel and then ten minutes on the fine "Three M" diamond wheel. For a final polish, the specimen was hand polished on a lead lap wheel embedded with six micron diamond paste [17]. To bring out the grain structure, the specimen was etched for 75 minutes with concentrated hydrofluoric acid.

---

[17] W. C. Allen, Personal Communication

b. Experimental Procedure

A Bausch and Lomb microscope equipped with a 45X objective and a 25X Spencer filar eyepiece was used to examine the specimens under the microscope. The divisions on the filar eyepiece were calibrated using a Bausch and Lomb stage micrometer. Each eyepiece division was found to be four microns.

The experimental procedure used in the fragmentation technique [18] was as follows:

1. A fragment with about 20-30 grains was found.
2. Only those grains near the center of the fragment, making sure not to include grains at the edge of the fragment, were measured. This was done to insure measuring only whole grains.
3. The maximum and minimum grain size within the fragment were determined.
4. The average grain size was determined by measuring a number of grains of intermediate size and averaging the results.
5. The same procedure was repeated for five or six other fragments.
6. The limits on the pore size and their location (at the grain boundary or the grain interior) were determined.
7. The results were recorded.

[18] H. C. Van Cott, Personal Communication

The polished section method was used as a check for the fragmentation technique with good agreement obtained for the samples checked. It is felt, from discussion with Van Cott, that a major error exists in the fragmentation technique when the grains become as large as the fragments investigated.

D. RESULTS

1. Bulk Density, Per Cent Moisture Absorption and Total Porosity

a. Bulk Density

Figure 3 through 6 are plots showing bulk density of the three compositions investigated versus time at temperature. These data are represented in Tables 1 through 4.

Bulk densities for the R (0.25% MgO) and the CR (2.0% MgO) compositions in Figure 3, the lowest temperature investigated, are very similar. It can be seen that both compositions yield densities of 3.95 for the seven hour fire. The C composition (100% Al_2O_3) reaches a maximum density of 3.87 for the five hour fire and remains constant. Both the R and CR composition increased in density over the entire range of time.

In Figure 4, at 1650°C, a divergence occurred between the R and CR compositions. The CR composition reached a maximum bulk density of 3.95 again, but the bulk density of the R

Figure 3

DENSITY VERSUS TIME AT 1550 °C

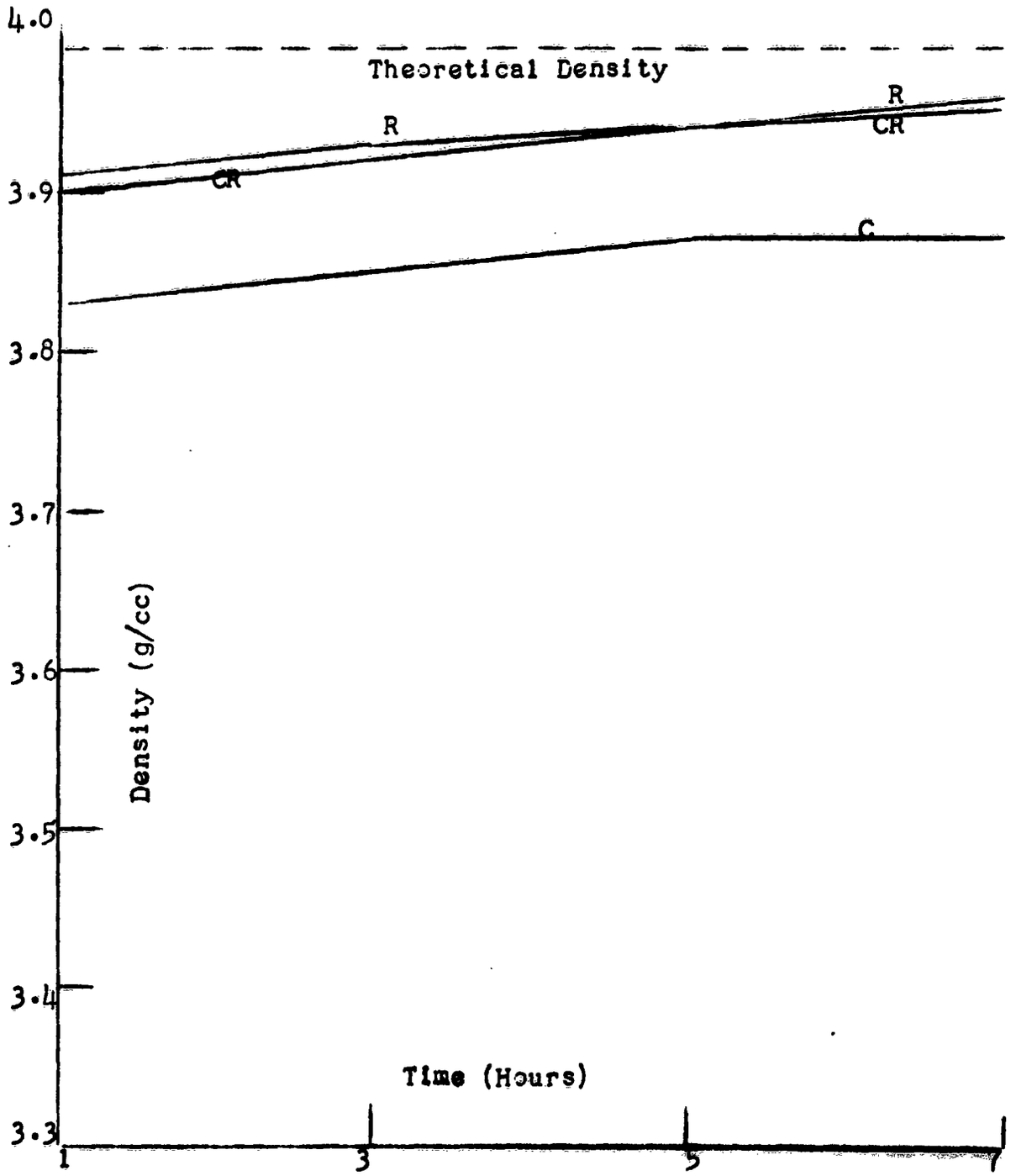

Figure 4

DENSITY VERSUS TIME AT 1650 °C

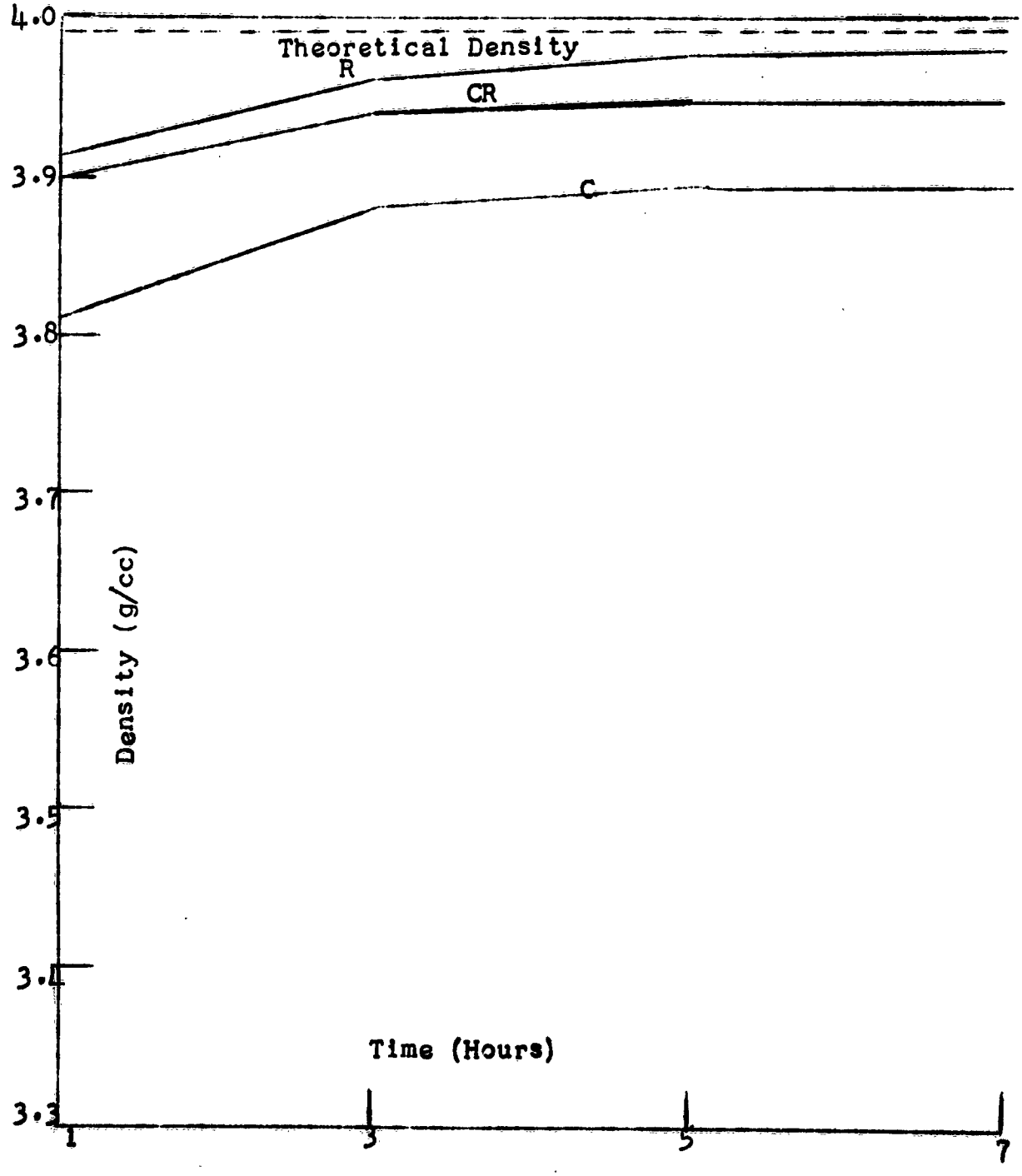

Figure 5

DENSITY VERSUS TIME AT 1700 °C

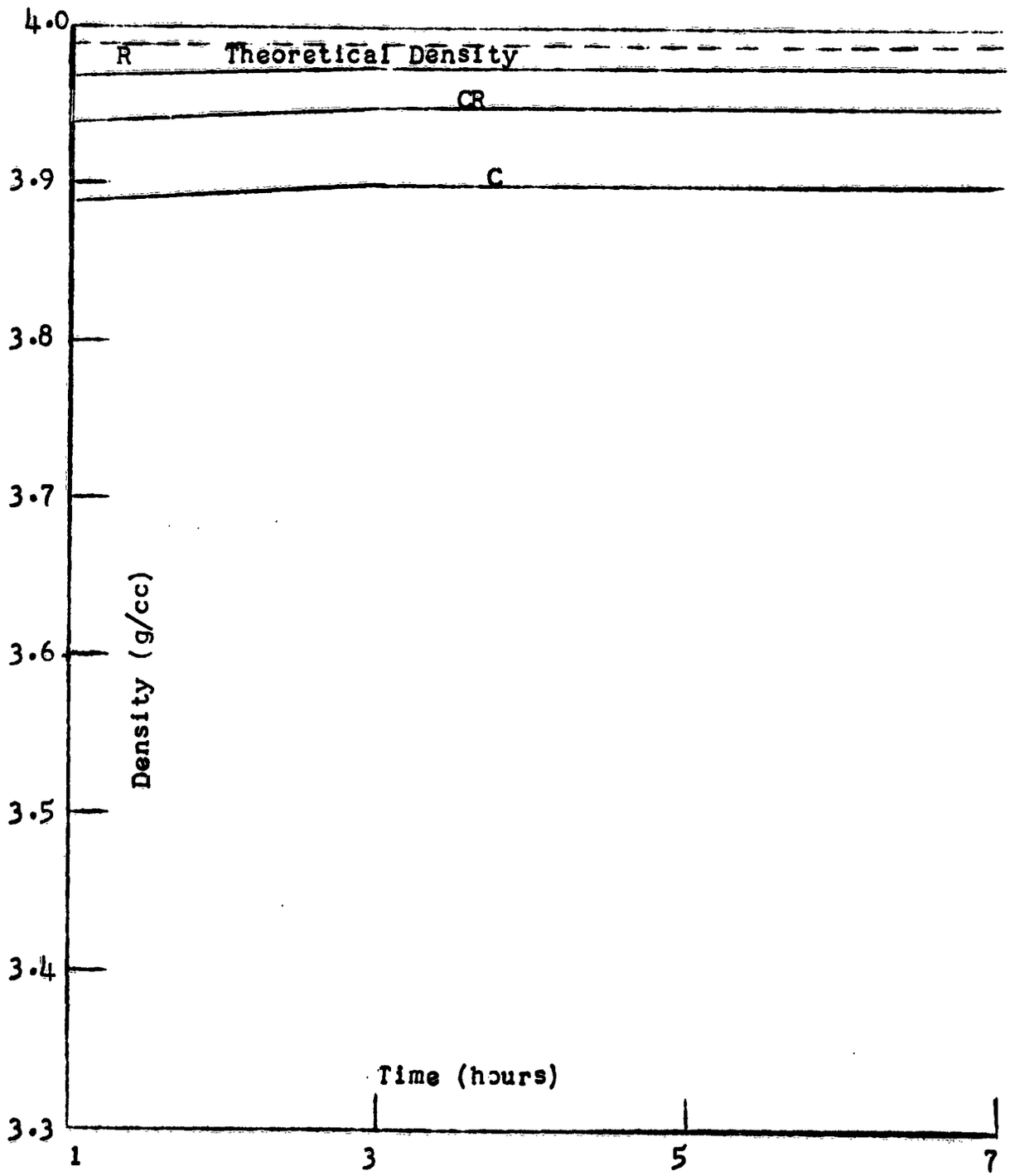

Figure 6

DENSITY VERSUS TIME AT 1750 °C

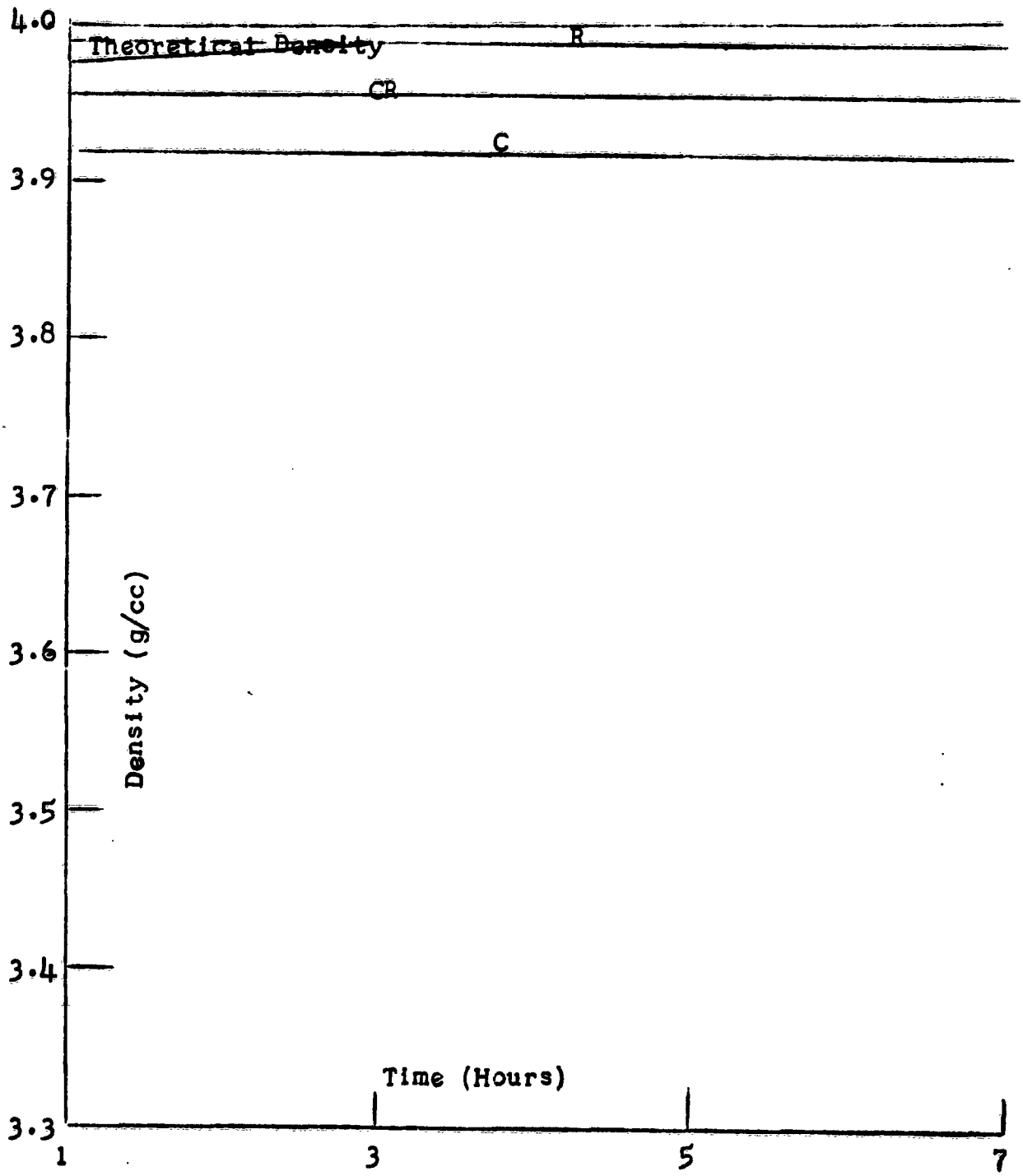

composition increased to 3.975. The maximum density obtained for the C composition is 3.89. All compositions attained maximum densities, which remained constant, during the five and seven hour fires.

The divergence between the R and CR compositions continues for both Figures 5 and 6. Figure 5 shows that each composition reached its maximum density, and maintained this density, for the three, five and seven hour fires. Maximum densities for the R, CR and C compositions were 3.975, 3.95 and 3.90 respectively. The R composition reached and maintained theoretical density from the three hour fire on. Both the CR and C compositions had a constant density over the entire time range 3.955 and 3.92 respectively.

Figures 7 through 10 are plots of bulk density versus temperature for one, three, five and seven hours respectively. In Figure 7, the R composition has the highest density at all temperatures. The CR composition most nearly approached the density of the R composition at 1550°C. The C composition had a lower density at 1650°C than at 1550°C. This composition had the lowest density at each of the temperatures investigated. These same general relationships held for Figures 8 through 10, except that no incongruity existed for the C composition at the other soaking times.

b. Per Cent Moisture Absorption

As seen from Tables 1 through 4, the only composition with any appreciable (greater than 0.00%) moisture absorption

Moisture Absorption, Bulk Density, Per Cent Total Porosity, and Per Cent Shrinkage for Samples Fired At 1550°C

Sample	% Moisture Absorption	Bulk Density	% Total Porosity	% Shrinkage
C51	0.20	3.83	4.01	20.2
R151	0.00	3.90	2.25	20.5
R251	0.00	3.92	1.75	20.5
CR151	0.00	3.91	2.00	20.6
CR251	0.00	3.89	2.50	20.4
C53	0.40	3.85	3.50	20.25
R153	0.00	3.94	1.25	20.75
R253	0.00	3.92	1.75	20.75
CR153	0.00	3.92	1.75	20.6
C55	0.00	3.87	3.00	20.35
R155	0.00	3.95	1.25	20.87
R255	0.00	3.93	1.25	20.87
CR155	0.00	3.94	1.25	21.0
CR255	0.00	3.94	1.25	20.6
C57	0.00	3.87	3.00	20.7
R157	0.00	3.95	0.87	20.9
R257	0.00	3.96	0.87	21.0
CR157	0.00	3.94	1.25	20.6
CR257	0.00	3.94	1.25	20.6

Note on Preceding Table:

1. The last digit of the sample number signifies time held at a particular temperature.
2. The number next to the letter signifies the sample number.
3. The number or numbers between the first and last digit signifies the temperature a sample is fired to.

TABLE 2

Moisture Absorption, Bulk Density, Per Cent Total Porsity, and Per Cent Shrinkage For Samples Fired At 1650°C

Sample	% Moisture Absorption	Bulk Density	% Total Porosity	% Shrinkage
C61	0.40	3.81	4.50	20.1
R161	0.00	3.93	1.50	20.9
CR61	0.00	3.94	1.25	21.0
CR161	0.00	3.93	1.50	20.7
CR261	0.00	3.92	1.75	20.7
C63	0.00	3.88	2.75	20.2
R163	0.00	3.96	0.75	20.9
R263	0.00	3.96	0.75	20.9
CR163	0.00	3.94	1.25	20.7
CR263	0.00	3.94	1.25	20.7
C65	0.00	3.89	2.50	20.5
R165	0.00	3.97	0.50	21.0
R265	0.00	3.98	0.25	21.2
CR165	0.00	3.95	1.00	21.0
CR265	0.00	3.94	1.25	20.6
C67	0.00	3.89	2.50	20.6
R167	0.00	3.97	0.50	21.2
R267	0.00	3.98	0.25	21.3
CR167	0.00	3.95	1.00	21.0
CR267	0.00	3.94	1.25	21.3

Table 3

MOISTURE ABSORPTION, BULK DENSITY, PER CENT TOTAL POROSITY, AND PER CENT SHRINKAGE FOR SAMPLES FIRED AT 1700°C

Sample	% Moisture Absorption	Bulk Density	% Total Porosity	% Shrinkage
C71	0.00	3.89	2.50	20.0
R171	0.00	3.97	0.50	21.1
CR171	0.00	3.94	1.25	20.8
CR271	0.00	3.94	1.25	20.6
C73	0.00	3.90	2.25	20.1
R173	0.00	3.97	0.50	21.4
R273	0.00	3.98	0.25	21.4
CR173	0.00	3.95	1.00	20.7
CR273	0.00	3.95	1.00	21.2
C75	0.02	3.90	2.25	20.4
R175	0.00	3.97	0.50	21.4
R275	0.00	3.98	0.25	21.4
CR175	0.00	3.95	1.00	21.1
CR275	0.00	3.95	1.00	20.8
C77	0.00	3.90	2.25	20.8
R177	0.00	3.98	0.25	21.4
R277	0.00	3.97	0.50	21.4
CR177	0.00	3.95	1.00	21.1
CR277	0.00	3.95	1.00	21.1

Table 4

MOISTURE ABSORPTION, BULK DENSITY, PER CENT TOTAL POROSITY, AND PER CENT SHRINKAGE FOR SAMPLES FIRED AT 1750°C

Sample	% Moisture Absorption	Bulk Density	% Total Porosity	% Shrinkage
C751	0.00	3.92	1.75	20.6
R1751	0.00	3.98	0.25	21.7
R2751	0.00	3.97	0.50	21.4
CR1751	0.00	3.95	1.00	20.9
CR2751	0.00	3.96	0.75	20.8
C753	0.00	3.92	1.75	20.8
R1753	0.00	3.99	0.00	21.6
R2753	0.00	3.99	0.00	21.7
CR1753	0.00	3.96	0.75	20.9
CR2753	0.00	3.95	1.00	21.0
C755	0.00	3.92	1.75	20.9
R1755	0.00	3.99	0.00=	21.8
R2755	0.00	3.99	0.00	21.7
CR1755	0.00	3.95	1.00	21.1
CR2755	0.00	3.96	0.75	20.9
C757	0.00	3.92	1.75	21.0
R1757	0.00	3.99	0.00	21.8
R2757	0.00	3.99	0.00	21.9
CR1757	0.00	3.95	1.00	21.2
CR2747	0.00	3.96	0.75	20.9

was the C composition. The maximum moisture absorption of 0.40% occurred at 1550°C for a three hour soak and 1650°C for a one hour soak.

3. Per Cent Total Porosity

The per cent total porosity of each sample was obtained directly from bulk density determinations by using the theoretical density of pure alumina (3.99) for this conversion. Little or no error exists for the 0.25% MgO composition. When 3.99 is used for the theoretical density of the 2.0% magnesia composition; an error of about 0.2% may occur. This error would lower the theoretical density of the 2.0% MgO composition to 3.98 and therefore, effect the per cent total porosity. The above error would change the total per cent porosity from 1.00% to 0.75% for a sample with a bulk density of 3.95.

Figures 11 through 14 are plots of per cent theoretical density and total per cent porosity versus time for each of the temperatures investigated. In Figure 11 both the R and CR compositions have fairly similar values for total porosity and per cent of theoretical density. The C composition had a higher total porosity than either the R or CR compositions. Minimum porosities of 0.87%° 1.25% and 3.0% were obtained for the R, CR and C compositions. It can be seen from Figure 12 that the CR composition starts to diverge from the R composition. Again, as in all these figures, the C composition

Figure 7

DENSITY VERSUS TEMPERATURE (°C) HELD FOR ONE HOUR AT TEMPERATURE

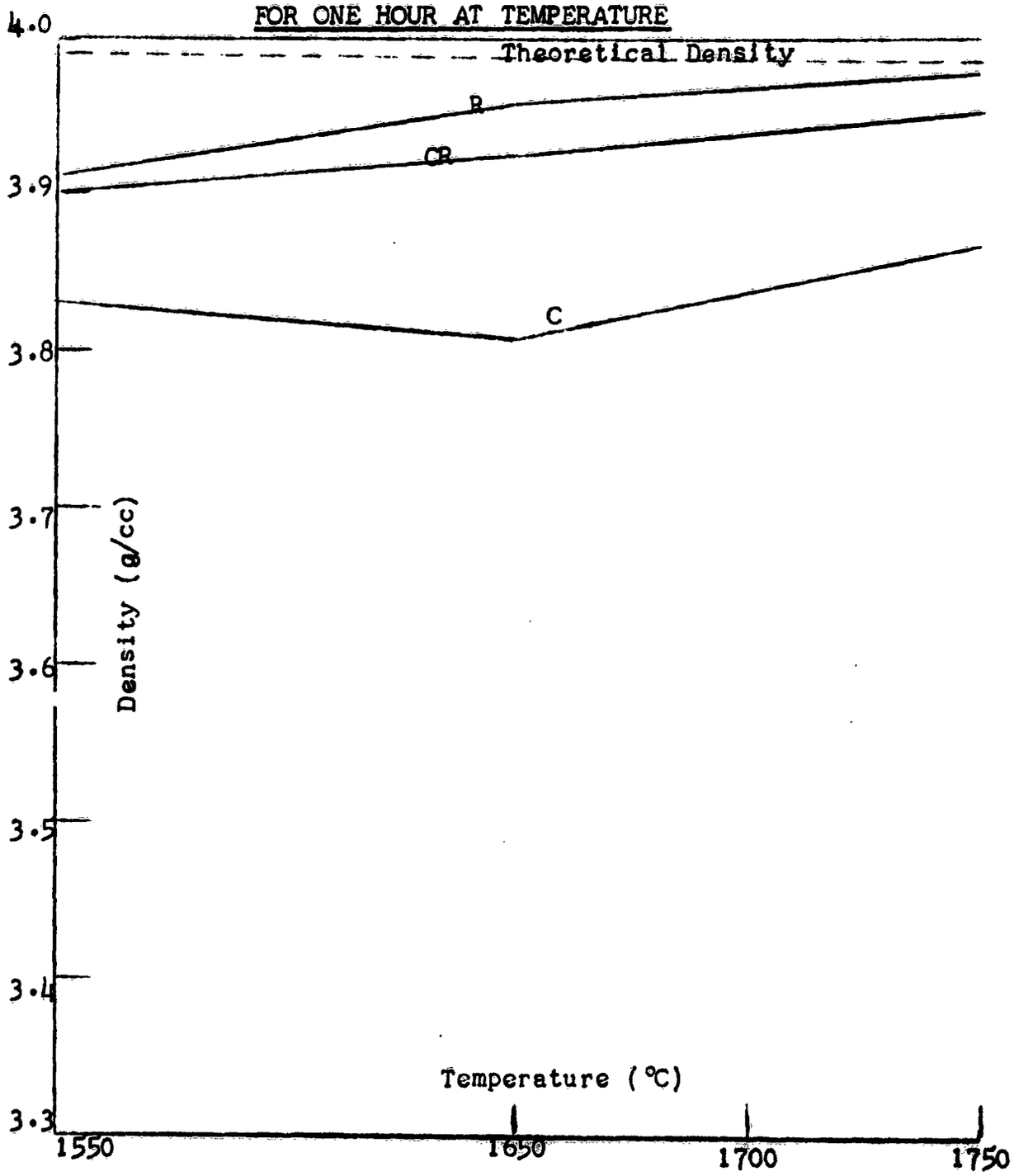

Figure 8

DENSITY VERUS TEMPERATURE (°C)

HELD FOR THREE HOURS AT TEMPERATURE

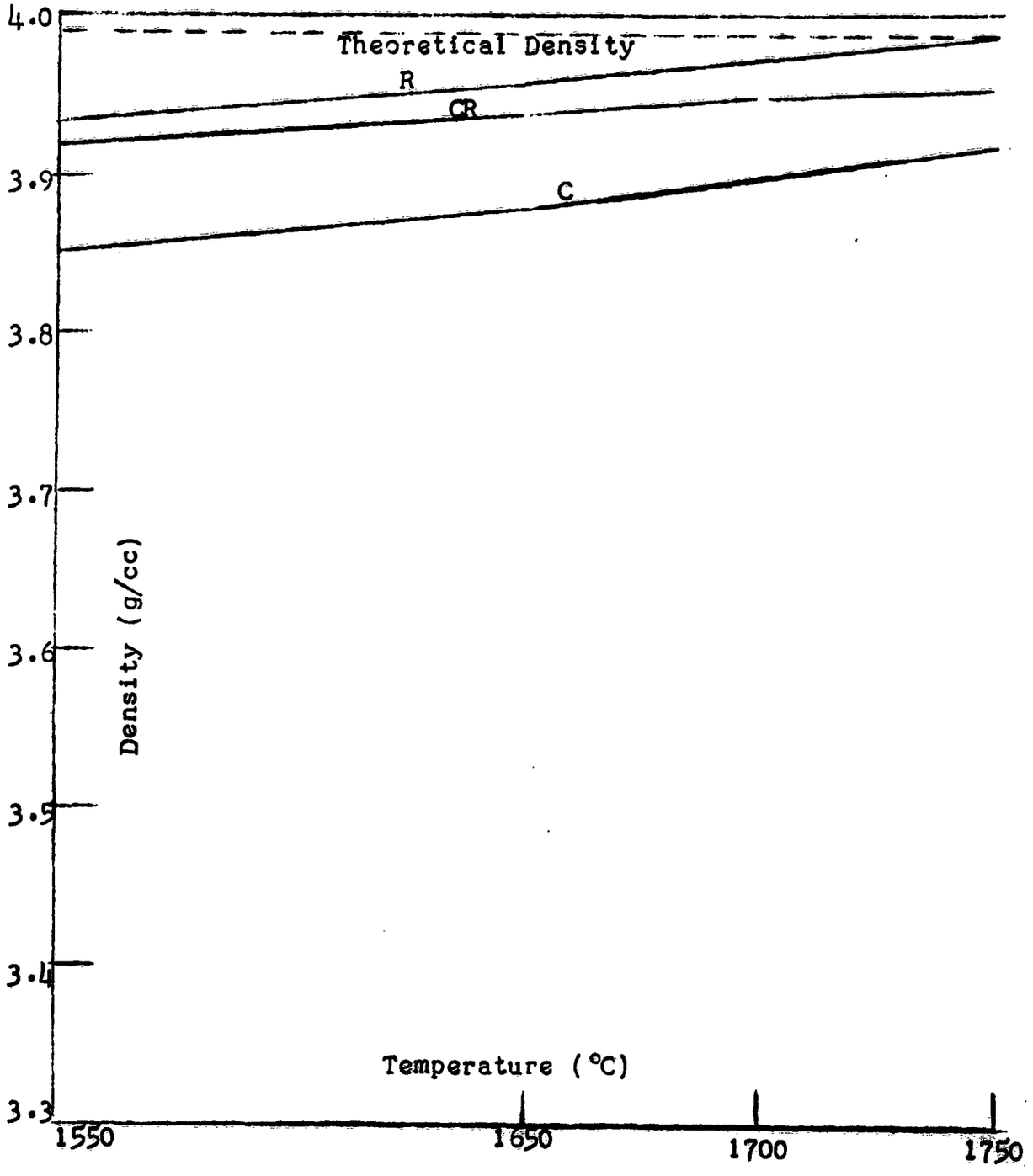

Figure 9

DENSITY VERSUS TEMPERATURE (°C)

HELD FOR FIVE HOURS AT TEMPERATURE

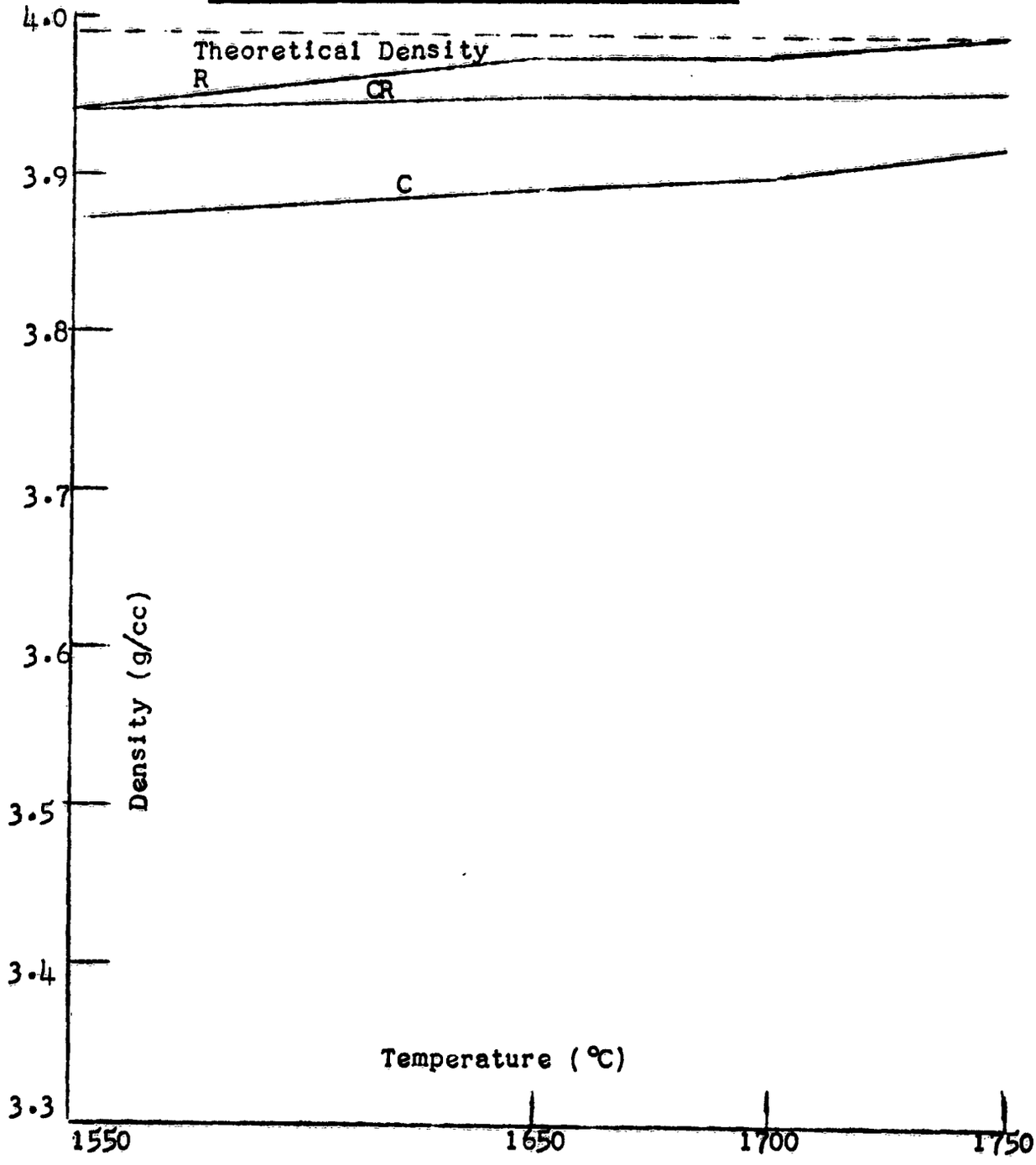

Figure 10

DENSITY VERSUS TEMPERATURE (°C)

HELD FOR SEVEN HOURS AT TEMPERATURE

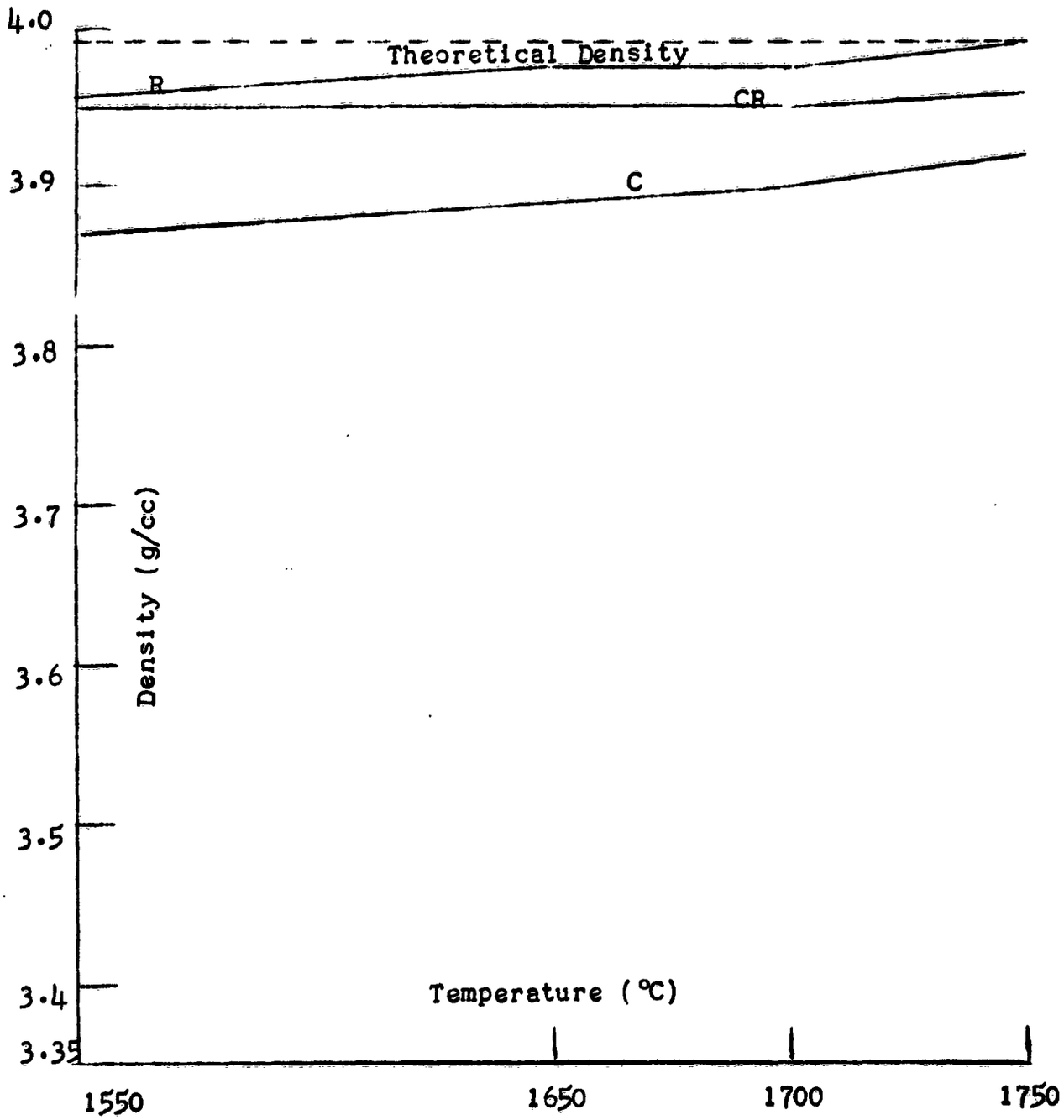

has the highest total porosity. The minimum total porosity occurred in the seven hour fire at 1650°C and was 0.37%, 1.00% and 2.5% for the R, CR and C compositions respectively. Figure 13 shows the same relationships between the compositions as the previous figure. Minimum total porosities were approached faster at this temperature (1700°C) than at lower temperatures. Minimum values of 0.37%, 1.00% and 2.25% were obtained for the R, CR and C compositions. In Figure 14 minimum values of total porosity were attained for every time investigated for the CR and C compositions. The R composition reached its minimal value at the three hour fire. The minimum values for the R, CR and C compositions were 0.00%, 0.87% and 1.75% respectively. Even with the assumption that the theoretical density of the 2.0% MgO composition is 3.98, a residual per cent total porosity of 0.63% was obtained for the CR composition. Therefore, only the R composition attained theoretical density.

B. Per Cent Linear Shrinkage

Figures 15 through 19 are plots of per cent linear shrinkage versus time for the temperatures under investigation. Variations of up to 0.4% linear shrinkage were obtained for two samples of the same composition fired together at the same temperature.

In Figure 15 both the R and CR compositions are fairly close together and maximum per cent shrinkages for each was 20.95 and 20.8 respectively. The shrinkage of the C composition

Figure 11

PER CENT OF THEORETICAL DENSITY AND TOTAL PER CENT POROSITY VERSUS TIME AT 1550°C

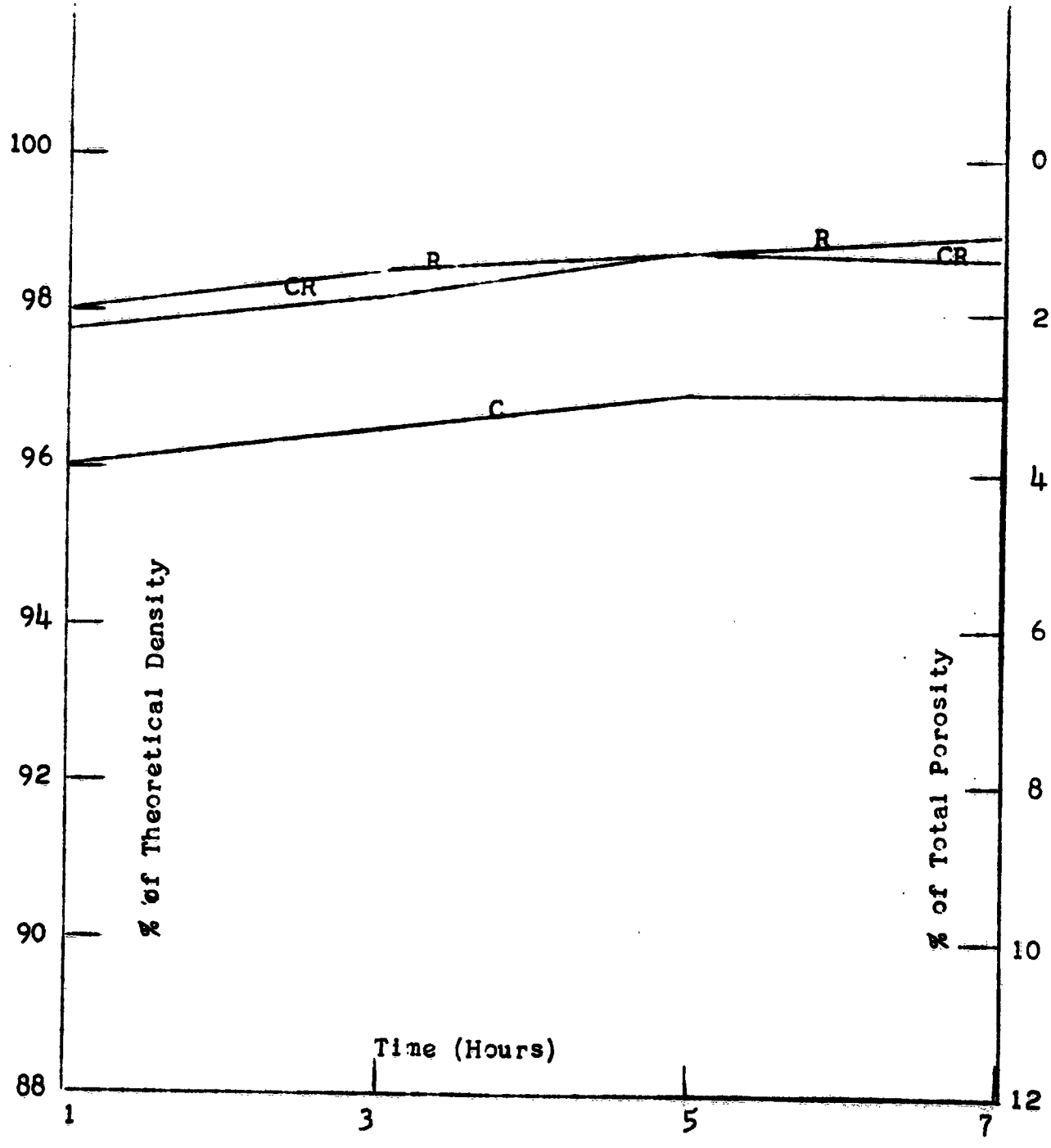

Figure 12

PER CENT OF THEORETICAL DENSITY AND TOTAL PER CENT POROSITY VERSUS TIME AT 1650 °C

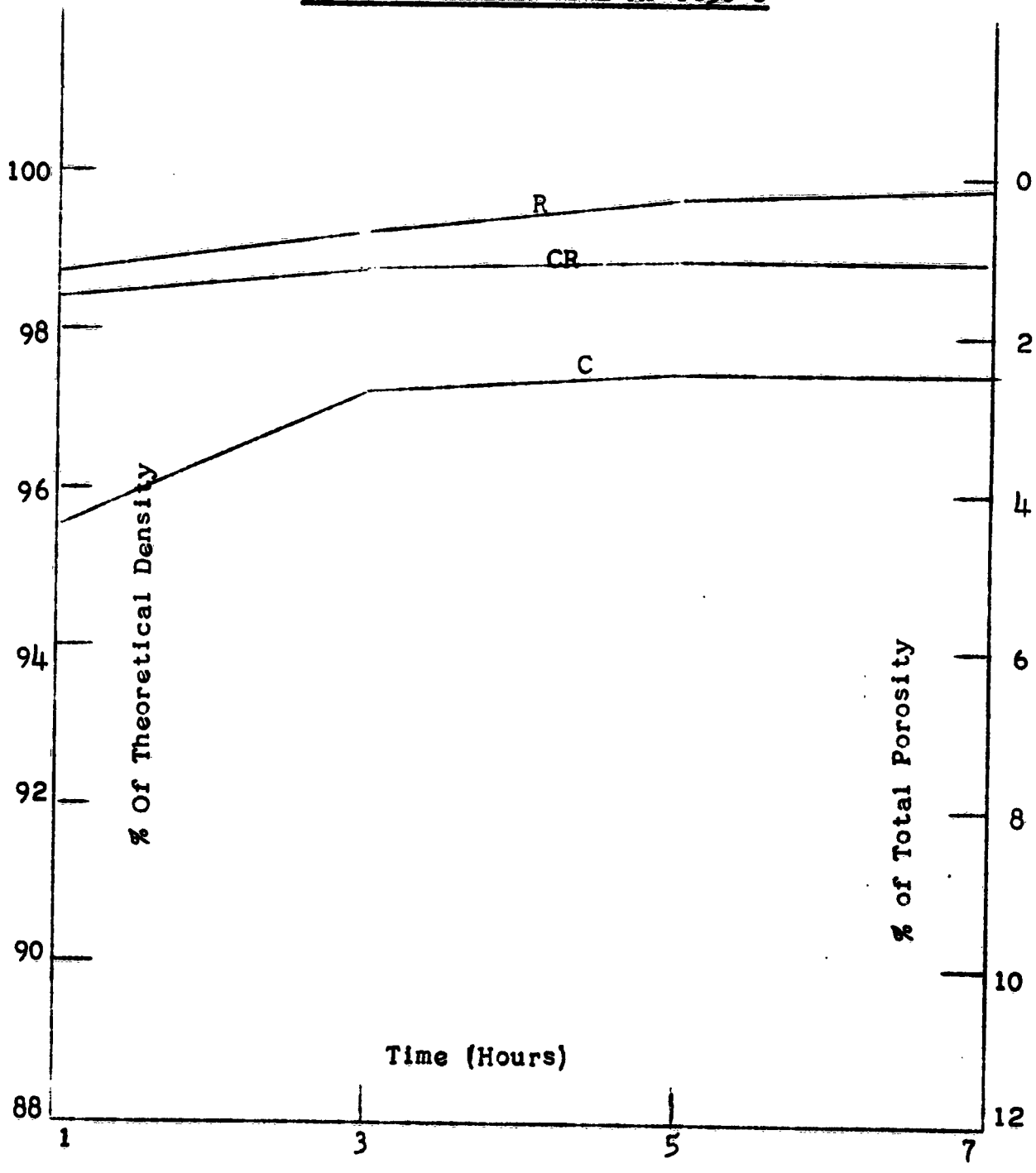

Figure 13

PER CENT OF THEORETICAL DENSITY AND TOTAL PER CENT POROSITY VERSUS TIME AT 1700°C

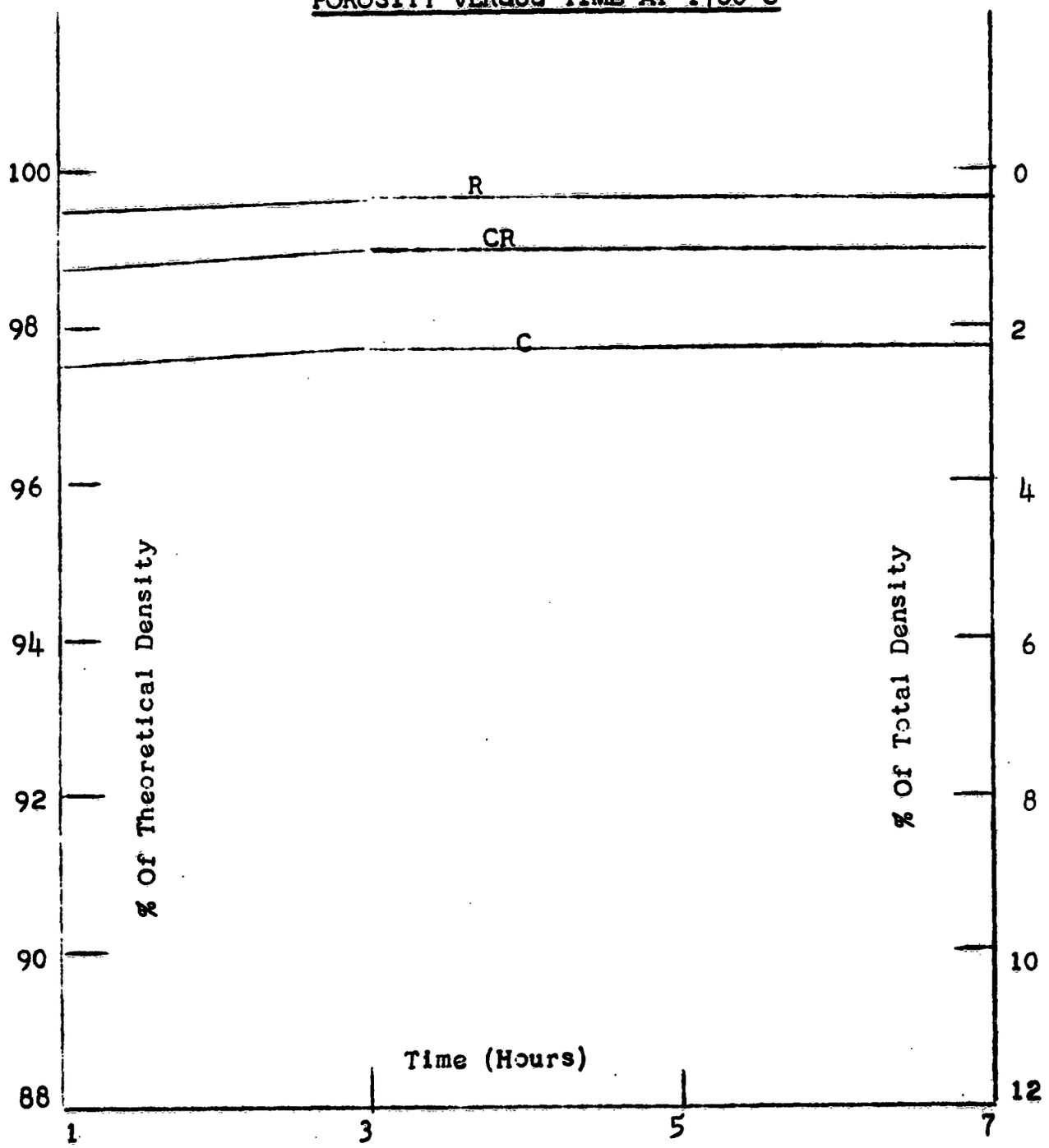

Figure 14

PER CENT OF THEORETICAL DENSITY AND TOTAL PER CENT POROSITY VERSUS TIME AT 1750°C

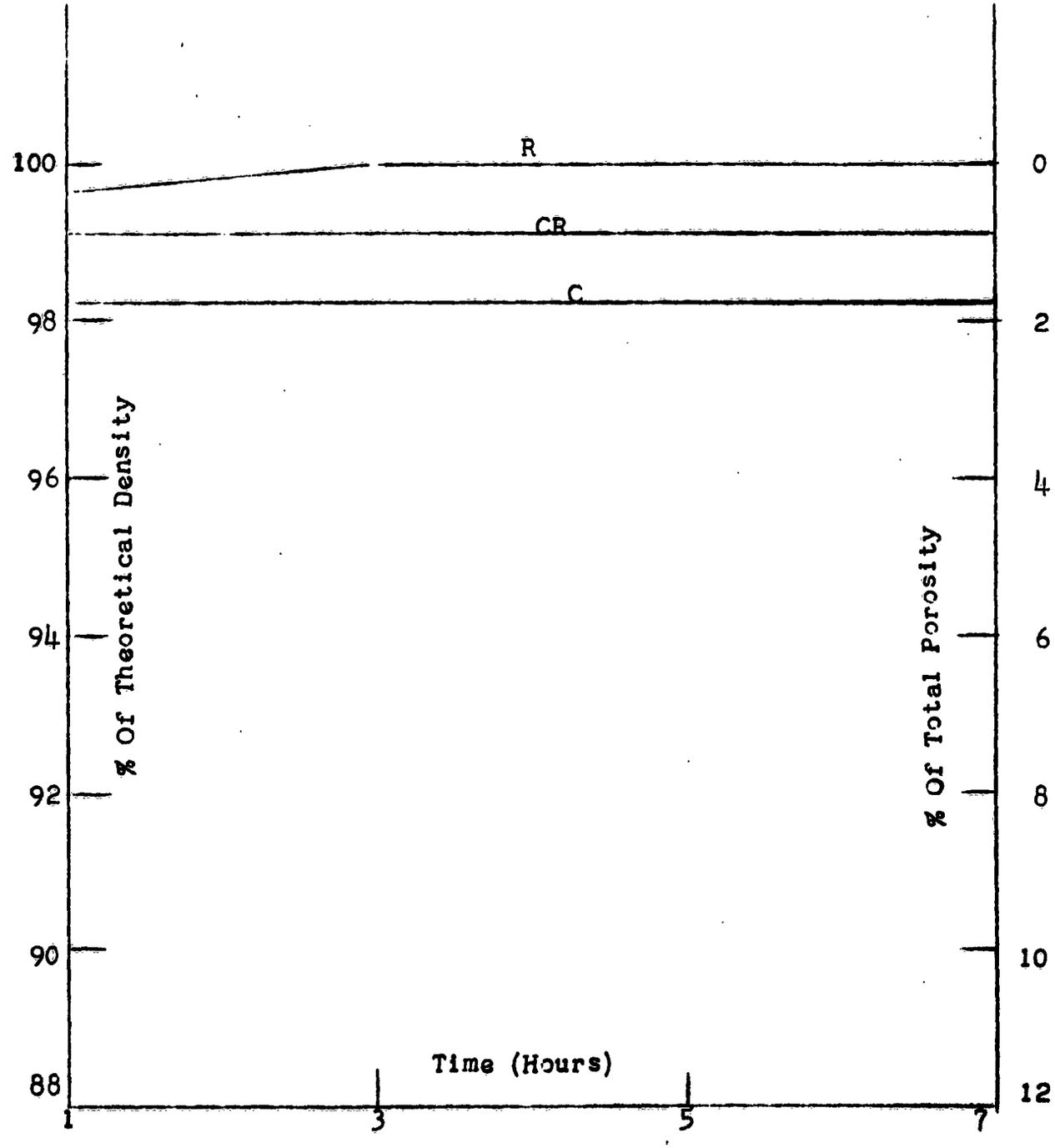

was less than the other compositions, which was in good agreement with density measurements. The maximum per cent shrinkage for this composition was 20.6%.

Figures 16 through 18 have the same relative relationships as in Figure 15, namely, the R composition had the highest per cent shrinkage, the CR composition next highest and the C composition the lowest per cent shrinkage. In Figures 17 and 18, at 1700°C and 1750°C respectively, the per cent shrinkage of the C composition approached the per cent shrinkage of the CR composition. At the same time, the R composition diverged from the CR composition. Maximum shrinkages occurred for all these compositions at 1750°C and a seven hour soak. They were 21.85%, 21.05% and 21.0% for the R, CR and C compositions respectively.

C. Microstructure

Microstructure determinations were made using the fragmentation method [19]. The error in determining average grain size varied with the grain size distribution and size of the grains. When the average grain size was ten microns or less, the error was approximately ±0.5 microns. In making determinations of average grain sizes between ten and twenty microns, the error was about ±1 micron. When exaggerated grain growth occurred, and an average grain size was greater than twenty microns, the error in the average grain size was approximately

[19] H. C. Van Cott, Personal Communication

Figure 15

PER CENT SHRINKAGE VERUS TIME AT 1550°C

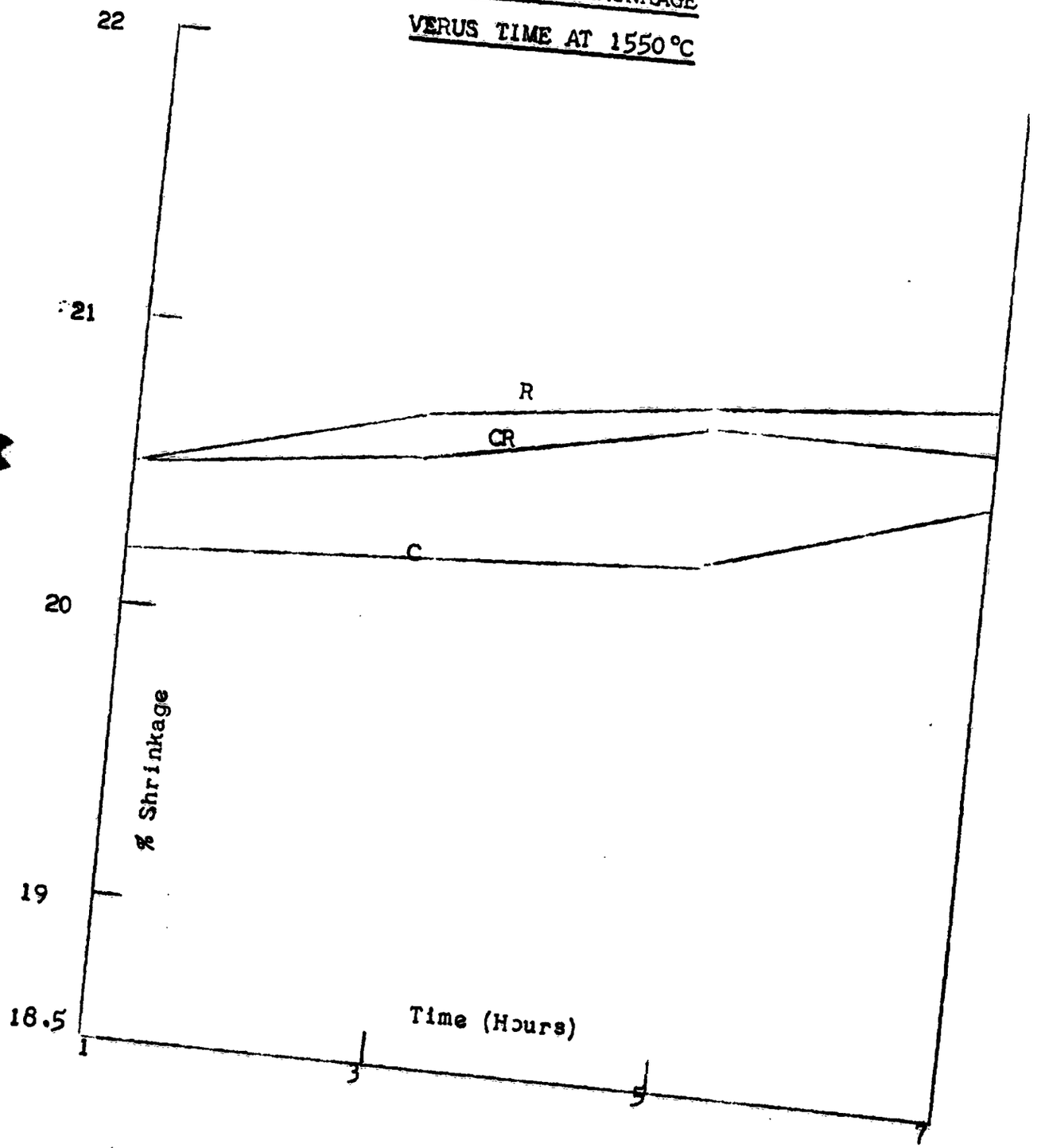

Figure 16

PER CENT SHRINKAGE VERSUS TIME AT 1650°C

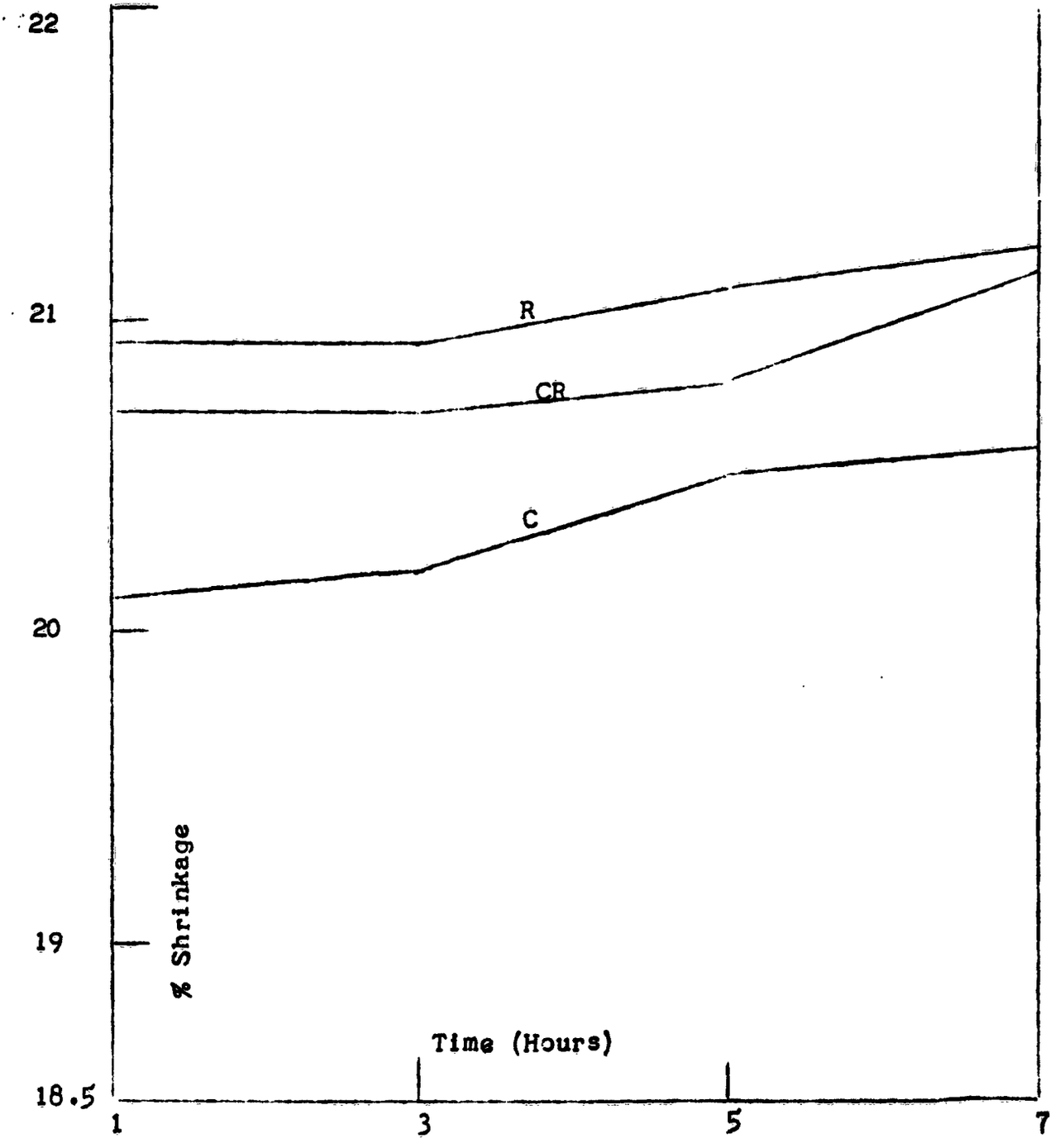

Figure 17

PER CENT SHRINKAGE VERSUS

TIME AT 1700 °C

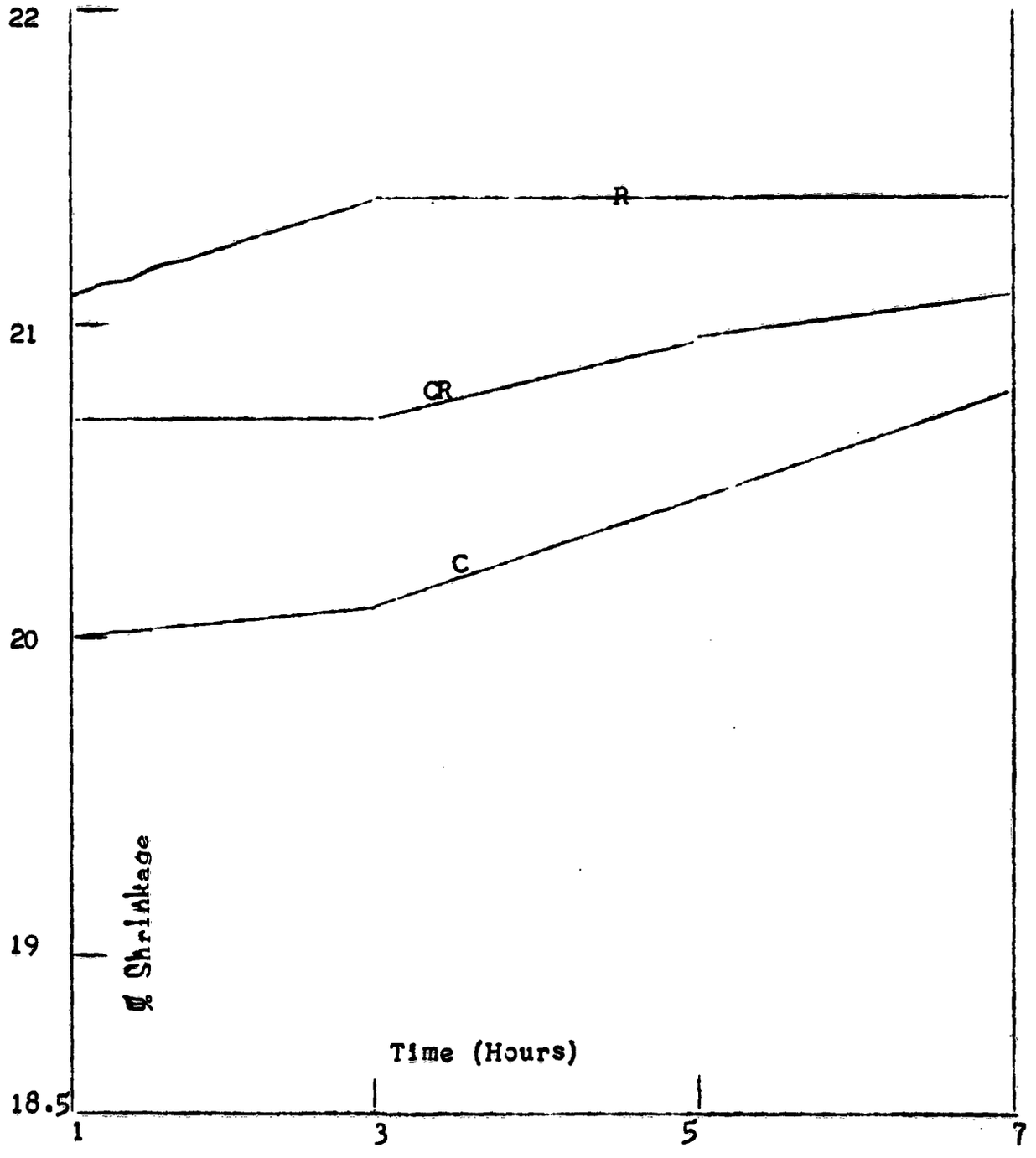

Figure 18

PER CENT SHRINKAGE VERSUS TIME AT 1750°C

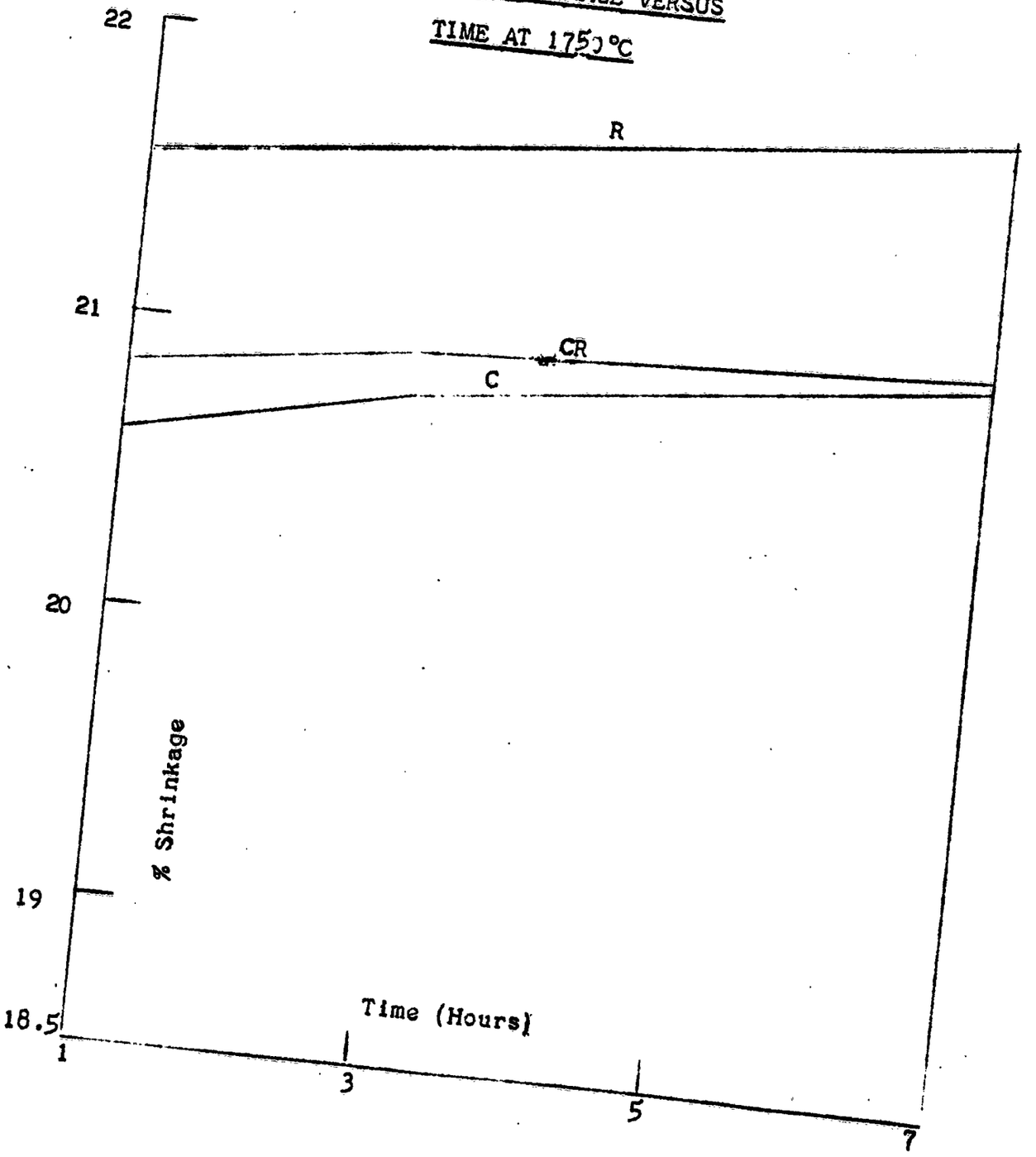

±10 microns. Where normal grain growth was found, and average grain size was between twenty and thirty microns, the error was about ±2 microns.

Figures 19 through 22 are graphs representing average grain size plotted against time for the four temperatures under investigation. Tables 5 through 8 contain all the variables measured with the microscope, namely, largest grain size, smallest grain size, average grain size, pore size and pore location. In Figures 19 and 20 the data for all compositions, within experimental error, lie on the same line. Pores for all compositions, except for samples C57, C63, C65 and C67 were located at the grain boundaries and are less than one micron. Some pores, in the four exceptions mentioned above, were found in the interior of the grain and their size was less than one micron. Figures 21 and 22 show a greater divergence in grain size as time and temperature were increased.

Exaggerated grain growth was noted for the C composition for all times and temperatures above 1650°C, and a maximum average grain size of forty microns was found. In the series of samples fired at 1750°C, the pore size for the C composition increased to a maximum of two microns. It was found that nearly all of the pores seen at the higher soaking times at 1700°C, were located within the grains.

In comparing the R and CR compositions at 1700°C and 1750°C, it was observed that the average grain size of the

R composition increased in comparison to the CR composition at 1750°C. This increase can be partially accounted for by the increase in experimental error, but there still remains a significant difference between the two compositions. The maximum grain size for both the R and CR compositions occurred at 1750°C and a seven hour soak and were twenty and sixteen microns respectively. Pore sizes of less than a micron were noted in Tables 7 and 8 for the R composition. Very few pores were found for the R composition at 1750°C with soaking times for more than one hour. It was noted that the few pores found at 1750°C were located within the grains. Pore sizes of up to two microns were noted for the CR composition. Pores were located at the grain boundary for samples fired at 1700°C and few pores were found for this composition at 1750°C. The pores found at the latter temperature were located almost equally between the grain boundary and grain interior.

Figure 19

GRAIN SIZE VERUS TIME

AT 1550 °C

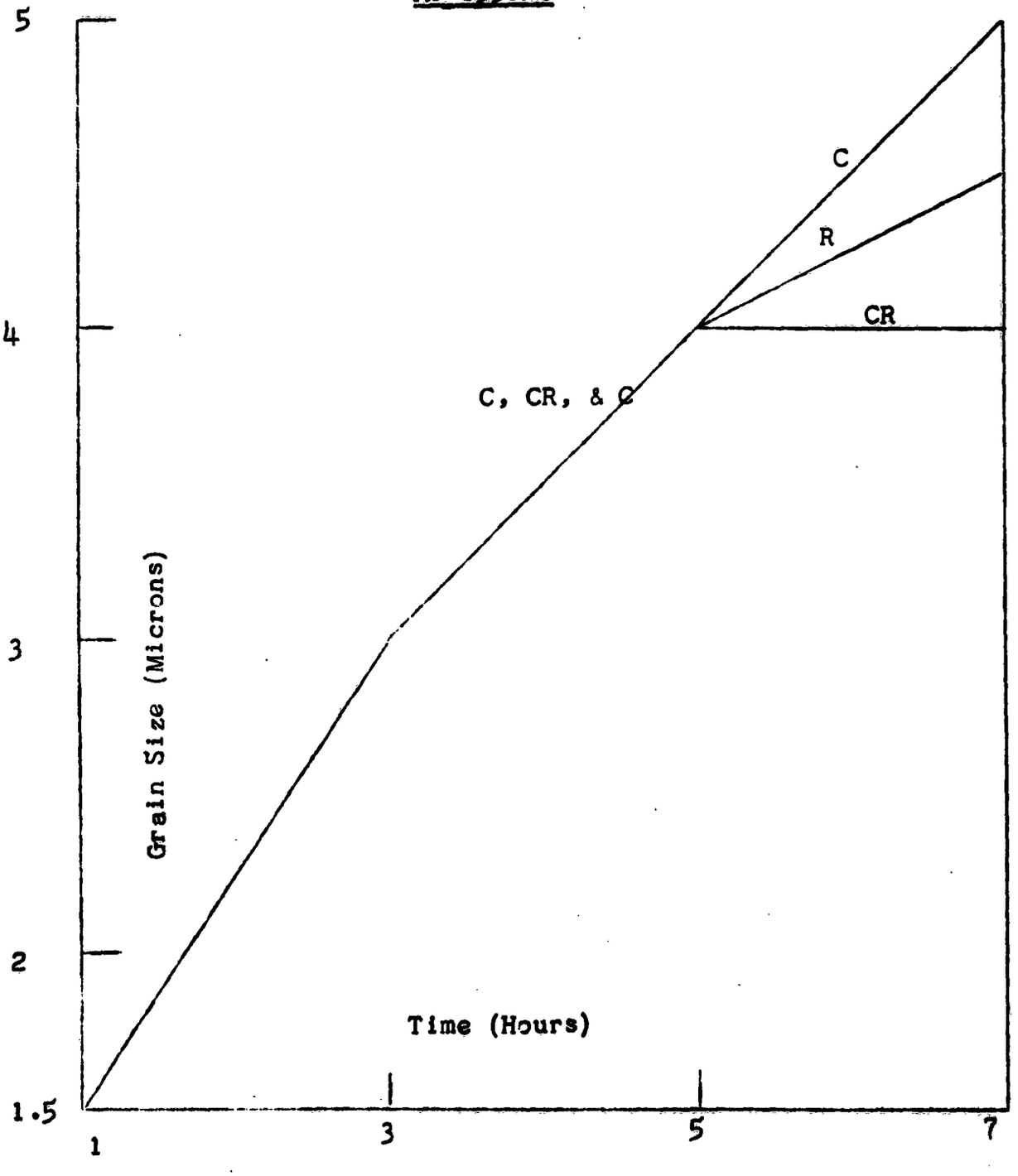

Figure 20

GRAIN SIZE VERSUS TIME

AT 1650°C

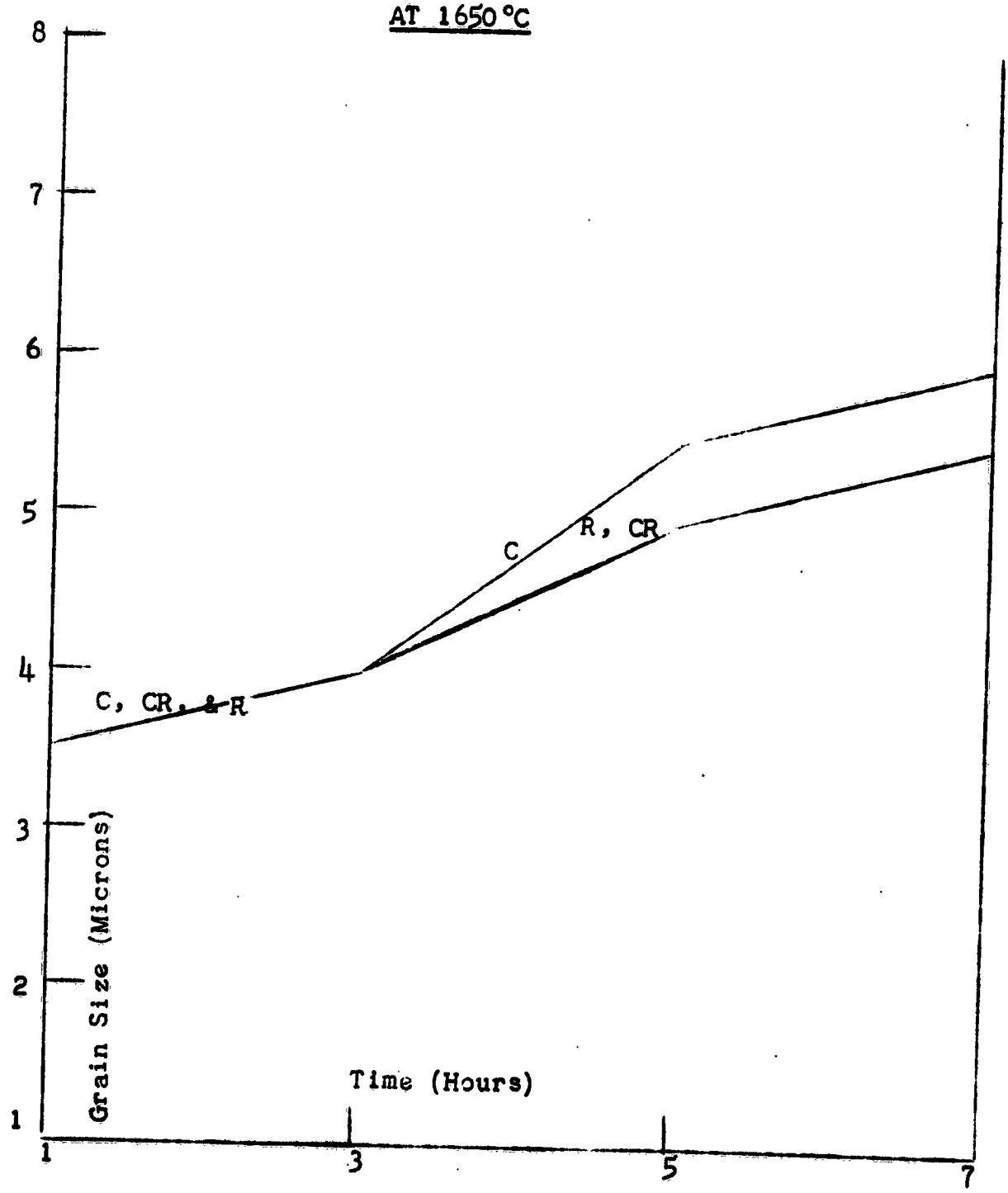

Figure 21

GRAIN SIZE VERUS TIME

AT 1700 °C

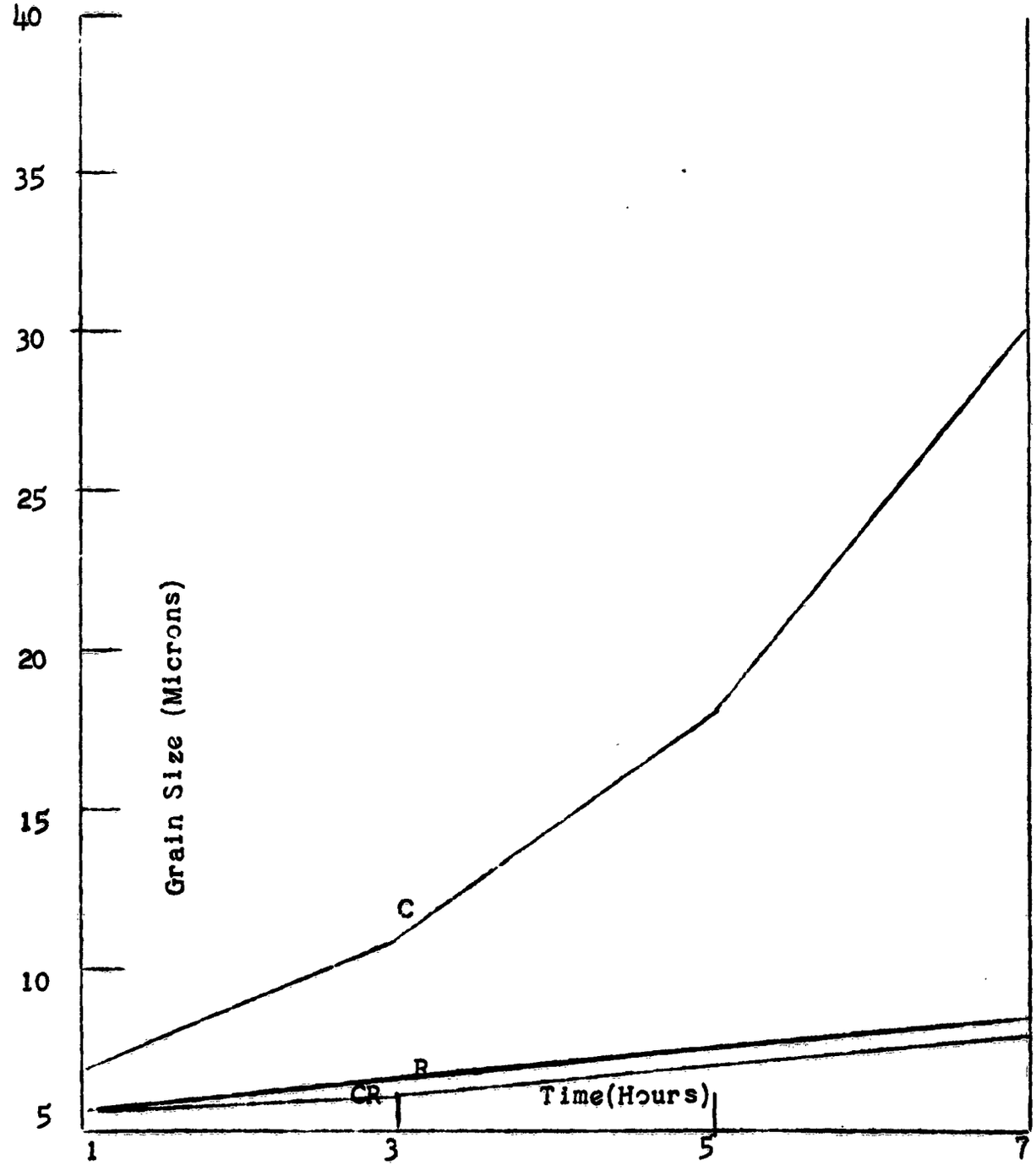

Figure 22

GRAIN SIZE VERSUS TIME

AT 1750°C

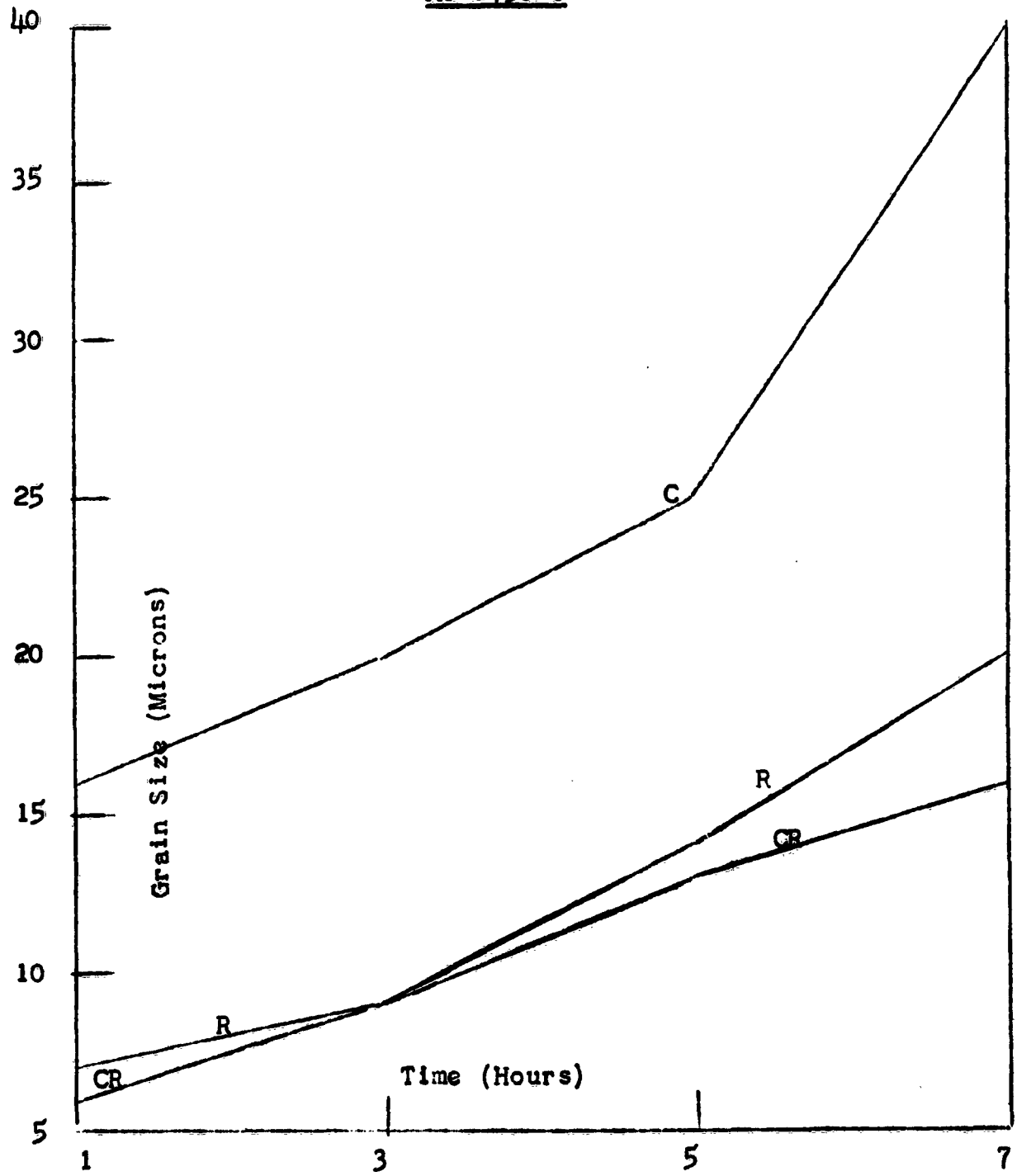

Table 5

MICROSCOPIC DETERMINATION

OF GRAIN SIZE, PORE SIZE, AND

PORE LOCATION AT 1550°C

Sample	Largest Grain Size (Microns)	Smallest Grain Size (Microns)	Average Grain Size (Microns)	Pore Size (Microns)	Pore Location
C51	4	under 1	1-2	.4	G. B.
C53	6	1	2-4	.4	G. B.
C55	8-6	2	3-5	.4	G. B.
C57	10-8	2-4	4-6	.8	G. B. & G. Int
R51	4	under 1	1-2	.4	G. B.
R53	4	1	2-4	.4	G. B.
R55	6	2-1	4	.4	G. B.
R57	6	2	4-5	.8-.4	G. B.
CR51	4	under 1	1-2	.4	G. B.
CR53	6-4	1	2-4	.4	G. B.
CR55	6	2-1	4	.8-.4	G. B.
CR57	7-6	2	4	.8-.4	G. B.

Note:

1. G. B. is an abbreviation for the grain boundary.

2. G. Int. is an abbreviation for the grain interior.

Table 6

MICROSCOPIC DETERMINATION OF GRAIN SIZE, PORE SIZE, AND PORE LOCATION AT 1650°C

Sample	Largest Grain Size (Microns)	Smallest Grain Size (Microns)	Average Grain Size (Microns)	Pore Size (Microns)	Pore Location
C61	6-4	2	4-3	.8-.4	G. B.
C63	6-5	3-2	4	.8	G. B. & G. Int.
C65	10-8	3-2	5	.8	G. B. & G. Int.
C67	12-9	3	6	.8	G. B. & G. Int.
R61	6-4	2	4-3	.8-.4	G. B.
R63	6-5	2	4	.8-.4	G. B.
R65	8-6	3-2	5	.8	G. B.
R67	9-8	3	6	.1-.8	G. B.
CR61	6-4	2	4-3	.4	G. B.
CR63	7-5	3-2	4	.8-.4	G. B.
CR65	8	3	5	.8	G. B.
CR67	10	3	6	.8	G. B.

Table 7

MICROSCOPIC DETERMINATION OF GRAIN SIZE, PORE SIZE, AND PORE LOCATION AT 1700°C

Sample	Largest Grain Size (Microns)	Smallest Grain Size (Microns)	Average Grain Size (Microns)	Pore Size (Microns)	Pore Location
C71	16	4-3	7	.8	G. B. & G. Int.
C73	25	4	12-10	.4	G. B. & G. Int.
C75	40	5	20-16	1.5-.4	G. B. & G. Int.
C77	70	8	30	1.5-.4	G. B. & G. Int.
R71	8-6	4-3	6-5	.8-.4	G. B.
R73	10-8	4-3	7-6	.8-.4	G. B.
R75	12-10	4	8-7	.8-.4	G. B.
R77	16-13	5	9-8	.8	G. B.
CR71	8-6	4-2	6-5	.8-.4	G. B.
CR73	9-8	4	6	.8	G. B.
CR75	10-9	4	7	1.5-.8	G. B.
CR77	12	5-4	8	1.5-.8	G. B.

Table 8

MICROSCOPIC DETERMINATION OF GRAIN SIZE, PORE SIZE, AND PORE LOCATION AT 1750°C

Sample	Largest Grain Size (Microns)	Smallest Grain Size (Microns)	Average Grain Size (Microns)	Pore Size (Microns)	Pore Location
C751	30	8	16	2-.4	G. Int.
C753	50-40	10	20	2-.4	G. Int.
C755	70	14-8	40-20	2-.4	G. Int.
C757	100	14-12	50-30	2-.4	G. Int.
R751	12	4	8-6	.4	G. B.
R753	20-16	6-4	10-8	very few pores	G. Int.
R755	30-25	8	16-12	very few pores	G. Int.
R757	40-30	12	22-18	very few pores	G. Int.
CR751	12	4	6	1-.4 few	G. B. & G. Int.
CR753	20-16	6-4	10-8	1-.4 few	G. B. & G. Int.
CR755	28-24	8-6	14-12	2-.4 few	G. B. & G. Int.
CR757	32-28	10-8	16	2-.4	G. B. & G. Int.

Figures 23 through 26 show the effect of grain size with temperature for four different soaking temperatures. In Figures 23, a divergence was noted between the C and the R and CR composition at temperatures above 1650°C. The variation between the R and CR composition could be attributed to experimental error. Figure 24 shows results that are similar to Figure 23 except that the difference in grain size between the C and the R and CR compositions has increased. The same effect can also be noted for Figure 25. Figure 26 shows a still further increase in the difference in average grain size between the compositions noted above. In addition, a noticeable difference was found to exist between the R and CR compositions.

E. DISCUSSION OF RESULTS

The results obtained showed that of the three compositions fired in vacuum, only the 0.25% MgO composition achieved theoretical density. Densities of the 2.0% MgO composition were found to be intermediate between the 0.25% MgO composition and pure alumina. Shrinkage and microstructure measurements correlated well with the density determinations. Microstructure measurements showed that exaggerated grain growth occurred primarily only in the pure alumina composition. A large difference was noted between the average grain size of the pure alumina and the 0.25 and 2.0% MgO compositions at the two highest temperatures investigated. Differences between the micro-

Figure 23

GRAIN SIZE VERSUS TEMPERATURE (°C)

HELD FOR ONE HOUR AT TEMPERATURE

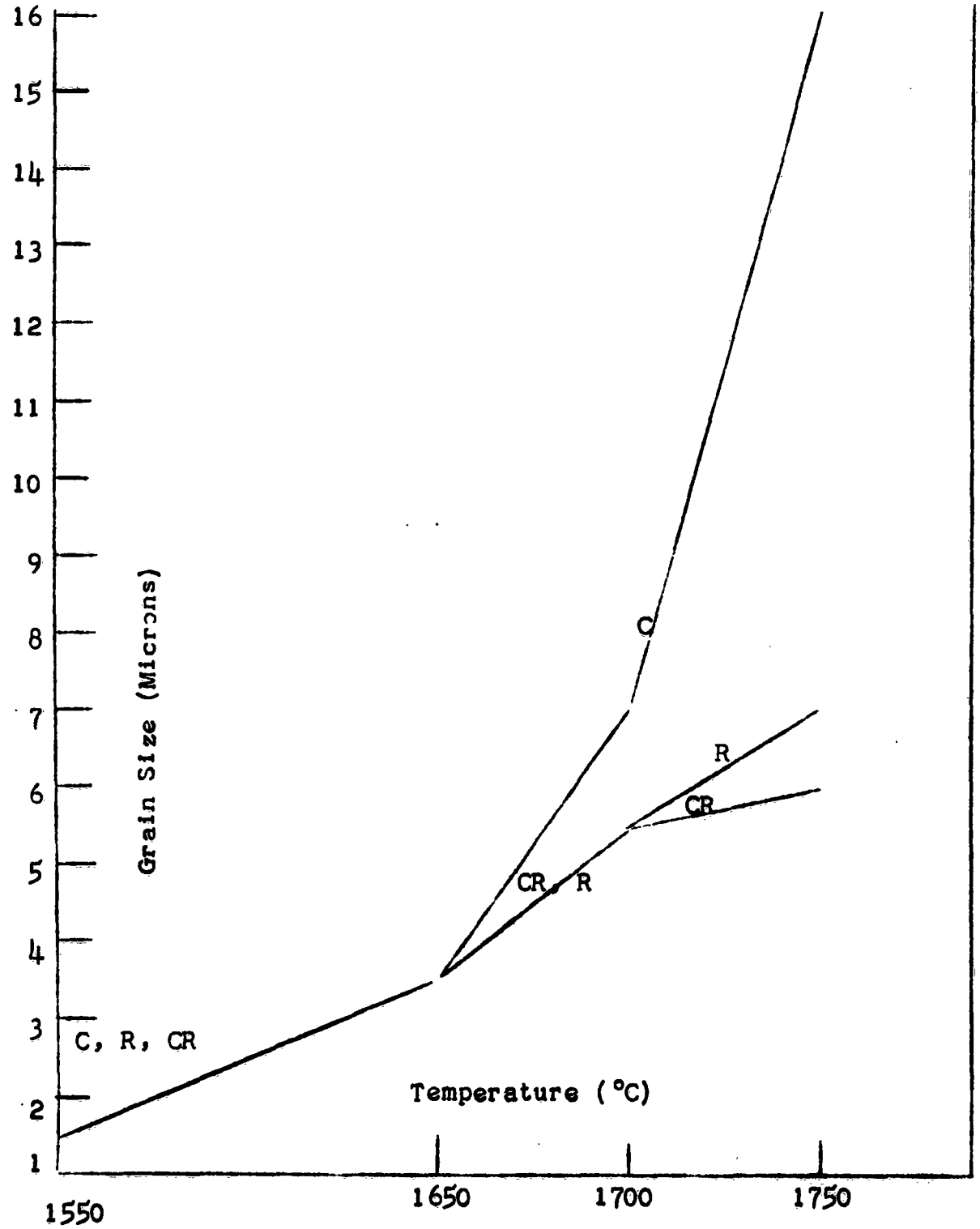

Figure 24

GRAIN SIZE VERSUS TEMPERATURE (°C)

HELD FOR THREE HOURS AT TEMPERATURE

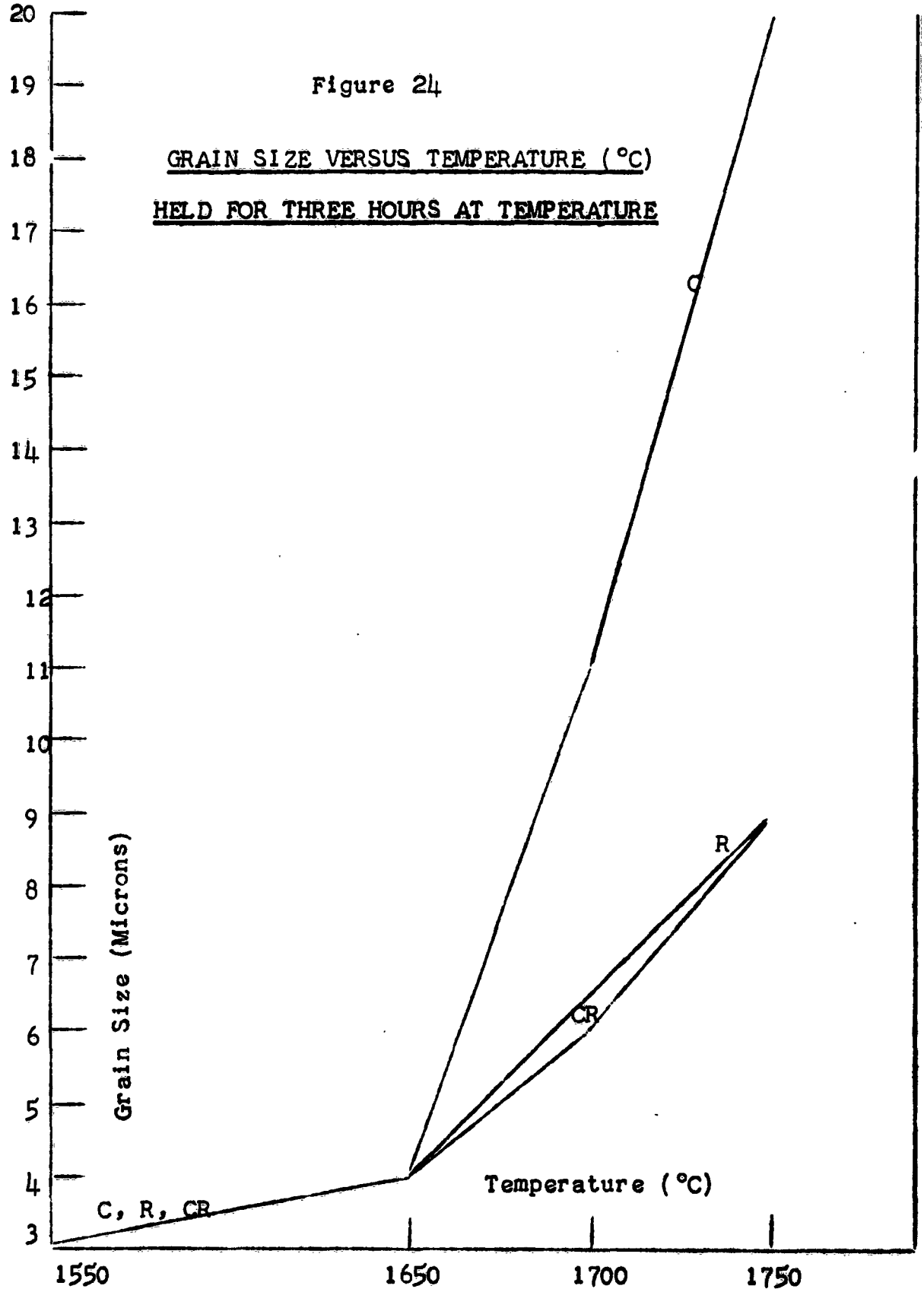

Figure 25

GRAIN SIZE VERSUS TEMPERATURE (°C)

HELD FOR FIVE HOURS AT TEMPERATURE

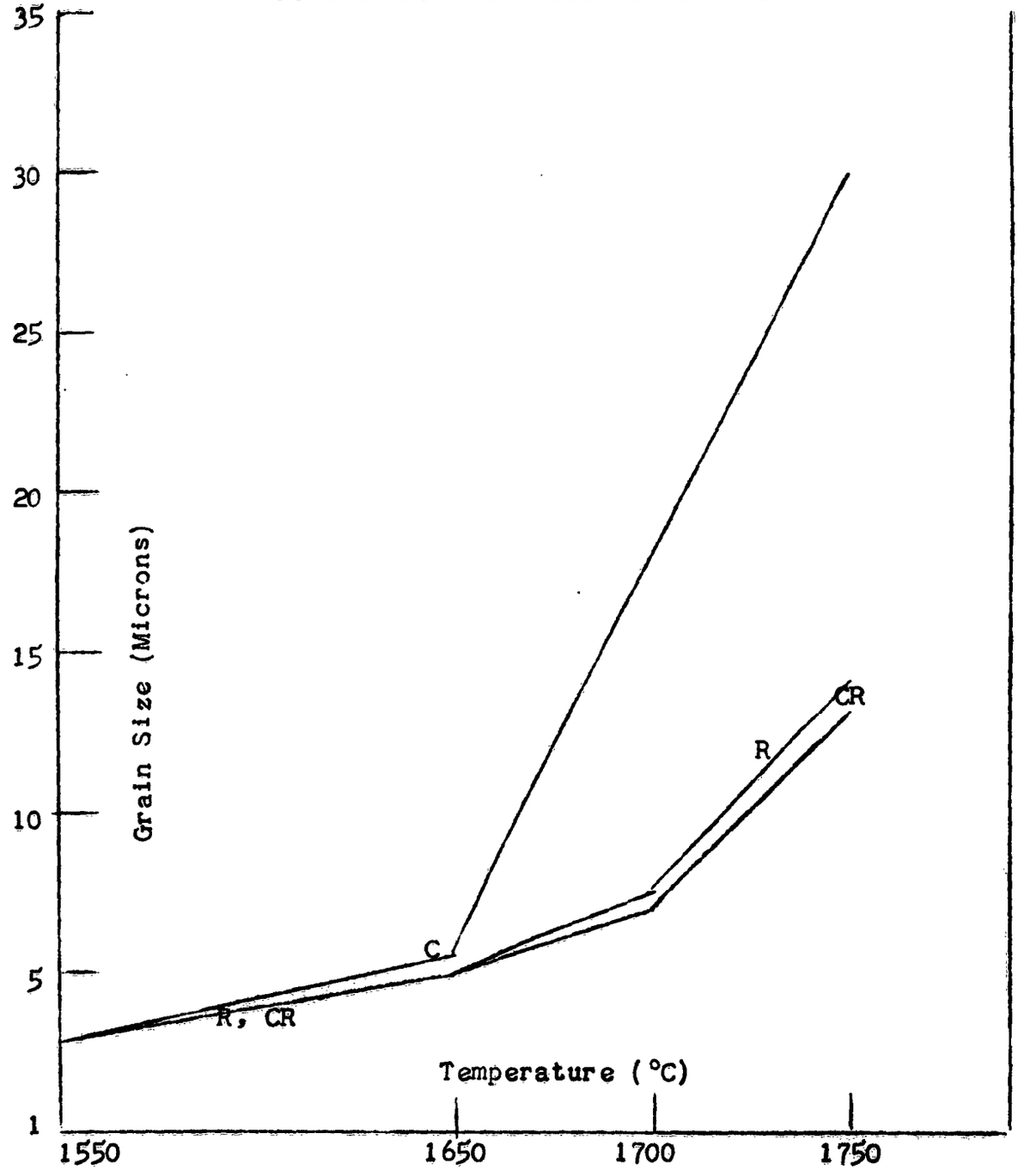

Figure 26

GRAIN SIZE VERSUS TEMPERATURE (°C)

HELD FOR SEVEN HOURS AT TEMPERATURE

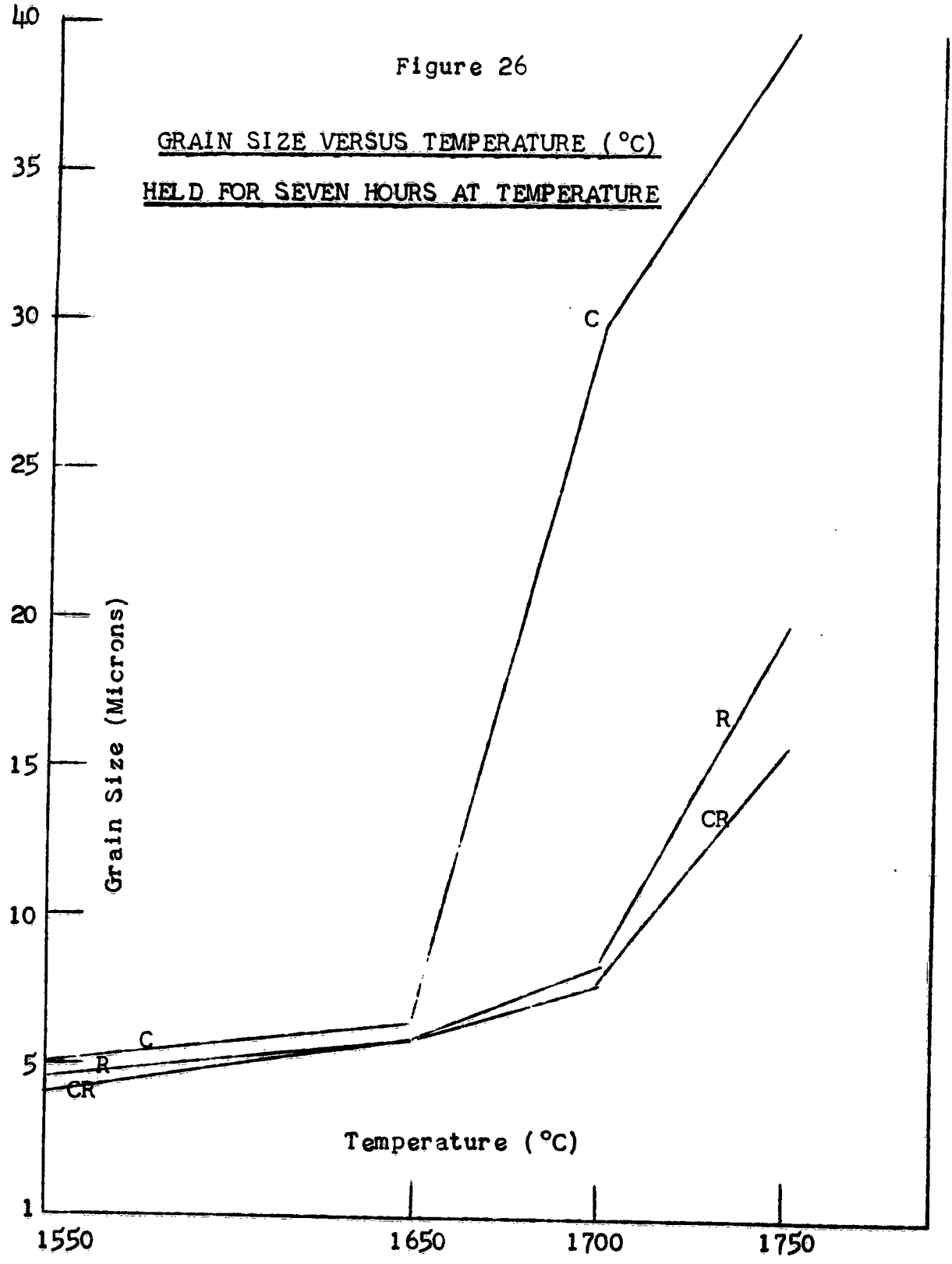

structure of the 0.25% MgO and the 2.0% MgO compositions were noted only at the longest time and highest temperature investigated.

Exaggerated grain growth nuclei were found at 1650°C to 1700°C. It was found that the pure alumina composition could not be sintered to theoretical density. The total porosity at 1700°C was 2.25%. This result is in good agreement with the value established by Coble. A high degree of densification was found for pure alumina. This degree of densification is comparable to the value obtained by Coble while using a dry hydrogen atmosphere. This degree of densification is high when compared with other aluminas fired in air to the same temperatures.

The increase in densification found can be attributed to both the starting material and vacuum firing. When the raw material used has a small uniform grain size, the sintering rate may be increased and exaggerated grain growth retarded. This retardation is due to the primary driving force for grain growth. It is known that large grains will grow at the expense of small grains. This was due to the smaller surface energy the large grains had with respect to the small grains [20]. The role vacuum plays in the densification of the pure alumina compositions may be the reduction of pressure on pores located at the grain boundary. This would tend to make the pore expand and thereby reduce the pressure within it and cause the pore to collapse.

[20] W. D. Kingery, Introduction to Ceramics (J. Wiley and Sons, Inc., New York, 1960) 353-401.

In the densification of the 0.25% MgO composition it was found that theoretical density was obtained for a three hour or more firing at 1750°C. Coble required nearly fifteen hours at 1675°C in order to obtain theoretical density in a dry hydrogen atmosphere[21]. Therefore, the results obtained in this investigation using vacuum, are in fairly good agreement. As shown by the results, a very high degree of densification was obtained at all temperatures investigated. Microstructure determinations show a great similarity in grain size between the 0.25% MgO and the 2.0% MgO compositions. The only noticeable variation found was at 1750°C and a seven hour soak. A comparison with the data obtained by Coble and the results obtained by this investigation shows good agreement. For example, Coble obtained an average grain size of ten microns for a seven hour fire at 1675°C. A value of six microns was obtained in this study for the average grain size at 1650°C and a seven hour fire. The maximum grain size for the 0.25% MgO composition was found to be twenty microns for a seven hour fire at 1750°C. The role vacuum played in the sintering of the 0.25% MgO composition was similar to that found by Coble with dry hydrogen.

It is felt that the mechanism operative may be different for vacuum than for dry hydrogen. In sintering alumina with dry hydrogen, it is felt that this atmosphere acts as a reducing agent on alumina and therefore, produces excess anionic vacancies

[21] R. L. Coble, "Sintering Crystalline Solids, Part I and II," J. of Appl. Phy., 32(5) (1961), 787-99.

which in turn enhance the sintering rate of the 0.25% MgO and pure alumina composition. It is felt that vacuum aids in the densification process by acting to reduce the pressure within the pore, thereby aiding in the collapse of the pore by external forces.

Results obtained for the 2.0% MgO composition show the densities to be intermediate between the 0.25% MgO and the pure alumina composition. Theoretical density could not be obtained for this composition. Microstructure determinations indicated that the microstructure of the 2.0% MgO composition was similar to the 0.25% MgO composition. An exception for the above was found for the seven hour firing at 1750°C.

The difference in microstructure of the seven hour firing at 1750°C may be attributed to three factors. The first may have been an error in determining the average grain size. The second factor may be that the 0.25% composition was at theoretical density and the inhibition of the pore phase located at the grain boundary on grain growth no longer existed [22]. Cahoon and Christensen [23] have shown that additions of magnesia to alumina inhibits grain growth. Therefore, it may have been a spinel phase at the grain boundary that inhibited grain growth, or a combination of all of the above.

[22] J. Burke, Kinetics of High Temperature Processes (Edited by W. D. Kingery. Technology Press Cambridge, Mass. and J. Wiley and Sons., New York, 1959)

[23] H. P. Cahoon and C. J. Christensen, "Sintering and Grain Growth of Alpha Alumina," J. Am. Ceram. Soc., 39(10) (1956), 337-44.

The difference in sintering of the 0.25% MgO composition from the 2.0% MgO composition may be attributed to two different phenomena. The 0.25% MgO composition could have entered the alumina structure as a solid solution [24]. If this occurred, an anionic deficient solid solution might have formed. This solid solution would have an additional number of vacancies above and beyond those found at equilibrium and as a result, increase the sintering rate of pure alumina. In the case of the 2.0% MgO composition, if the phase diagram [25] is to be believed, a solid solution spinel phase would exist in equilibrium with pure alumina. More likely, if the work of Arlett is assumed, part of this composition would enter the structure as a solid solution and the remainder would be deposited as a second spinel phase. This phase most probably would be found at the grain boundaries. A further postulation might be that the spinel phase at the grain boundary acts as a pore does and inhibits densification. In this manner it is possible for the 2.0% MgO composition to be intermediate between the pure alumina and 0.25% MgO compositions in its sintering characteristics.

F, CONCULSIONS

1. This investigation has shown that by firing in vacuum, high densities can be obtained at comparatively low temperatures for all the compositions investigated. At 1550°C (2820°F) densities of 3.87, 3.955 and 3.94 were obtained for the C, R, and CR compositions respectively. The total porosities for these compositions were 3.00, 0.87 and 1.25 respectively. Per cent moisture absorptions were 0.00 for all of the above compositions at 1550°C and at soaking time greater than 3 hours.

2. High densities, as well as theoretically dense bodies, have been prepared by using a vacuum for the 0.25% magnesia composition.

3. Exaggerated grain growth was found at temperatures at or above 1650°C for the pure alumina composition. Normal grain growth was found for both the 0.25% and the 2.0% magnesia compositions.

4. A mcehanism for the effect vacuum played in sintering was proposed as the reduction of the pressure of the ambient atmosphere within the pore.

5. A possible mechanism was postulated for the difference in grain size and densification characteristics between the 0.25% and the 2.0% magnesia compositions. The postulated mechanism was the formation of a solid solution for the 0.25% magnesia composition and the formation of both a solid solution and second spinel phase which inhibits sintering of the 2.0% magnesia composition.

G. FUTURE WORK

1. Determination of Electrical properties of the most promising compositions investigated in vacuum.

2. A sintering study of the three compositions investigated will be undertaken in a dry hydrogen atmosphere. The compositions will be fired at 1550, 1650, 1700 and 1750 °C for 1, 3, 5 and 7 hours soaking times. Determination of Bulk density total porosity, per cent shrinkage, moisture absorption. grain size and pore location will be made.

Distribution List for Reports Prepared Under Contract NOw 62-0710-d

1. RRMA-34, Bureau of Naval Weapons, Washington 25, D. C.
2. RAAV-321, Bureau of Naval Weapons, Washington 25, D. C.
3. PID-232, Bureau of Naval Weapons, Washington 25, D. C.
4. RMGA-811, Bureau of Naval Weapons, Washington 25, D. C.
5. DLI-3, Bureau of Naval Weapons, Washington 25, D. C. (2)
6. Armed Services Technical Information Agency, Arlington Hall, Arlington, Virginia (10)
7. Commanding Officer, Naval Air Development Center (EL-72), Johnsville, Pa.
8. Commanding Officer, Naval Air Material Center (AML), Philadelphia, Pa.
9. Code 423, Office of Naval Research, Washington 25, D. C.
10. Aerospace Industries Association, 7660 Beverley Boulevard, Los Angeles, Calif. (2)
11. Aeronautical Systems Division, Wright-Patterson Air Force Base, Ohio Attn: ASRCMC
12. National Aeronautics and Space Administration, Washington 25, D. C.
13. Lewis Research Center, NASA, 21000 Brookpark Road, Cleveland 11, Ohio.
14. Gladding, McBean and Company, 2901 Los Feliz Boulevard, Los Angeles 39, Calif.
15. Vitro Laboratories, West Orange Lab., 200 Pleasant Valley Way, West Orange, New Jersey, Attn. Dr. S. Grand.
16. Shenango China, Inc., P.O. Box 120, New Castle, Pennsylvania
17. Raytheon Company, Missile Systems Division, Bedford, Massachusetts, Attn: Mr. Robert O. Howe.
18. Boeing Airplane Company, Aerospace Division, P.O. Box 3707, Seattle 24, Washington, Attn: Mr. W. M. Sterry.
19. Office of Naval Research, c/o Princeton University, Chemical Sciences Building, Princeton, New Jersey, Attn: Mr. J. H. Levy

20. Avco Research and Advanced Development, 201 Lowell Street Wilmington, Massachusetts, Attn: Metals and Ceramics R&D.

21. Mr. Karl Schwartzwalder, AC Spark Plug Division, General Motors Corp., Flint Michigan.

22. Mr. Herman H. Frahme, Alberox Corporation, Industrial Park, New Bedford, Massachusetts.

23. Mr. John Duke, Duco Company, Butler, Pennsylvania.

24. Commanding Officer, Naval Air Material Center, Philadelphia 12, Pennsylvania, Attn: Technical Library, SE-354.

25. Raytheon Company, Missile and Space Division, Bedfored, Massachusetts, Attn: Mr. Wm. Shakespeare

26. National Beryllia Corporation, First and Haskell Avenues Haskell, New Jersey, Attn: Mr. P. S. Hessinger

27. Battelle Memorial Institute, 505 King Avenue, Columbus Ohio, Attn: Mr. Charles E. Day.

28. Scientific and Technical Information Facility, Attn: NASA Representative (S-AK/OL), P.O. Box 5700, Bethesda, Maryland.